Department of Environment Systems
Graduate School of Frontier Sciences
The University of Tokyo

2017

Master's Thesis

CFD based analytical approach of the annual performance of a solar absorption chiller with an underground cold thermal storage and an indirect seawater cooling system

Submitted August 24, 2017

Adviser: Assistant Professor Masaatsu Aichi
Co-Adviser: Associate Professor Takeshi Iimoto

ミッチェル　悠　チャベス　岡田

Michel Yu Chavez Okada

Abstract

This paper presents a computer fluid dynamics (CFD) based analytical approach of the annual performance of a solar absorption chiller with an underground cold thermal storage and an indirect seawater cooling system.

CFD simulations of an evacuated tube solar collector, seawater indirect helical coil heat exchanger and an underground cold-water tank are performed using ANSYS Fluent in order to obtain the key parameters of these components.

Analytical functions using these parameters are obtained and an Excel worksheet tool is created in order to do an annual simulation of the system.

A one-year simulation of the designed solar absorption chiller system is done at a building located in Veracruz, Mexico by using the Excel tool in order to obtain energy and costs information and compare it to a water powered chiller using a cooling tower and the same chiller using the indirect seawater cooling system.

Keywords:

Solar absorption chiller, underground thermal storage, indirect seawater cooling system, evacuated tube solar collector, CFD.

Acknowledgement

In this space, I would like to thank the many people who have supported me and encouraged me throughout this experience.

First of all, I am very grateful to my professor Aichi for all the support and tolerance during these 2 years. Countless advices and proposals have led to the conclusion of my research. Thank you.

I would like to thank JICA for providing me the scholarship and support, as well as the good memories and contacts, which made this experience possible.

I would like to thank my mother Etsuko and my dad Claudio, as well as my Japanese grandparents for raising me and providing me the tools and values to become the person I am today and support throughout the writing of this document.

I would like to thank my girlfriend Ana for all her support and company through all this time.

I would like to thank my friends from the childhood Parada, Palazuelos, Baca, Baez, Montero, Uribe for keeping in touch through all these years, as well as Ceron and many others who I'm sure know who they are. I would also like to thank my lab mates Kento, Morigaki, Morikawa, Ma, Kabil, Crystal who have made this a great experience.

I would like to acknowledge the Mexican and Japanese smash community for all the good times, experiences and support during these 2 years in Japan.

Finally, I would like to dedicate this work to my grandparents Claudio and Yolanda, who always kept encouraging me to study a master's degree and have supported my throughout the years.

Table of contents

List of Figures

List of Tables

Nomenclatures

Symbols

$\frac{\dot{Q}}{A}$	Useful energy extracted from collector per m^2 (kWh)
$F'(\tau\alpha)_{en}$	Effective transmittance-absorptivity product at (tm – ta) = 0 for direct solar radiation Gb at normal incidence
τ	Collector transmissivity
α	Collector absorptivity
$K_{\theta b}(\theta)$	Incidence angle modifier for direct irradiance
Gb	Beam irradiance in tilted collector plane (W/m2)
$K_{\theta d}$	Incidence angle modifier for diffuse irradiance
Gd	Diffuse irradiance in tilted collector plane (W/m2)
u	Wind speed in the collector plane (m/s)
G^*	Total (beam + diffuse) solar radiation in the collector plane (W/m2)
tm	(tin + tout)/2, it is the mean fluid temperature between inlet and outlet of the collector (C)
ta	Ambient temperature close to the collector (in the shade) (C)
E_L	Long wave radiation in the collector plane (W/m2)
σ	Stephan Boltzmann constant σ = 5.6697 x 10^-8 W/m2K4
Ta	Ambient temperature close to the collector (in the shade) (K)
c1	Heat loss coefficient at (tm – ta) = 0 (W/m2K)

c2	Temperature dependence in the heat loss coefficient (W/m2K2)
c3	Wind speed dependence of the heat losses (J/m3K)
c4	Long wave irradiance dependence of the heat losses
c5	Effective thermal capacitance (J/m2K)
c6	Wind dependence on the collector zero loss efficiency (s/m)
Q_{BC}	Building cooling load at specified air temperature.
Q_{PC}	Building peak cooling load
t_{dc}	Design cooling temperature
t_{bc}	Building balance point temperature
t_a	Ambient temperature
T_c	Temperature of cooling water
T_h	Temperature of heat medium
k	Turbulence kinetic energy
u_i	Velocity component in tenor notation
μ_t	Turbulent viscosity
σ_k	Prandtl number for k
σ_ϵ	Prandtl number for ϵ
G_k	Production of turbulence kinetic energy due to mean velocity gradients
G_b	Production of turbulent kinetic energy due to buoyancy
Y_M	Contribution of fluctuating dilatation in compressible flow

S_k, S_ϵ	User defined source terms
C1ϵ, C2ϵ, C3ϵ	Constants.
keff	Is the effective thermal conductivity k+kt, where kt is the turbulence thermal conductivity of the model being used
$\vec{J}_j$	Is the diffusion flux of species j
$\overline{\overline{\tau_{eff}}}$	Is the effective shear force
h	Enthalpy of the flow according if its compressible or incompressible
Re	Reynolds number
V	Fluid velocity (ft/s)
D_i	Internal diameter (in)
μ	Fluid viscosity (cp)
ρ	Fluid density (lbm/ft^3)
Q	Flow rate (gpm)
2r	Pipe inner diameter
2Rc	Coil diameter = Pitch circle diameter (PCD)
H	Pitch
α	Helix angle
δ	Ratio of Pipe diameter to Coil diameter is called curvature ratio = r/Rc
λ	Ratio of pitch to developed length of one turn (H/2pi*R) = non-dimensional pitch

q	Total heat transferred (W)
U	Overall heat transfer coefficient (W/m2K)
ΔT_{lm}	Logarithmic mean temperature difference (K)
A	Total surface area of contact (m2)
T_{hin}, T_{hout}	Inlet and outlet temperature of the hot fluid (K)
T_{cin}, T_{cout}	Inlet and outlet temperature of the cold fluid (K)
$TC^*(z^*_c)$	Dimensionless thermocline thickness
$S(v^*,t^*)$	S parameter function in dynamic state (discharging)
$S(t^*)$	S parameter function in static state
v^*	Dimensionless velocity of the thermocline
t^*	Dimensionless time
z^*	Dimensionless tank height
z^*_c	Dimensionless thermocline position at a certain time
α	Thermal diffusivity

Chapter 1. General Introduction

Background

The IPCC Fourth Assessment Report (AR4) concluded that "Most of the observed increase in global average temperature since the mid-20th century is very likely due to the observed increase in anthropogenic greenhouse gas concentrations."

Recent data confirm that consumption of fossil fuels accounts for the majority of global anthropogenic GHG emissions. Emissions continue to grow and CO2 concentrations had increased to over 390 ppm, or 39% above preindustrial levels, by the end of 2010.

The residential sector represents 27% of global CO_2 emissions, as well as 17% of global energy consumption, having great potential on the mitigation of climate change.

In the United States, the residential building sector spends around 7.79 quadrillion Btu/year, as shown in Figure 1 by the Department of Energy (DOE).

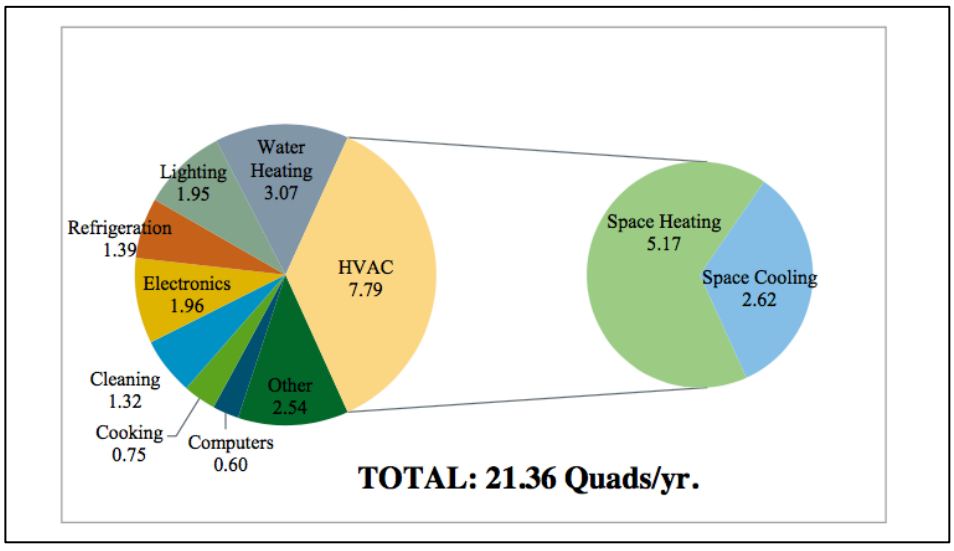

Figure 1. US residential building sector primary energy consumptions (Quad/year).

Source. Prioritization tool (2013)

In this sector, space heating and cooling represent 43% of total primary energy use, with the space cooling consuming 2.62 quads/year.

In the commercial building sector, the ratio is similar as observed in Figure 2.

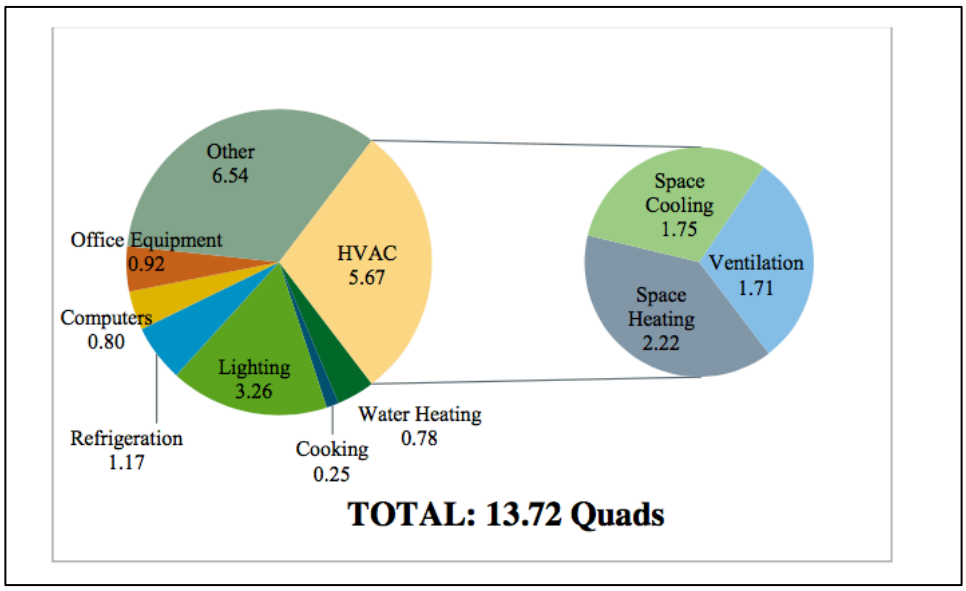

Figure 2. U.S. commercial building sector primary energy consumption (Quads/year). Source. Prioritization Tool (2013)

As observed, in the commercial building industry, space cooling consumes 1.75 quad/year.

The most common type of air conditioning equipment is the vapor-compression air conditioner, which uses a compressor to run the vapor-compression refrigeration cycle consuming large amounts of electricity.

We can see in Figure 3 that the space cooling technology that corresponds to the entirety of the residential and commercial building sectors in the United States use the vapor-compression technology.

There are many types of space cooling technology but they can be largely divided into four types depending on their operation principles as vapor-compression, thermally driven, electro-mechanical and solid-state technology.

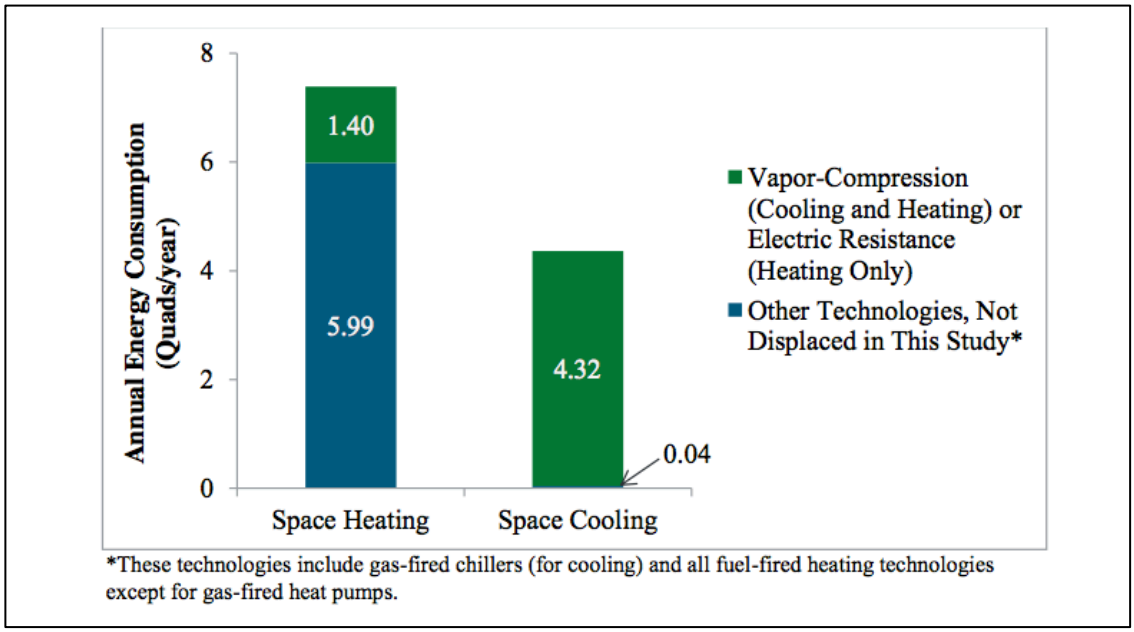

Figure 3. U.S. building sector HVAC primary annual energy consumption by technology. Source. Prioritization Tool (2013)

The total efficiency of each type of space cooling technology depends greatly on the climate zone characteristics such as annual temperature distribution, humidity, sun hours, etc.

In Figure 4 we can see a distribution of the space cooling equipment energy consumption by region in the United States.

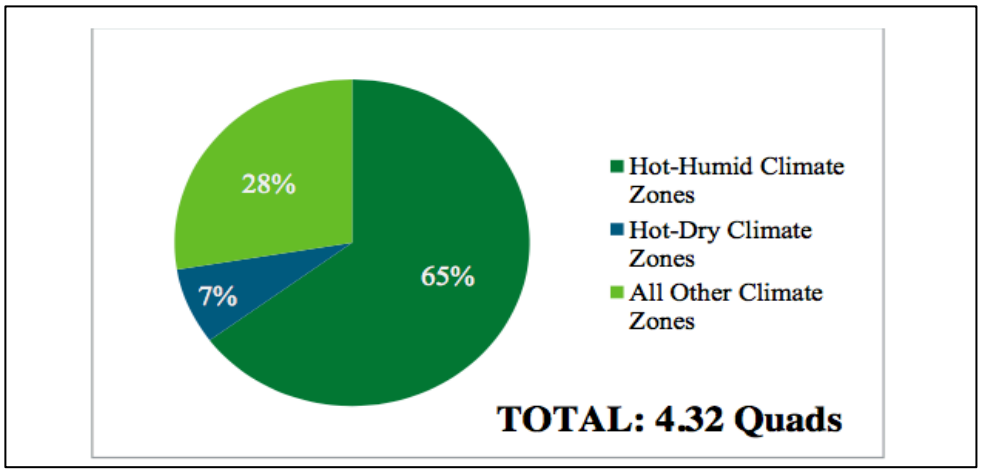

Figure 4. Climate zone breakdown of cooling energy consumption. Source. Prioritization tool (2013)

It is important to notice that hot-humid climate zones consume 65% of the energy of space cooling technology; therefore these regions are of interest for the purpose of this research.

In Mexico, households heating energy consumption accounts only 3% of the total energy consumption, but air conditioning accounts for 15% and water heating for 29%. Refrigeration accounts for 22% (CONUEE, 2006), but, as mentioned before, it is important to differentiate by zones to get a better idea of the air conditioning consumption.

In Mexico, the electricity bill varies depending on the location of the consumer and is divided into 7 regions (see Figure 5).

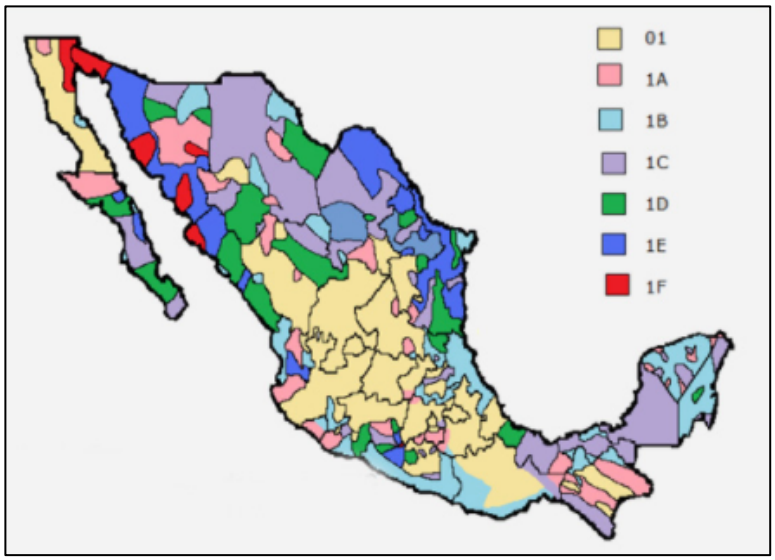

Figure 5. Electricity Bill in Mexico.*Comision Federal de Electricidad (CFE)*

Between 2012 and 2016, the average electricity consumption due to air conditioning of the 1B and 1C region has increased 56% and 50% respectively (CONUEE, 2017). These areas correspond to the coastal zones and southern zones of Mexico, therefore, it is of our interest to find a cooling technology that performs well under these conditions and can reduce the consumption of electricity. Due to this, Veracruz, Mexico was selected as the target region for the purpose of this research.

The most significant drawback of the other types of space cooling equipment is that often they are not cost effective, making them unattractive for the consumer. This is one of the major reasons that other cooling technologies haven't deployed as much as the vapor-compression technology. Due to this, in order to make alternative space cooling more cost-effective, most of the times innovative and creative ways of using the available resources is necessary.

Cooling equipment options

Ground source heat pump

One of the most promising air conditioning equipment in the actuality is the ground source heat pump, which uses an underground heat exchanger loop to extract or reject heat depending if its either heating or cooling. This technology takes advantage of the underground temperature, which due to the thermal inertia of the ground maintains an almost constant temperature close to the annual mean temperature throughout the year (see Figure 6).

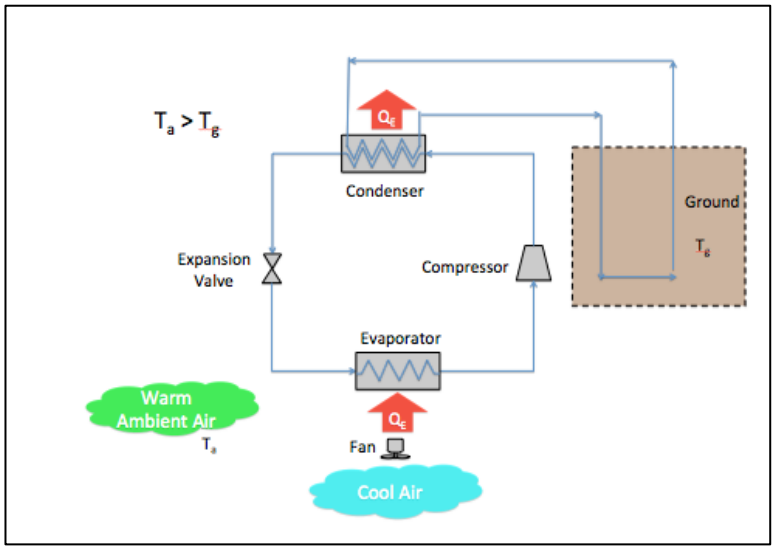

Figure 6. Closed loop ground source heat pump diagram

Depending on the soil thermal conductivity, ground water conditions and temperature difference between ground and air, this technology can attain higher COPs and EERs than traditional air source heat pumps, making up for its high initial costs due to drilling and excavation, and site analysis.

Depending on the area where it's going to be installed, several loop designs can be considered in order to make it cost effective. The most common loop designs are the vertical loop, horizontal loop, horizontal trench, pond loop and slinky loop.

This technology has been implemented in the United States, Europe and Japan with success, but it is more known for its heating performance rather than its cooling performance.

There are two major drawbacks of this technology when considering its implementation in Veracruz, Mexico.

As observed in Table 1, Veracruz is a highly cooling load inclined area, having more than 85% of the time a cooling load requirement to maintain a comfort temperature.

Bin (F)/(F)	Tair (F)	Tair (C)	Hours
105/109	107	41.7	0
100/104	102	38.9	1
95/99	97	36.1	56
90/94	92	33.3	512
85/89	87	30.6	1135
80/84	82	27.8	1494
75/79	77	25.0	2303
70/74	72	22.2	1981
65/69	67	19.4	1024
60/64	62	16.7	218
55/59	57	13.9	27
50/54	52	11.1	4
45/49	47	8.3	5
40/44	42	5.6	0
35/39	37	2.8	0
30/34	32	0.0	0
25/29	27	-2.8	0
20/24	22	-5.6	0
15/19	17	-8.3	0
Mean annual temperature	77.4	25.2	
Total hours			8760

Table 1. Bin data of Veracruz annual temperature

Temperatures above 19.4 °C require a cooling load. Temperatures below 16.7 °C require a heating load. It is well documented that when the ambient air is between 16.7 °C and 19.4 °C, there is no need for a thermal load.

As observed, the mean annual temperature is 25.2 °C, which would make a relatively low temperature difference with the ambient temperature, which would yield a relatively low EER, making it hard to compensate for its high initial installation costs.

Another issue is that because of the heavily inclined cooling loads, heat stagnation will start to occur, increasing the ground temperature continuously and reducing the systems EER as it continues to operate.

Seawater air conditioning

There are mainly two types of seawater air conditioning. Indirect seawater air conditioning and direct seawater air conditioning. These options are less popular, but have some significant advantages.

Water has almost 4 times the specific heat capacity of common land materials (sand, clay, silt, etc.), making the seawater surface temperature daily fluctuations relatively low due to the thermal inertia (see Figure 7). Also, unlike ground, after few meters from the surface, seawater temperature decreases steeply with depth, creating a large temperature difference between the heat sink and the ambient air.

Indirect seawater air conditioning

Indirect seawater air conditioning is very similar to a ground source heat pump but instead of using the ground as the heat sink, it uses the sea.

High-density polyethylene (HDPE), which is the most common material used in heat pumps loops, is highly resistant to salinity and marine growth.

This technology presents some advantages over the issues that ground source heat pumps has to overcome.

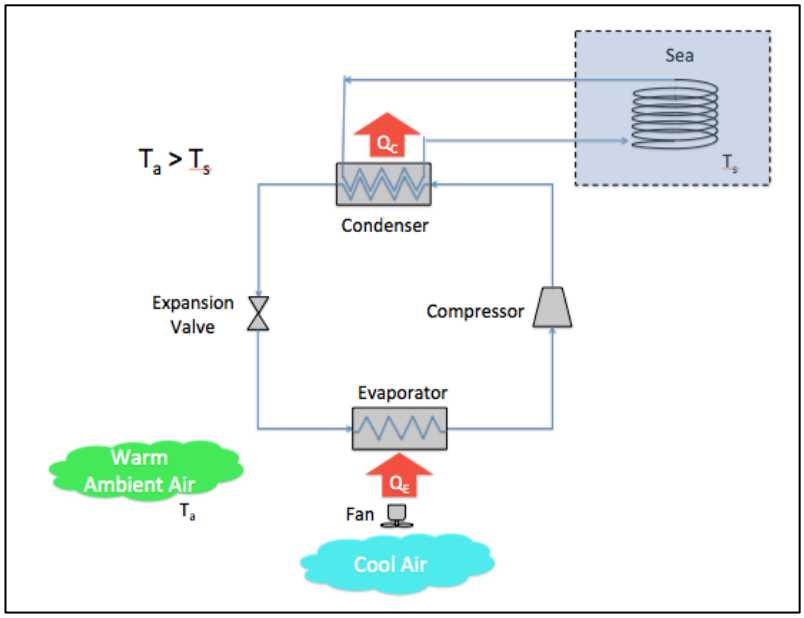

Figure 7. Simple seawater source heat pump diagram

One of the most significant advantages is that there are virtually no drilling or excavation costs compared to the ground source heat pump, making installation costs more accessible. Another advantage over the ground source heat pump is that due to the continuous current flow of the sea, there would be little to no heat stagnation, keeping the system performance consistent.

Direct seawater air conditioning (SWAC)

The direct seawater air conditioning system pumps deep seawater, which has a very low temperature (approximately 7 °C), to a heat exchanger station in land in order to cool the working fluid to the required temperature, which is pumped directly to the building cooling distribution system (see Figure 8). The waste seawater is then pumped back to a semi-deep layer in order to avoid environmental impact due to "cold shock" (Elsafty, 2009).

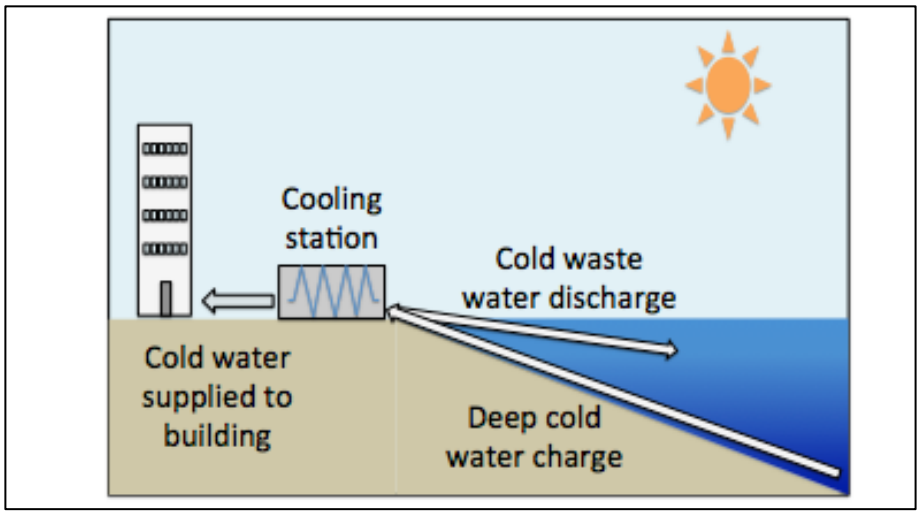

Figure 9. Simple schematic of SWAC system

The issue with the implementation of these types of seawater air conditioning in Veracruz, Mexico is because of the bathymetry of the region as shown in Figure 10.

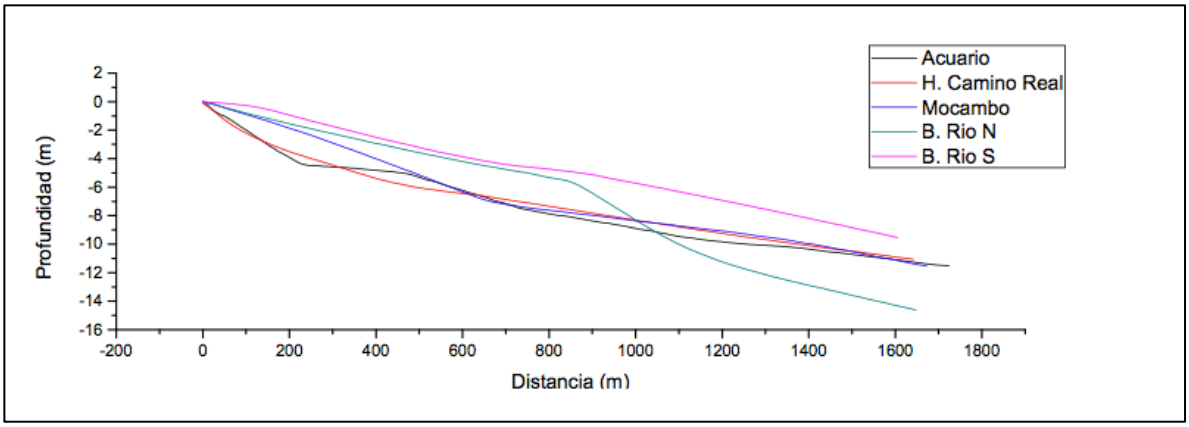

Figure 10. Bathymetry of several Veracruz beaches. Sectur, 2014

As observed, after a distance of almost 2 km there's barely 14 m of depth, which has still the same or very close temperature to the sea surface, which generates a relatively small temperature difference. Therefore, in order to attain a sufficiently low temperature, very long distances of piping need to be installed making it not cost effective.

Evaporative coolers

Evaporative coolers take advantage of the large latent heat necessary to have a phase transition of a substance (water, e.g). There are many different configurations, but they mainly function through the evaporative cooling cycle. Water is pumped into an evaporative pad, which is a porous material that separates water particles. Hot air is passed through this pad and some water particles evaporate, extracting large amounts of heat due to the phase change latent heat and this in turn reduces the temperature of the now humid air. The amount of heat is maintained, but the temperature of the air is decreased. This type of systems cooling potential depends greatly on the difference between the wet bulb and dry bulb temperature, therefore, it is more suited towards arid climates. In some cases, a desiccant cooling cycle is added in order to maximize this difference (see Figure 11).

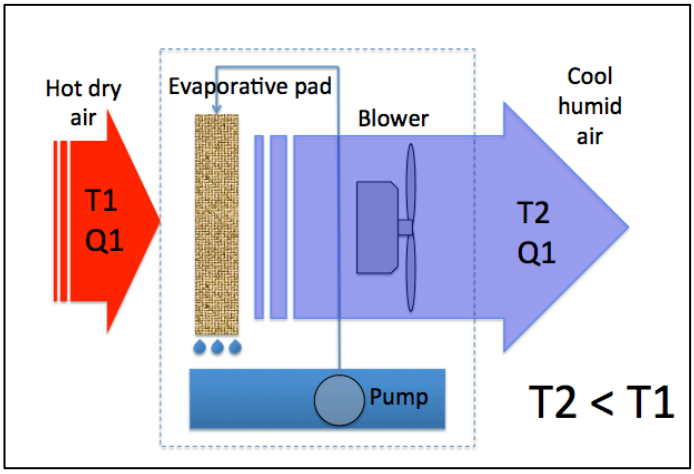

Figure 11. Evaporative cooling diagram

Due to its coastal location, the humidity in Veracruz is extreme, having an average annual relative humidity of 83.6%, therefore using standard desiccant cooling cycle is not enough to reduce the humidity of the entering air down to a level acceptable for evaporative cooling to occur effectively. In this type of region, additional equipment, such as an

additional desiccant wheel or a chiller has to be installed in order to reduce the humidity of the entering air, which in turn increases installation costs significantly.

Solar air conditioning

Solar air conditioning is used in areas where high solar irradiation is available. This type of technology is expanding in hot climates due to its convenient relationship that whenever irradiation is high, ambient temperature is high, and also the cooling capacity of the equipment is high. Solar air conditioning can be greatly divided into solar electric cooling and solar thermal cooling systems.

Solar thermal cooling systems

In solar thermal systems, solar thermal collectors are used to accumulate solar radiation in the form of hot water or steam, which is used to run a refrigeration cycle. These systems can be divided into closed cycle and open cycle.

Closed cycle: A refrigerant runs through a thermally driven refrigeration cycle in order to produce chilled water. Closed cycle consists mainly of three different types of refrigeration cycles: Absorption, adsorption and ejector jet.

Absorption refrigeration cycle: An absorption refrigeration cycle is very similar to a vapor-compression cycle in that they both have a condenser, expansion valve and an evaporator. The part that changes is how the compression of the refrigerant takes place.

After getting through the evaporator, the refrigerant, which is usually water in the case of water-lithium bromide types or ammonia in the case of ammonia-water type, goes into an absorber chamber, which contains a sorbent material, either lithium bromide or water depending on the type. In this chamber the gas-state refrigerant is absorbed by the liquid sorbent and is pumped into a generator where heat is added through a heat exchanger

connected to the solar thermal collectors. This heat is enough to evaporate the refrigerant separating it from the sorbent. The refrigerant, now as a gas again, goes to the condenser to continue the refrigeration cycle, while the sorbent goes to back to the absorber chamber through a valve and cooled in order to repeat the cycle (see Figure12).

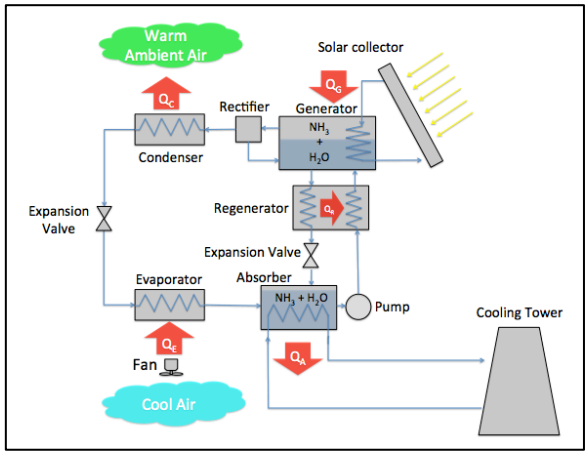

Figure 12. Solar absorption chiller diagram

A great advantage of the absorption system is that the only mechanical component that it uses is the circulating pump, which consumes very small quantities of electricity compared to a compressor.

Adsorption refrigeration cycle: The adsorption refrigeration cycle is similar to the absorption refrigeration cycle, except that it uses a solid adsorber instead and it works on two steps or more steps.

At the beginning of the cycle, the adsorber contains high concentration of refrigerant and is located inside a generator. The adsorber is a porous material that absorbs the refrigerant when the temperature is low, but releases it when the temperature is high. In the first step, heat is added and the adsorber starts to release the refrigerant increasing the pressure of the generator. The gas flows to a condenser and the further cycle is the same as

the traditional refrigeration cycle. In the second step, the adsorber is cooled in order to absorb the incoming refrigerant from the evaporator to continue the cycle (see Figure 13).

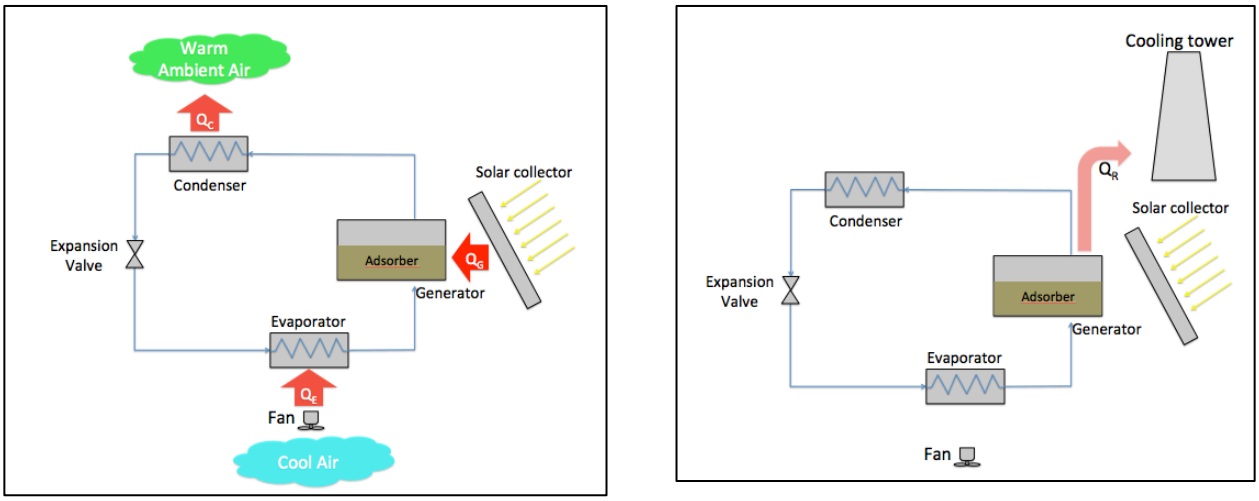

Figure 13. Two steps of the solar adsorption chiller diagram a) First step of cycle, b) Second step of cycle

This type of equipment usually contains more than 1 generator and rotates between them in order to maintain a continuous supply of cool air.

Ejector jet refrigeration cycle: In the generator, the primary fluid is heated by the heat from the solar collectors and increases its pressure. The high-pressure fluid enters the jet ejector, which increases further more the pressure of the refrigerant and also creates a low pressure area at the bottom part that brings a secondary fluid from the evaporator. Both fluids are mixed in the jet ejector and go through a condenser where the residual heat is rejected. The fluid goes to a separator where the primary and secondary fluids are sent to the pump and to the expansion valve respectively. The secondary fluid goes through the evaporator and back to the jet ejector to continue the cycle (see Figure 14).

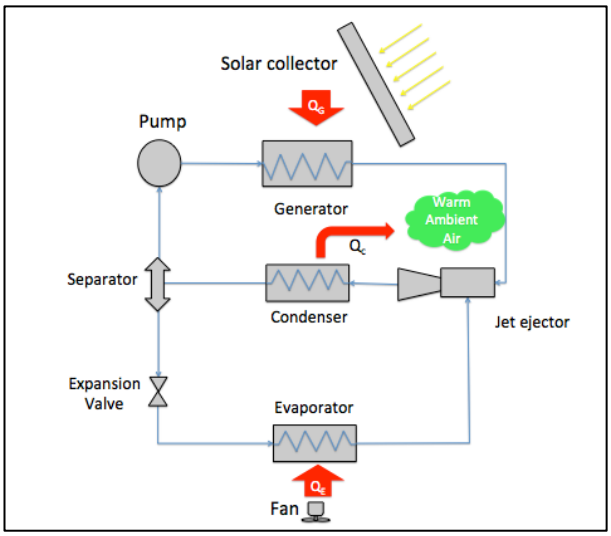

Figure 14. Ejector Jet cooling diagram

Open cycle: These systems are called desiccant evaporative cooling systems and use the same basic principle as the evaporative coolers, but they use a low-grade solar heat (60-90 °C) in order to regenerate the desiccant wheel.

Hot humid air enters the desiccant wheel and gets its humidity absorbed by it and becomes hot dry air. The hot dry air goes to the evaporative pad and continues the evaporative cooling cycle.

Humid air from the building goes to the generator, which receives heat from the solar thermal collectors, and heats up. The hot air evaporates the water particles at the opposite side of the desiccant wheel and dries it to continue the cycle (see Figure 15).

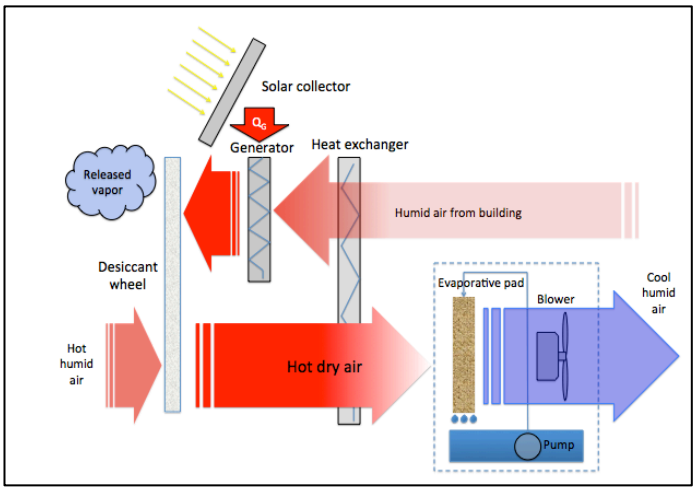

Figure 15. Solar evaporative cooling with desiccant wheel

Solar electric cooling systems

These systems use photovoltaic cells to produce electricity to run a traditional vapor-compression refrigeration cycle (see Figure 16).

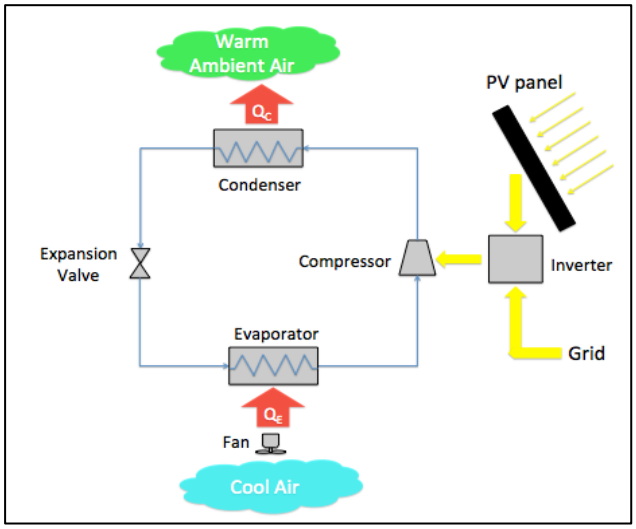

Figure 16. Solar Photovoltaic cooling

Kim et al. presented a state of the art review of solar air conditioning systems. In his work he compared solar electric, solar thermal and some emerging technologies in order to view economic feasibility and energy efficiency of these systems.

According to Kim's research (appendix A), the single effect water-lithium bromide solar absorption chiller is the most economically viable option with a cost of 1000 €/kW_c, followed closely by a double effect absorption chiller and a single effect adsorption system at 1200 €/kW_c.

Ghafoor et al. presented a research about a worldwide overview of the solar thermal cooling technologies. In his paper he described the advantages and disadvantages of each of the solar air conditioning technologies. He further performed a cost analysis including the area of collector and storage tank volume of several solar cooling systems estimating their costs per kilowatt of cooling capacity and gathered them in a table (see appendix B).

According to the author's research, a water-lithium bromide solar absorption chiller is the most economical option with a range of 1500-2000 €/kW_c followed by a solar adsorption chiller using flat plate collectors with a range of 2000-2500 €/kW_c.

He further performed a comparison of these solar thermal cooling technologies in terms of COP by using experimental data and simulation results concluding that the COP of a solar absorption system lies between 0.6 - 0.8 for simulation results and from 0.4 - 0.85 for experimental data. Solar adsorption chillers have a lower COP between 0.2 - 0.6 both for simulated and experimental systems. He also mentions that the most dominant technology in the actuality among solar thermal cooling technology is the solar absorption chiller.

Comparing the above-mentioned options with their respective advantages and disadvantages, we decided to select a single fired water-lithium bromide solar absorption chiller system for the purpose of this research.

Chapter 2. Solar Absorption Chiller System

In this section we will briefly describe the traditional components that are necessary for the correct functioning of a solar absorption chiller (Types of solar collectors, thermal storage tanks, Cooling towers, etc.).

A solar absorption chiller is composed by several components that must be sized according to site-specific needs. In Figure 17 we can observe the components of a traditional solar absorption chiller system.

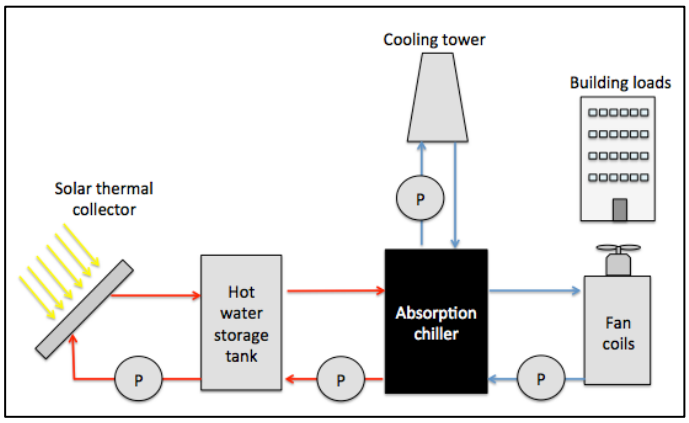

Figure 17. Solar absorption chiller main components

The main components of the solar absorption chiller system are the solar thermal collectors, the thermal storage tank, the cooling tower and the fan coils.

Absorption chiller

There are several manufacturers of absorption chillers worldwide (Appendix C), but for the purpose of this paper we selected a 50 ton Yazaki absorption chiller (see Figure 18). The complete absorption chiller specifications sheet can be seen in Appendix D.

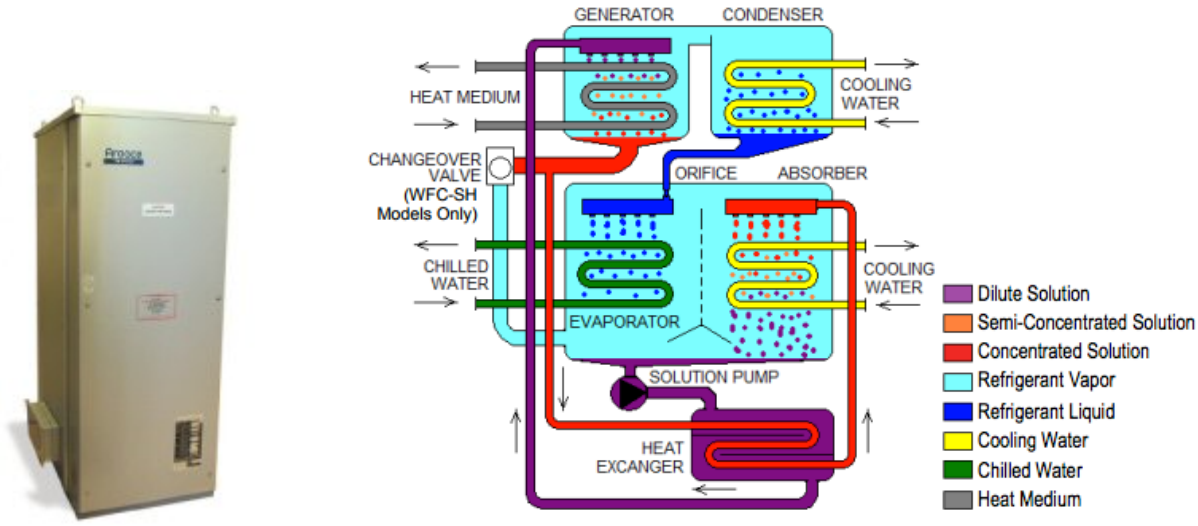

Figure 18. Yazaki single fire water-lithium bromide absorption chiller, http://www.yazakienergy.com/

Table 2 describes the most important characteristics of the selected chiller.

	Rated values		
	Inlet T (°C)	Outlet T (°C)	Water Flow (m3/s)
Cooling Water	31	35	0.026
Heat Medium	88	83	0.012
Chilled Water	12.5	7	0.008

Table 2. Characteristics of the Yazaki 50 ton absorption chiller

Solar thermal collectors

Solar thermal collectors are used to gather heat from the sun in order to increase the temperature of a working fluid. They are commonly composed by an absorber plate, which is

usually painted black in order to absorb the most amount of irradiation. Actual absorbers can absorb more than 98% of the heat of the sun. This absorber is coupled to a heat exchanger, which transfers heat to the working fluid.

In order to minimize convection losses to the ambient, the absorbers top surface is usually covered with a semi-transparent glass with high transmissivity for the absorber to receive as much solar irradiation as possible while avoiding its contact with exterior air.

A solar thermal collector's efficiency depends greatly on the above mentioned factors. Low efficiency collectors required a greater collector area.

There are several types of solar thermal collectors, but for the application of solar cooling, mainly the following three are used.

Flat plate collector: The flat plate collector usually consists of a flat plate absorber with a glass cover on top of it. The sides and the bottom are usually covered by a high thermal insulation material to prevent further convection and conduction losses (see Figure 19).

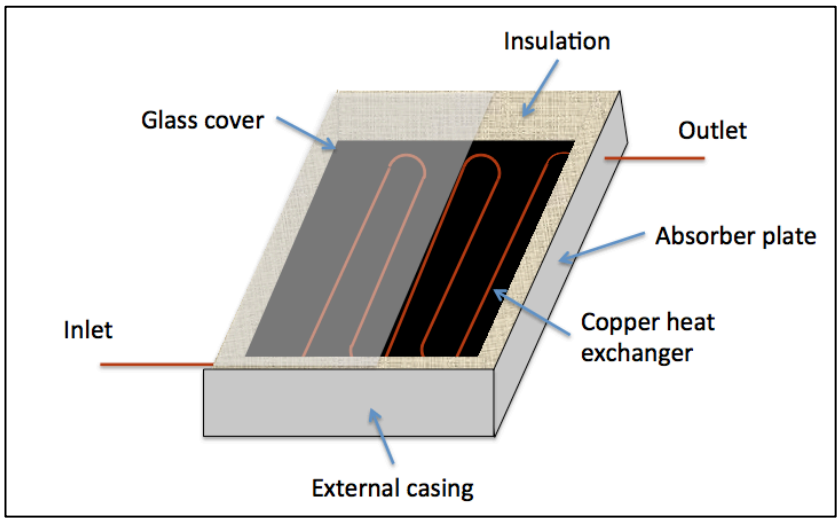

Figure 19. Flat plate solar thermal collector

The copper heat exchanger has direct contact with the absorber in order to transfer heat through conduction.

This type of collector is the simplest and it usually has the lowest prices on the market, but it is mostly used for lower temperature applications in the range of 30-80 °C (Kalogirou, 2004). This is due to the fact that due to the low thermal resistance of the glass cover, convection losses increase significantly as the temperature of the working fluid increases and the temperature difference with ambient becomes large

A table of the typical characteristics of a flat plate collector can be found at Appendix E.

Evacuated tube solar collector

All evacuated tube solar collectors consist of a long flat or round absorber covered by a cylindrical glass evacuated tube. This tube maintains a vacuum between two glass cylinders, increasing thermal resistance significantly and thus reducing its convection losses to the ambient (see Figure 20).

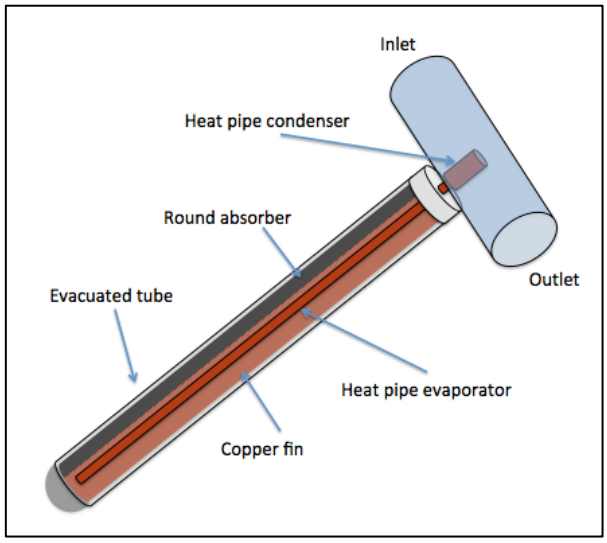

Figure 20. Evacuated tube solar collector

Several evacuated tubes are aligned in series in order to increase the overall absorber area.

They are divided into 3 types depending on how the heat is transferred to the working fluid into integrated tank, U pipe and heat pipe.

The integrated tank contains a tank at the top of the evacuated tube. The water from the tank enters the tubes and has direct contact with the absorber, which heats the water up. Due to the thermosyphon effect, the hot water from the bottom of the evacuated tube raises and goes to the top of the tank, while cold water descends to the bottom of the tube to be heated and so on.

The U pipe or direct flow has a U shaped pipe that goes along the evacuated tube, which transports the water. The pipe is usually a copper pipe and is connected to the absorber directly or through fins in order to increase contact area. The water enters the U pipe and gets heat up due to conduction.

The heat pipe type contains a heat pipe located inside the evacuated tube. A heat pipe is a heat exchanger that contains a heat transfer fluid with a relatively low boiling point. Usually ethanol is used, but in some cases water can be used if a vacuum is generated inside the heat pipe in order to reduce the pressure to lower its boiling point.

The part of the heat pipe that is inside the evacuated tube in contact with the absorber or fins is the evaporator and the condenser part is located outside, and it is in contact with the pipe (commonly copper) that transports the water.

The liquid at the evaporator heats up, phase changing to gas and ascends to the condenser, where it transfers its heat to the cold water through the copper walls and condenses to repeat the cycle.

The evacuated tube collector is used for a medium temperature range of 50-200 °C (Kalogirou, 2004) and it's the most commonly used for solar absorption chiller applications due to its operation temperature range and costs relation.

A table of the typical characteristics of an evacuated tube solar collector can be found at Appendix F.

Compound parabolic solar concentrators

These types of collectors are cylindrical tubes that have a parabolic concentrator that reflects the incident irradiation to the absorber, which can be flat or round (see Figure 21).

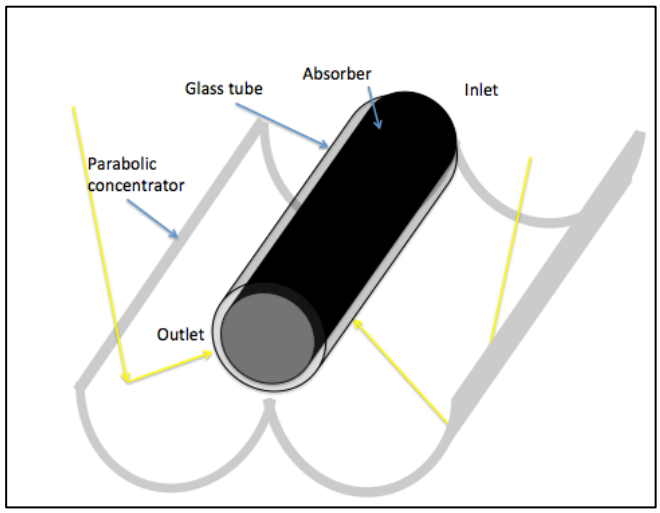

Figure 21. Compound parabolic solar concentrator (CPC)

The absorber is usually covered with glass in order to reduce convection losses, as well as to avoid dust or particles into the absorber.

The concentrator has a reflective coating in order to reflect as much irradiance as possible and they are most commonly designed as linear trough collectors.

This type of collector can work well in the range of 60 up to 240 °C (Kalogirou, 2004) due to the high concentration of irradiance at the absorber.

A table of the typical characteristics of a compound parabolic solar concentrator can be seen at Appendix G.

Figure 22 shows some common collector efficiency depending on the inlet temperature.

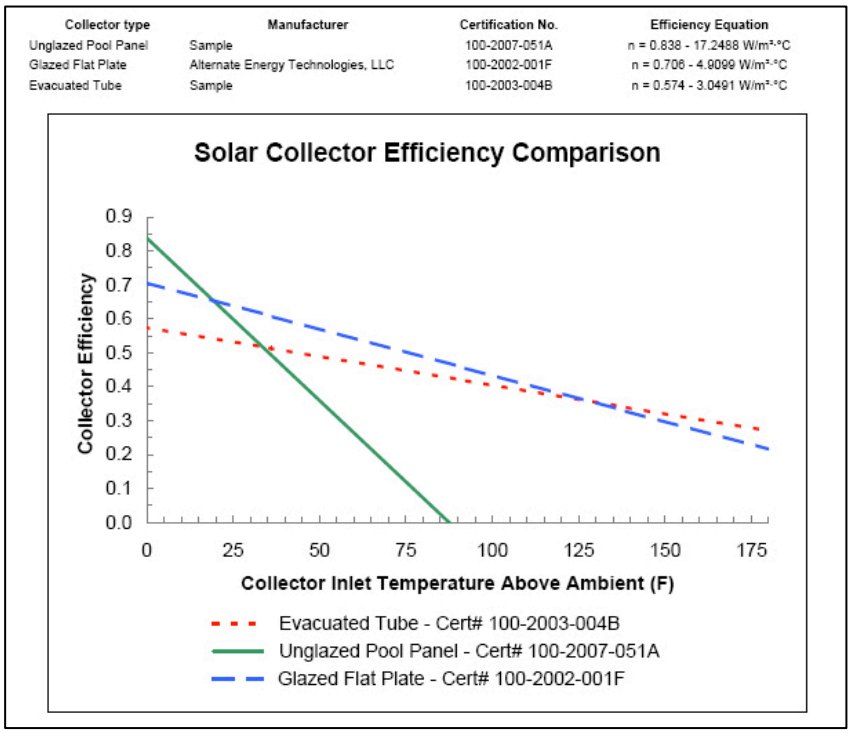

Figure 22. Solar collector efficiency comparison. Solar rating and certification corporation (http://www.solar-rating.org/)

The start point of the curve depends on the optical losses related to the absorptivity of the absorber and the transmissivity of the glazing material. This is why unglazed pool panel has the highest starting point.

Further we can clearly observe how collector efficiency decreases as the difference between the inlet temperature and the ambient temperature increases due to convection losses, especially in the case of unglazed due to no protection from convective heat transfer.

Another important factor that affects the collector overal efficiency is the incidence angle modifier (IAM).

The total irradiation or global horizontal irradiance (GHI) that strikes a surface is composed mainly by the direct normal irradiation (DNI) and the diffuse horizontal irradiation (DHI). There is also the ground reflected component, but it is minimal and most of the times it is neglected.

The DNI is the direct ray that comes directly from the sun to a surface perpendicular to it. Some of the rays coming from the sun strike clouds and water particles throughout their way and scatter the rays creating diffuse irradiation, which is the DHI.

Depending on the angle of incidence of the solar beam, the amount of the solar heat flux to the absorber changes significantly.

In the case of a flat plate collector, the maximum amount of heat flux can be obtained when the sun is perpendicular to the plane of the absorber plate, which in this case gives an incidence angle modifier of one.

In the case of a cylindrical absorber, the longitudinal and transversal angles must be considered thoroughly (see Figure 23).

The sun moves in the transversal plane through the day-night cycle, while it moves to the longitudinal plane throughout the year. This is why collectors are usually placed differently depending on their purpose. For example, if a collector output is required to be at its highest during winter, then the collector should be angled in the longitudinal plane in such a way that the sun incidence angle is at its highest during winter's sun position. In the case of a solar absorption chiller, max outputs are usually desired during summer time where the peak loads tend to occur.

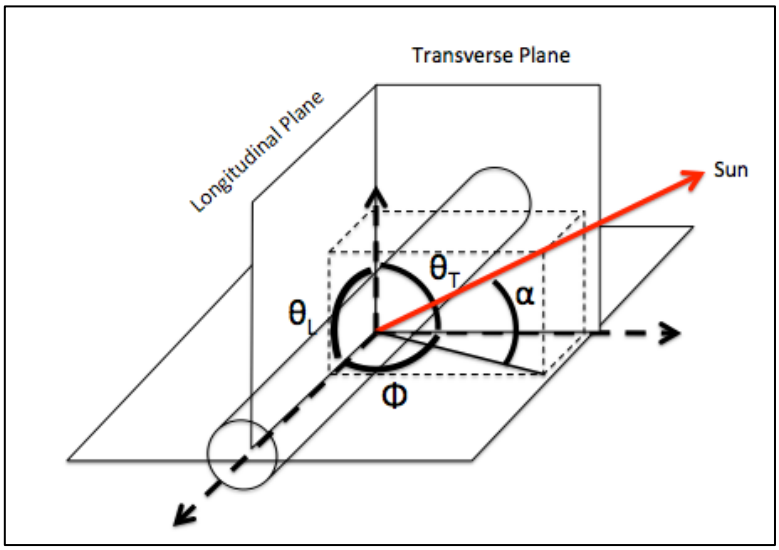

Figure 23. Description of transversal and longitudinal angle components for the solar angle

https://www.osti.gov/scitech/servlets/purl/345030

Due to its shape, cylindrical absorbers have the benefit that they can passively track the sun during the day-night cycle while the sun is traveling through the transversal angle. This advantage lets the cylindrical absorber collector to have higher heat fluxes throughout the day compared to a standing flat absorber collector, although it is important to mention that in order to increase the overall efficiency of a collector, some systems use an active tracking system that allows the collector to stay at a perpendicular angle to the sun during longer sun hours.

Cylindrical absorbers also benefit slightly from the DHI that can strike the cylindrical absorber from many different angles.

In the case of an evacuated tube solar collector, a portion of the rays that strike the vacuum tube reflects to the tube next to it, increasing the incidence angle modifier as well. This component depends on the spacing between the tubes and it varies greatly depending on the manufacturer.

Even though generally the flat plate collector is considered more accessible, it is worth mentioning that recently the evacuated tube solar collectors costs have decreased significantly due to the Chinese market expanding through Asia and Europe (Ghafoor, 2014).

Competition is increasing and prices are dropping rapidly due to the improvement of the manufacturing processes making ETCs more competitive and more accessible than flat plate collectors in some cases. The recommendation on which collector to use depends on the author according to literature.

Muhammad et al, member of the American society of heating, refrigerating and air conditioning society recommends the use of ETCs for the case of single effect absorption chillers as shown Appendix H.

Considering the above-mentioned information, the evacuated tube solar collector was selected for the purpose of this research.

Thermal storage tank

The solar collector generates hot water, but in order to control the temperature of the generated water, the flow has to be adjusted continuously. The absorption chiller only accepts a certain range of flow rate, this is why in order to provide a constant flow, a hot water buffer tank must be implemented between the collector and the absorption chiller.

Asides from this, a thermal storage tank can also be considered. One significant disadvantage of the solar absorption chiller is that it can only work as long as there is solar irradiation available, which makes it incapable of providing cooling loads at night, this is why in some cases a thermal storage tank can be added to the system.

There are many types of thermal storage systems, but we will only briefly explain the ones that are relevant for the purpose of this research.

Hot water buffer / storage tank

This is the most common type of storage tank used in solar absorption systems. It serves as a buffer and a storage tank at the same time.

It can be a two tanks (one for high temperature and one for low temperature) or a single thermocline tank.

Water has a high specific heat capacity of approximately 4203 kJ/m^{3}K at 85 °C. This allows water to store high amounts of sensible heat per volume compared to other common materials.

In order to resist the high temperatures, the storage tank is usually made of an inner and outer case of stainless steel, which is also resistant to outer conditions and is strong enough to contain great volumes of water. Between the two cases, a thick layer of thermal insulation material is located to reduce convection losses. Thermal insulation is very important, especially during nighttime where the temperature difference between the tank and the ambient air could be large.

The size of the tank depends on the amount of load to be covered, but due to the low COP of the single effect absorption chiller (0.7), it is usually big.

To get a better idea, a simple calculation gives us a rough estimate that for the absorption chiller of interest to run a straight hour in rated capacity conditions it required 43.2 m^3 of water. This could increase the costs of the installation greatly due to the scale of the tank and the high costs of the required materials, not to mention the space constrains due to the size of the tank.

Phase change material

A phase change material (PCM) is a material that has a convenient phase change temperature in the operation range and can benefit from its large latent heat of fusion. This allows the storage of great amounts of heat in relatively small volumes.

Ice is a common example of a phase change material. Ice has a specific heat capacity of 2.05 kJ/kgK, but whenever it reaches its point of fusion, it requires 333.6 kJ/kg for the phase transition, which is more than 100 times its specific heat capacity (see Figure 24).

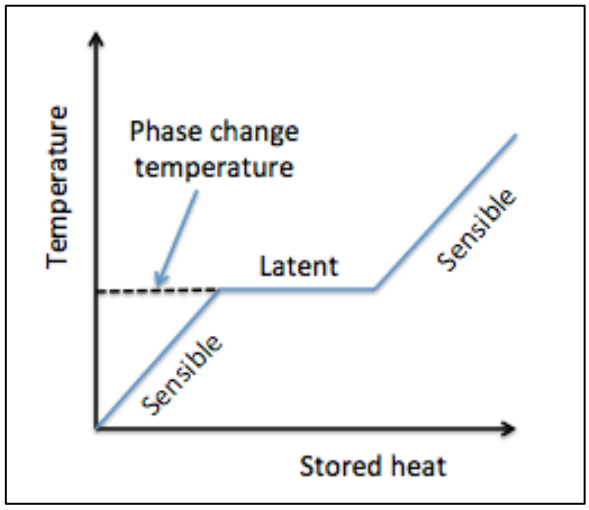

Figure 24. Sensible and latent graph heat of phase change materials

There are several thermal, physical, chemical, kinetic and economical characteristics that must be considered for the application and usefulness of a PCM (see Figure 25).

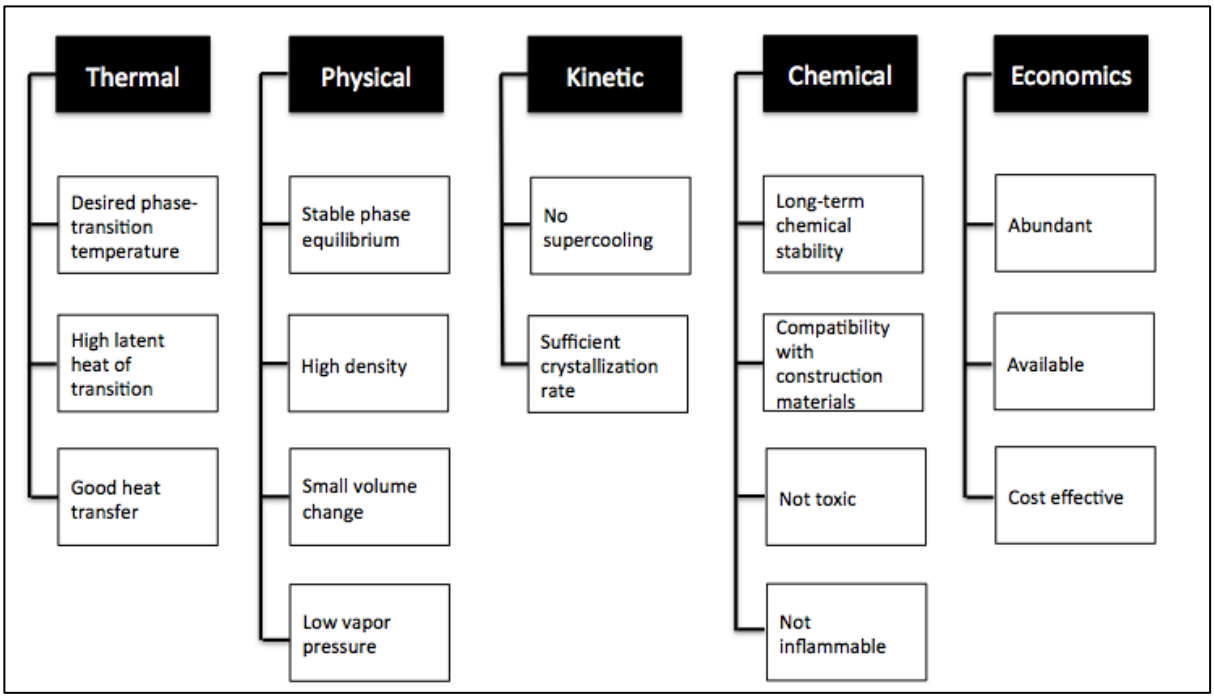

Figure 25. Desirable characteristics of PCM

If one or more desirable characteristics of the PCM are not met, additional control measures need to be implemented, which could affect installation costs severely.

Phase change materials can be classified into organic, inorganic and eutectic. Each of these has its pros and cons, and thorough consideration must be taken on which type to use for a specific application.

Organics can be further classified into paraffins and non-paraffins. Paraffins consist of chains of n-alkanes CH_3-(CH_2)-CH_3 where as non-paraffins are mostly esters, fatty acids, alcohols and glycols (Abhat et al., 1981). One advantage of paraffins is that their melting and fusion points can be manipulated by increasing or decreasing their chain length, making them flexible for many application ranges. Non-paraffins have the widest range among PCMs with each of them having different characteristics, but in often they have low thermal conductivity.

Inorganic PCMs can be classified into salt hydrates and metallics, where salt hydrates are alloys of inorganic salts and water with crystal formations and metallics include the low melting point metals and metal eutectics. Salt hydrates have a high heat of fusion per unit volume, as well as a relatively high thermal conductivity and small volume changes in phase transition. Metallics are still in the experimental stage, but one of their attractive properties is their high thermal conductivity.

The eutectic is a minimum-melting composition of two or more components, each of which melts and freezes congruently forming a mixture of the component crystals during crystallization (George et al. 1989). This gives them the advantage of having sharp melting points.

Much research has been done regarding the use of PCMs as a thermal storage material in domestic solar water heating applications, but not as much for solar cooling systems.

Depending on the location of the PCM, these systems can be classified as integrated PCM storage vessels and integrated PCM solar collector storage.

PCM integrated storage vessels

This type of system has the PCM inside the thermal storage tank and is the most common type of PCM thermal storage.

Agyenim et al. (2007) investigated the possibility of integrating a hot thermal storage tank to a LiBr/H_2O solar absorption chiller system to meet the peak cooling loads of a three bedroom house on Cardiff, Wales. The experimental setup consisted of a shell and tube heat exchanger with erythritol as the PCM on the shell side. His results showed that 100 liters of erythritol would be able to provide approximately 4.4 hours of cooling at peak loads based on a COP of 0.7.

Agyenim et al. (2016) further performed experimental research to investigate the performance of a 4.5 kW absorption chiller with PCM as a thermal storage. This time 20 kg of Erythritol were used in four experimental setups each having a heat transfer enhancement techniques as circular fins, longitudinal fins and multi-tube system. His experiments demonstrated that the multi-tube system performed best, melting the PCM completely in 275 minutes. He also mentions that in order to cover 4 hours of 100% peak cooling load, 242 kg of PCM are required with the multi-tube heat exchanger configuration.

Stalin et al. (2014) investigated theoretically the use of PCMs in an absorption chiller system using solar energy and waste heat. His theoretical design shows that the PCM storage helps to run the system uninterruptedly during the designed 1 hour.

Gil et al. (2013) performed experimental analysis on a PCM thermal storage tank for a solar cooling system for a building in Seville. The actual experimental setup had a dry cooler instead of an absorption chiller and an electrical boiler as the heat supply instead of the solar thermal collector. They tried two different PCM storage tanks with heat exchangers, but one had fins and the other didn't.

Integrated PCM solar collector storage

This configuration has the PCM integrated inside the collector it self, which saves space and potentially costs due to smaller storage tank sizes.

No research has been found of solar absorption chiller systems using integrated PCM solar collector storage, though it's worth mentioning that this type of configuration has had good results in domestic solar hot water systems.

Rabin et al. (1995) developed an integrated PCM solar collector for solar hot water system using salt hydrate and eutectic mixture as the PCM. The PCM is placed inside the box shaped solar collector with a heat exchanger on the top and the PCM at the bottom. Kumar et

al (2001) used a similar box collector design with finned heat exchangers and using paraffin wax instead. As a result, it was observed that the collector could provide the desired temperature range.

Mettawee et al. (2006) integrated the PCM in a well-insulated triangular prism shaped collector (Figure 26). In their design, the absorber plate was in direct contact with the PCM and the water pipe was inserted inside the PCM. Their results showed that during the charging process, because of the melting of the PCM, the heat transfer coefficient increased significantly. They further investigated the effects of the mass flow rate on the energy storage and release and found out that higher mass flow rates yield higher in both.

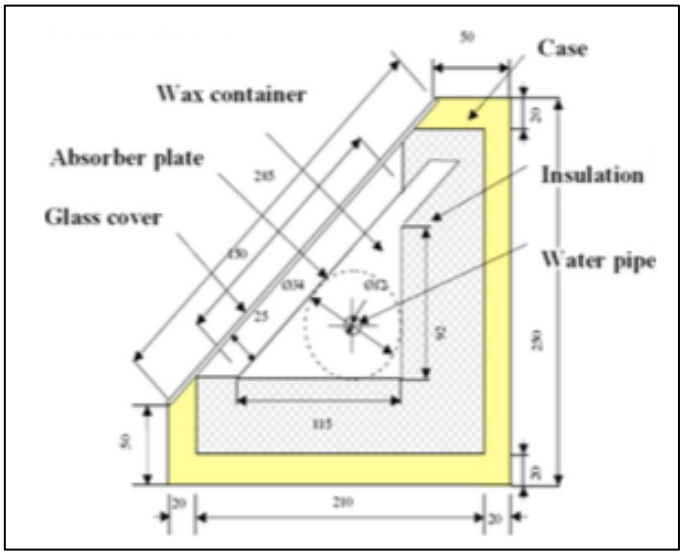

Figure 26. Solar thermal collector with integrated PCM (Mettawee et al.)

Felinski et al. (2016) did an experimental study on the thermal performance of an evacuated tube solar collector containing paraffin as PCM as seen in figure 27. Their work indicated that the integration of the PCM extended the operating time of the ETC system. The temperature of the water was approximately 45 °C, which is relatively low compared to the traditional ETC, but this resulted on less heat losses due to a smaller temperature difference with ambient. Their results also showed that the amount of useful heat obtained with their

design increased by 45%-79% depending on the mass flow rate of the water during discharge cycle.

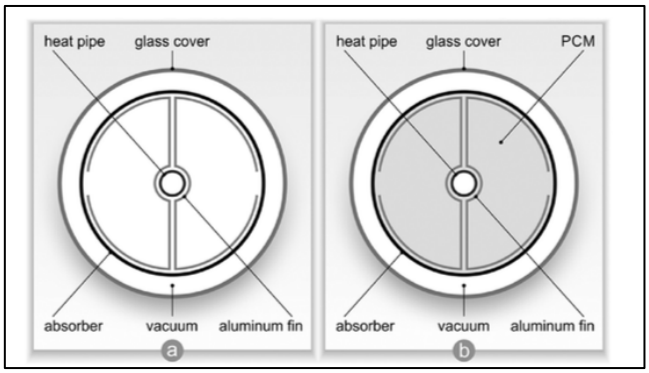

Figure 27. Evacuated tube solar collector with integrated PCM. Felinski et al.

PCM have notable advantages due to their higher energy density by reducing occupied space as well as storage vessel costs, but it is worth mentioning that PCMs greatest disadvantages is their costs due to being relatively new to the market, and their low thermal conductivity, which has to be increased by using heat exchangers or fins. This could adversely increase the costs of the system installation compared to a sensible thermal storage tank.

Pintaldi et al. (2016) performed an energetic evaluation and comparison between a latent storage system and a sensible storage system. He compared commercially available liquid sensible storage materials with PCMs for a triple effect absorption chiller, which was powered by parabolic trough collectors delivering heat at 200 °C. They developed a numerical model in order to simulate the latent heat storage system, which was validated with experimental data and they added it as an external library in TRNSYS. Their results showed that the PCM storage system functioned with high storage efficiency compared to the sensible heat storage system due to less heat losses because of the reduced storage size, but it

showed that the solar collectors have a higher yield when functioning with a sensible heat storage material, and as a result, the sensible heat storage provided higher annual performance.

Noro et al. (2014) analyzed and compared economically a liquid sensible storage and a PCM heat storage in a solar cooling system. A transient simulation was done using TRNSYS of a cold storage and a hot storage. They analyzed the case in which both tanks have sensible storage (water), only cold storage with PCM and only hot storage with PCM. The results showed that the PCM solar storage only performs better during periods when the mean temperature of the storage is near the fusion point of the PCM. Their analysis also showed that the greater investment cost of PCM technology is only justified whenever high natural gas tariffs are present, or when a lower cost PCM are available.

From the above-mentioned factors, it can be discussed that the greatest disadvantages of sensible thermal storage tanks are their size and their lower thermal efficiency due to heat losses. It can also be discussed that latent thermal storages have overall lower performances due to their poor thermal conductivity even with heat transfer enhancers such as fins.

Regarding costs, latent thermal storage can have a smaller vessel size, but has to include heat exchanger accessories and PCM costs, and it could also possible increase maintenance costs due to some PCM properties such as continuous thermal expansion and contraction, corrosion, crystallization, etc.

Because none of the above-mentioned options was convincing enough, we decided to evaluate the possibility of using an underground storage tank for the purpose of this research.

Underground thermal storage tank

Whenever space constrains are present and storage thermal efficiency is key, an underground thermal storage tank can be considered.

A list of thermal conductivities and thermal diffusivities of common soil materials can be found in Table 3.

Soil thermal properties		
Thermal texture class	Thermal Conductivity W/m°K	Thermal Diffusivity cm^2/sec
Sand (or gravel)	0.77	0.0045
Silt	1.67	---
Clay	1.11	0.0054
Loam	0.91	0.0049
Saturated sand	2.5	0.0093
Saturated silt or clay	1.67	0.006

Table 3. Thermal conductivities of common soil materials

A list of thermal conductivities of common rock types can also be found in Appendix I. Soil and rocks present a wide variety of thermal conductivities, but it is well known that most of them are relatively low. This is the main reason why underground thermal storage tanks have lower heat losses. The other significant reason is that because it is underground, there is virtually no convection losses from the wind and no direct radiation heat transfer from the sun either. Another important characteristic worth mentioning is that as time passes, the ground would start to gain heat, increasing its temperature due to heat stagnation. This would in turn reduce the temperature difference between the ground and the storage tank reducing even more the conduction losses.

Serag et al. (2013) performed a mathematical analysis of a double effect absorption chiller using an underground thermal storage tank to store hot water at a temperature around 180 °C. In his work he developed a mathematical model in order to simulate the steady state radiation, convection and conduction occurring inside the storage tank. In his work, he demonstrated that high thermal efficiencies can be reached such as 96.7% for the most efficient design when ambient temperature is 45 °C and of 91.8% for the least efficient design when ambient air is at 20 °C. In his work he also mentions that soil thermal conductivity has little effect on the storage efficiency (see Figure 28).

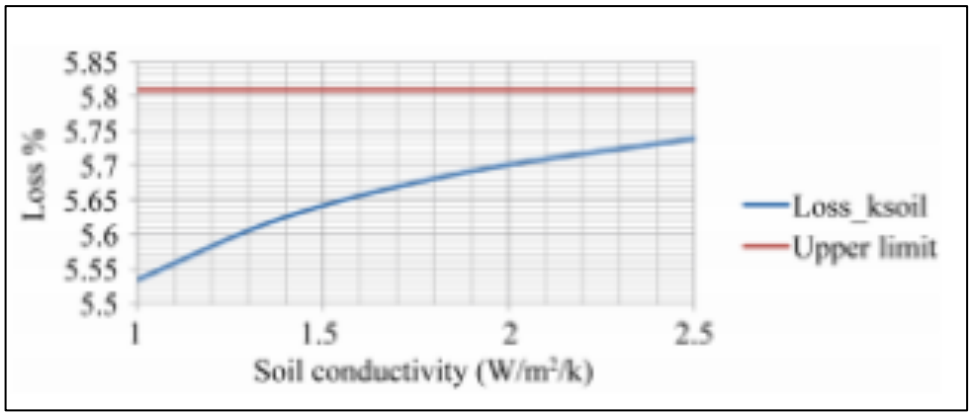

Figure 28. Effect of soil conductivity on heat loss of underground thermal tank. Serag 2013

Underground hot water storage tanks have a lower heat loss compared to a hot storage tank on the surface, though still significant loss is observed due to the large temperature difference, unless expensive insulation material is added.

An underground cold-water storage tank on the other hand has several advantages over the underground hot storage tank.

The main advantage is that it has much lower temperature difference with the soil. As mentioned in chapter 1, underground temperature is approximately the year average temperature, which in the case of Veracruz is 25 °C. The chilled water from the chiller inlet

and outlet has a rated temperature of 12.5 °C and 7 °C respectively, whereas the heat medium has a inlet temperature of 83 °C and an outlet temperature of 88 °C. Storing the heat medium would yield a temperature difference more than three times greater than storing the chilled water, which would result in much higher heat losses.

Another significant advantage of storing the chilled water is that it opens flexibility on the construction material of the tank, possibly making it more accessible.

A disadvantage is that storing the chilled water means an overall lower exergy of the system when considering domestic hot water generation, but if the main priority of the underground storage tank is to provide cooling loads, this would not be detrimental.

Taking into account the above mentioned arguments, we decided to use a hot water buffer tank between the ETCs and the chiller, and an underground cold storage tank as a thermal storage for the purpose of this research.

Cooling tower

The absorption chiller receives heat from the solar thermal collectors and also from the fan coils through the condenser. This residual heat has to be disposed for a correct functioning of the system.

A cooling tower is the traditional heat sink used in the air conditioning industry. They can be classified into open circuit or closed circuit depending if the working fluid has contact to the exterior air.

In an open circuit, the water has direct contact with the air. Water is pumped to the top of the cooling tower where it is discharged into a pack of fills, which increase the contact area of water to air. The water goes down due to gravity while passing through the fills while

cooling down in the process. The cooling occurs through sensible heat transfer but also through evaporation, therefore, this type of cooling towers capacity is limited to the wet bulb temperature. There are water particle losses due to the constant evaporation, as well as purging due to contaminants and particles; therefore a recharge pump is constantly charging the system with water.

In a closed loop circuit or dry cooler, there is no direct contact between the water and the air, thus transfer heat occurs through a bundle of pipes that act as a heat exchanger. In this type of cooling tower, the cooling capacity is limited by the dry bulb temperature. Some cooling towers are mixed, in which they combine the cooling system of the open loop, but transfer heat through a heat exchanger in order to avoid exposure of the working fluid.

The performance of an open cooling tower depends highly on the wet bulb temperature, which is dependent on the relative humidity of the region. As mentioned earlier, Veracruz has a high annual average humidity of 83.6%, greatly limiting the performance of the cooling tower, not to mention water consumption, the need to charge and clean water, fog formation, and the risk of legionella bacteria growth (Helm et al. 2007). A dry cooler doesn't has these drawbacks, but its performance would be limited even more due to the high dry bulb temperatures throughout the year

Due the above-mentioned factors, we decided to consider the use of the sea as a heat sink.

Seawater as a heat sink

The thermal properties of the sea have been used for rejecting or extracting heat for heating and cooling systems purposes for a long time.

There are mainly three ways to use the seawater as a heat sink/heat reservoir and they are direct seawater utilization system, indirect seawater utilization system and seawater cooling tower.

Although direct seawater utilization system is very similar to SWAC in some aspects as intake and outfall system, central plants and distribution piping, they have some slight differences. In the case of direct seawater utilization system, a heat pump is used either for cooling or heating depending on the thermal loads. The seawater is pumped to the central plant structure. Then, it is filtered and pumped through the condenser of the heat pump, where heat transfer occurs with the heat pump's refrigerant. The extracted seawater is then discharged to the sea.

When designing the intake of this type of systems, the depth of the sea becomes an important factor. The intake should be positioned at least 2.5 m from the bottom of the sea in order to avoid extracting debris from the sea. Air cannot be extracted to the piping system; therefore the heat must be submerged at all times. It is also necessary to consider some depth in order to avoid boats colliding with the pipe head. The temperature of the water discharged to the sea must also be regulated in order to avoid thermal stresses due to high temperature differentials between seawater inlet and outlet. In China, the Quality Standard for State Oceanic Water restricts the discharge in seawater cooling systems to a temperature difference of 4 °C (Zhen et al. 2007).

Chien et al. (1986) estimated that in 1985, the total installed cooling capacity of systems utilizing seawater condenser cooling systems in Hong Kong exceeded 1 GW (285,000 tons). In his work, he mentions that there is a 10-15% reduction in energy consumption compared to indirect cooling systems.

Mitchell et al. performed a review on the existing surface water heat pump systems. In his work, he also gathered several technical recommendation and know-how through empirical data.

Zhen et al. (2013) did an economic analysis on the feasibility of a district cooling and heating system with seawater as a heat source and sink in Dalian, China. The author compared the costs of a traditional heat pump the seawater source heat pump system and his results indicated that the seawater source heat pump is profitable in the majority of scenarios.

Indirect seawater utilization systems use a heat exchanger between the condenser and the seawater; therefore there is no direct contact between condenser and seawater.

The advantages of an indirect seawater utilization system over a direct one is that using freshwater in the heat pump or chiller can reduce maintenance costs compared to salt water, not to mention the extraction of debris and marine growth in the condenser of the main equipment. Also, in the case of a direct sea water utilization system a backup chiller is required to cover up during maintenance.

Akashi et al. (2003) performed an energy and cost analysis of a cooling plant system with indirect seawater utilization system for air conditioning in a commercial building in Nagasaki. In his work, direct measurement of the energy and the costs were done to obtain data, and a model-based simulation analysis was performed. He then compared the results of the indirect seawater utilization system (case 1) with a system with the same chiller using a cooling tower system (case 2), an air source heat pump (case 3) and a direct seawater utilization system (case 4).

His results indicated that the air source heat pump would perform lowest on COP and running costs due to the high ambient air temperature of the region. Then he compared the

COP of the chillers of case 1 and case 2, and even though wet bulb temperature was lower than seawater temperature throughout the year, it is not possible for case 2 to use that temperature for the condenser, which would yield a higher COP for case 1 throughout the year, especially during summer time, but when comparing the COP of the entire system, the COP of case 1 was slightly lower due to the higher electricity consumption due to the additional pump of seawater. Although when including the loads necessary for charging the cooling tower water, the electric consumption of case 2 would increase 1.79 times of case 1.

When comparing the COP of the chillers of case 1 and case 4, even though the cooling water of direct seawater should be higher, the use of titanium heat exchangers, which are used in order to avoid corrosion, would lower the thermal performance, yielding a lower COP for case 4 than case 1 throughout the year, but regarding the COP of the entire system, case 4 would have slightly higher COPs than case 1 due to the additional pumps for freshwater. He further mentions that the high initial costs due to the titanium heat exchangers and the additional backup chiller required for case 4, the slight difference in COP would not make up for the high investment cost, making case 1 the most feasible option.

Taking into account the above-mentioned information, we decided to use an indirect seawater utilization system for the purpose of this research.

The design of the seawater heat exchanger will be similar to those used in heat pump's pond loops. This type of heat exchanger consists of an array of multiple high-density polyethylene (HDPE) helical coil heat exchangers arranged in parallel or in series.

The helical coil loop is attached to a structure and fixed with weights at the bottom of the water body. We considered this design because the scale of our equipment is small compared to the scale of the chillers researched by many of the above-mentioned authors, therefore, there is no need for a central plant or a seawater pump, reducing overall costs.

A helical coil design was selected because this design tends to have higher heat transfer rates than a linear pipe. This is mainly because of the centrifugal force applied at the flow near the axis of the helical coil to be greater to the centrifugal force applied to the flow away from the axis, which makes the flow near the axis to go towards the outer walls. This causes a bifurcation of the flow at the helical coil walls leading to higher heat transfer rates (Jayakumar et al. 2012).

Because this is a conjugate heat transfer problem, forced convection due to the natural current of the sea will be key to determining the overall heat transfer coefficient of the design.

Summary

In summary, using the information from this chapter, our design looks like the Figure 29.

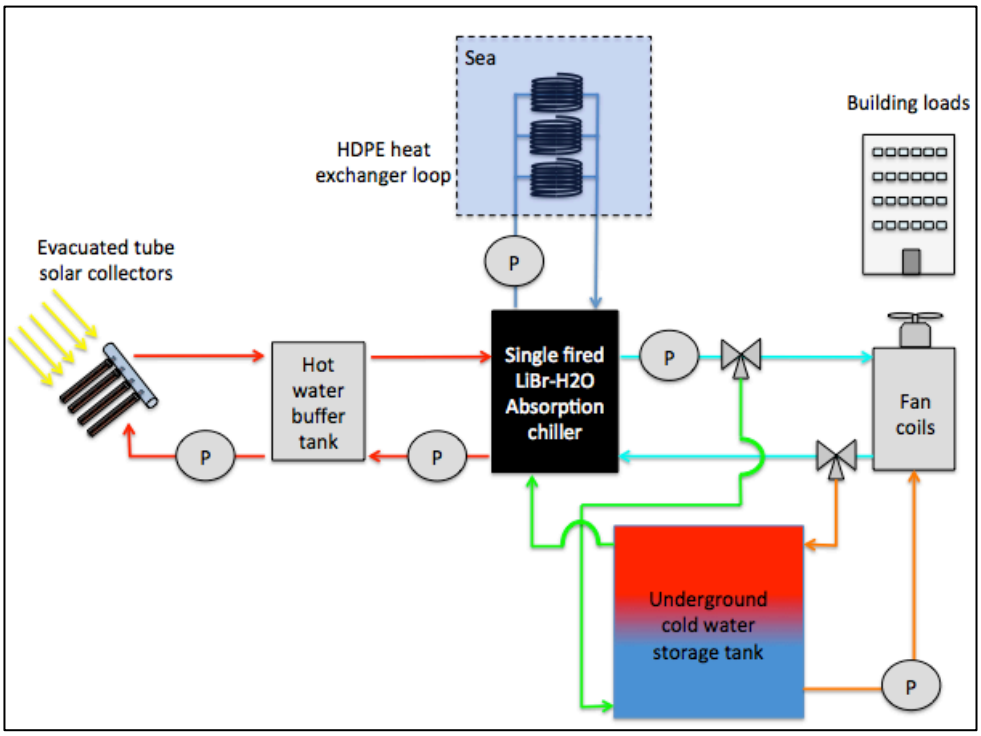

Figure 29. Proposed design of the solar absorption chiller to be studied

The system level simulation

Now that the components for our solar absorption chiller have been determined, we proceeded to propose a method to simulate the entire system throughout a year.

A system simulation requires the performance and inputs and outputs of each of the components and the results of their interaction, also because a transient simulation is required, it is necessary to define a step size and calculate the results per step.

Due to the complexity of some of the components required for system level simulation, we decided to use a numerical approach by using the computer fluid dynamics (CFD) software ANSYS Fluent.

It is well known that doing one year simulations using a CFD approach is inconvenient because it requires extremely high computational demands, as well as long time for convergence, especially in the case of a system level simulation, therefore, a different approach was proposed for the system level simulation.

It was agreed to do CFD simulations of the components in order to extract some key parameters, and then use an analytical approach to do the one-year system level simulation in order to avoid the above-mentioned issues.

Microsoft Excel was proposed to gather the data and calculate the one-year system level simulation. This is due to Excel having a flexible user interface, which could let us perform several comparisons in different scenarios, as well as being fast in the calculations, not to mention its ability to plot the results in many convenient ways.

Chiller sizing and Building loads

Weather data of Veracruz, Mexico was obtained through the National renewable energy laboratory (NREL) National solar radiation data base (NSRDB) viewer, which is an interactive geographic information system (GIS) application from which weather data such as dry bulb temperature, humidity, solar irradiation, wind velocity, etc. can be downloaded. This data can be configured into either 1 hour or 30 minutes time steps for one year.

The building load conditions were set according to the American Society of Heating and Refrigerating and Air-conditioning Engineers (ASHRAE) and Air Conditioning Contractors of America (ACCA) standards.

An analysis of the data was done in order to find out how many cooling load and heating load hours were required. For this, it is necessary to set some conditions.

It is well known by the HVAC industry that when the ambient temperature is in the range of 19.4 and 15.5 °C no heating or cooling load is required due to these ambient temperature yielding a comfort temperature inside the building. Having this in mind, the analysis showed that out of the 8756 hours of one whole year, 8588 required a cooling load, and 0 hours required a heating load. The remaining 172 hours were in the comfort temperature range, therefore this region is complete one sided to cooling loads.

From the above analysis it was decided to oversize the chiller by setting a high design cooling temperature, which is the temperature when the building peak cooling load occurs. The highest temperature in the obtained data is 43.2 °C, therefore we set our design cooling temperature slightly above that value at 44 °C. The building peak cooling load was set as the same as the chiller rated capacity, which is 50 tons (176 kW). The building balance point temperature, which is the temperature the thermostat is set, was set to 19.4 °C.

The way the building loads are calculated is through an interpolation of the design cooling temperature and the peak cooling load with the actual ambient temperature and the balance point temperature such that:

$$Q_{BC} = (\frac{Q_{PC}}{t_{dc} - t_{bc}})(t_a - t_{bc})1$$

Where:

Q_{BC} Building cooling load at specified air temperature.

Q_{PC} Building peak cooling load

t_{dc} Design cooling temperature

t_{bc} Building balance point temperature

t_a Ambient temperature

With this we can obtain the necessary cooling load the chiller has to provide in order to cover that particular time step's building load.

Cooling capacity factor

It is important to notice that the rated chiller's cooling capacity can increase or decrease depending on the cooling capacity factor (CCF) as well as with a flow correction factor (FCF).

Figure 30 shows the correction factors of the 50 ton Yazaki absorption chiller that we are going to use for this research.

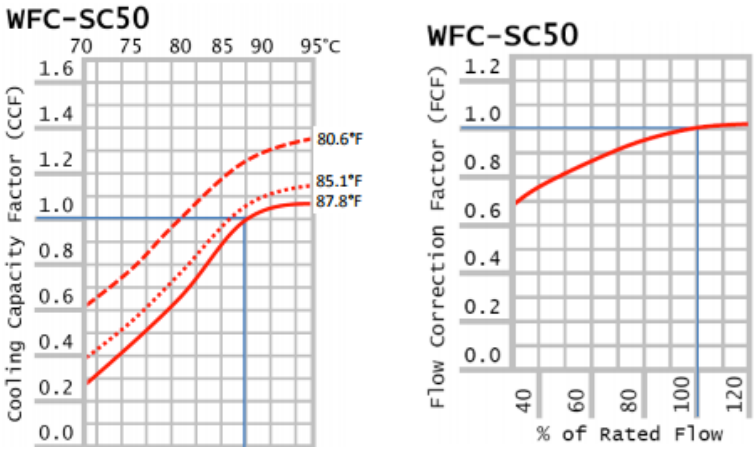

Figure 30. Characteristic curves of the correction factors of the 50 ton Yazaki absorption chiller

The x axis at the CCF curve is the heat medium temperature. The different curves represent the cooling water inlet temperatures to the condenser.

In our control design of the system, we decided to use a rated flow rate from the hot buffer tank to the absorption chiller; therefore, the FCF won't affect our particular case.

The CCF is affected by two components. One is the temperature of the heat medium and the other one is the temperature of the cooling water to the condenser.

In order to make use of these corrections, a polynomial interpolation was performed to create a function of the curve in terms of the heat medium temperature. The best fit was obtained with the following 5th degree polynomial:

$$CCF = 4.386E10^{-8}T_h^5 - 3.9934E10^{-5}T_h^4 + 0.0145T_h^3 - 2.6245T_h^2 + 236.9037T_h - 8532.1543$$

Where:

T_h Temperature of heat medium

This yielded an R^2 of 0.9987, which is an acceptable fit. Then, in order to take into account for the cooling water temperature effect, we can observe that the curves move upward in the y axis linearly with lower cooling water temperatures, therefore, we did a linear interpolation of the above CCF function to displace the curve in the y axis.

$$CCF^* = -0.0417 * (87.8 - T_c) + CCF$$

Where:

T_c Temperature of cooling water

With these equations, it is possible to know the CCF at any specific heat medium temperature and a cooling water temperature combination with acceptable accuracy.

Chapter 3. The Evacuated tube solar collector and hot thermal storage tank

In this chapter we will proceed to explain the calculations performed in order to obtain the performance of the evacuated tube solar collector and hot thermal storage tank system.

In the solar collector market, it is of great importance to standardize the way the solar collectors are measured in order to obtain an unbiased result of the collector efficiency of different providers. In order to do this, a separate organization usually tests and evaluates the performance of the collectors using the same standards and conditions. In Europe, the Quality Assurance in Solar Heating and Cooling Technology (QAiST) project was ran in order to develop the European Standards for the solar thermal market for quality assurance of the products and to enhance competitiveness of European manufacturers. In this project, the EN12795 was developed, which is the standard for solar thermal collectors. In this standard, several test conditions and requirements are thoroughly mentioned in order to obtain a comparable result among the several manufacturers.

One of the objectives of these tests is to obtain the useful energy from a square meter of a collector under similar climate and load conditions, which could be used to compare the collector's performance. An alternative way of comparing the collector's efficiency is by using the power curve, which is a curve that indicates the collector power output vs the temperature difference between the fluid entering the collector and the ambient air.

The EN12975 has two methods to calculate the thermal performance of the collector, the steady-state (SS) method and the quasi-dynamic method (QDT).

The steady-state method is derived from the ASHRAE 93-77 and ISO 9806 standards. In this method the performance is determined under clear sky conditions and high irradiance

levels. When using the steady-state method in the case of evaluating an ETC with circular absorber, which has the ability to absorb irradiance from transverse angles, can create an important bias in the results because it does not include a complete incidence angle modifier properties as well as lacking a heat capacitance term (Pettersson 2011). The QDT method makes up for these adjustments, as well as including a more complete characterization of the solar thermal collector with the addition of extra parameters compared to the SS method, therefore, for the purpose of this work, the QDT method will be used in order to evaluate the annual performance of the evacuated tube solar collector.

The following equation represents the useful energy extracted from a collector according to the QDT method (Fischer et al.)

$$\frac{\dot{Q}}{A} = F'(\tau\alpha)_{en}K_{\theta b}(\theta)Gb + F'(\tau\alpha)_{en}K_{\theta d}Gd - c_6 uG^* - c_1(t_m - t_a) - c_2(t_m - t_a)^2 - c_3 u(t_m - t_a) + c_4\left(E_L - \sigma {T_a}^4\right) - c_5 dt_m/dt$$

Where:

$\frac{\dot{Q}}{A}$	Useful energy extracted from collector per m^2 (kWh)
$F'(\tau\alpha)_{en}$	Effective transmittance-absorptivity product at (tm – ta) = 0 for direct solar radiation Gb at normal incidence
τ	Collector transmissivity
α	Collector absorptivity
$K_{\theta b}(\theta)$	Incidence angle modifier for direct irradiance
Gb	Beam irradiance in tilted collector plane (W/m2)
$K_{\theta d}$	Incidence angle modifier for diffuse irradiance
Gd	Diffuse irradiance in tilted collector plane (W/m2)
u	Wind speed in the collector plane (m/s)
G^*	Total (beam + diffuse) solar radiation in the collector plane (W/m2)
tm	(tin + tout)/2, it is the mean fluid temperature between inlet and outlet of the collector (C)
ta	Ambient temperature close to the collector (in the shade) (C)

E_L	Long wave radiation in the collector plane (W/m2)
σ	Stephan Boltzmann constant
Ta	Ambient temperature close to the collector (in the shade) (K)
c1	Heat loss coefficient at (tm – ta) = 0 (W/m2K)
c2	Temperature dependence in the heat loss coefficient (W/m2K2)
c3	Wind speed dependence of the heat losses (J/m3K)
c4	Long wave irradiance dependence of the heat losses
c5	Effective thermal capacitance (J/m2K)
c6	Wind dependence on the collector zero loss efficiency (s/m)

In order to obtain the necessary values and characteristics of an evacuated tube solar collector, simulations in ANSYS Fluent are performed. The main purpose of doing this is to find a value for $F'(\tau\alpha)_{en}$ for the simulated design.

Simulation in ANSYS Fluent

Simulation in ANSYS Fluent is performed in order to calculate the collector efficiency factor times the effective transmittance-absorptivity product, $F'(\tau\alpha)_{en}$, in order to be able to use the QDT method.

The following considerations were taken for the simulation:

1) Heat pipe effective thermal conductivity changes with inclination angle due to the effects on gravity on the heat pipe's working fluid.
2) There are no convection losses (Tm – Ta) = 0
3) The heat transfer fluid flow (water) is 0.02 kg/s*m2, where m2 is the area of absorber. This value is a standard value taken from the ISO9806-1 and ANSI/ASHRAE standard 93 for doing thermal performance tests.
4) A total solar irradiation at the collector greater than 700 W/m2 with a diffuse fraction less than 30% (EN 12975).

Estimation of inclination angle and heat pipe's effective thermal conductivity.

In order to calculate F'(ta)en, the inclination angle of the collector from the horizontal is required (see Table 4).

Optimal tilt angle for the collector from the vertical in Veracruz, Mexico

Jan	Feb	Mar	Apr	May	Jun
55°	63°	71°	79°	87°	94°
Jul	Aug	Sep	Oct	Nov	Dec
87°	79°	71°	63°	55°	48°

Source: http://solarelectricityhandbook.com/solar-angle-calculator.html

The highest cooling load according to the regions temperature data occurs in April 27th. The highest average temperatures can be observed in April, May, June, July, August and September, all being between 28 – 29 °C. Considering the hottest months and the peak day, it would be prudent to select an angle of 80°, but it is important to consider the effect that this would have in the heat pipe performance.

The effective thermal conductivity of the heat pipe changes depending on the inclination angle. This is due to the liquid having a harder time to go at the bottom of the heat pipe at steeper angles. Also, as the angle becomes steeper, the mean temperature of the heat pipe increases very rapidly, reaching faster to its heat transfer performance limit.

Danh et al. (2011) obtained experimental results for the effective thermal conductivity of oscillating heat pipes at different angles. As observed on Figure 31, the heat pipes have a continuous high effective thermal conductivity until reaching an angle of 60°, where their effective thermal conductivity starts to decline rapidly, therefore, an angle which does not surpass 60° degrees is highly desired.

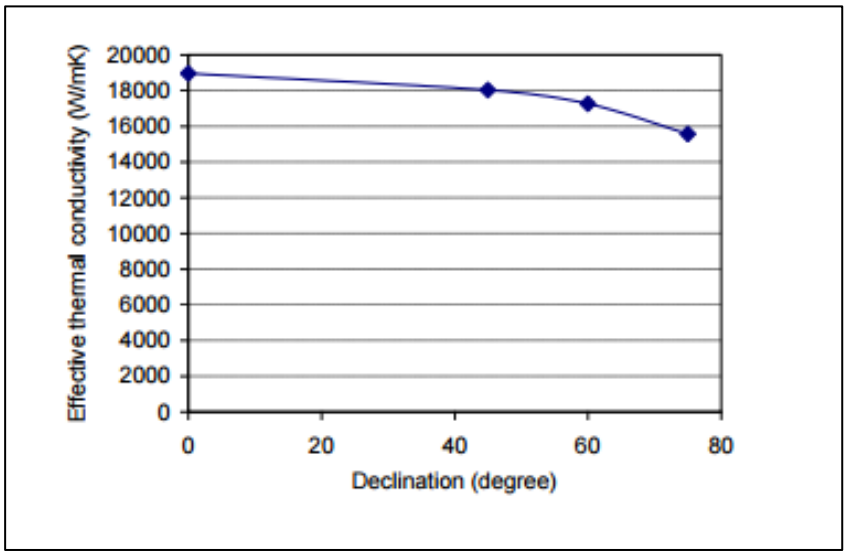

Figure 31. Effective thermal conductivity of heat pipe as a function of angle, Dahn (2011)

Fischer et al. (2012) did a research on the effect of the angle on the performance of a heat pipe used in an evacuated tube solar collector. In his work, he tested 10 heat pipes of the same type at different angles and measured their power output. Figure 32 shows an average of the results of these tests.

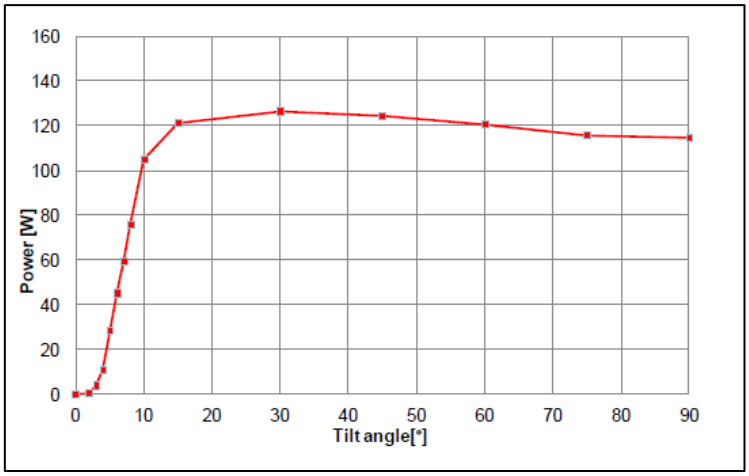

Figure 32. Effective thermal conductivity as a function of angle. Fischer et al. (2012)

As observed, his results indicate that an inclination of 30° from the horizontal yield the highest power output, which is similar to Danh's results.

Using these data, it is concluded that an inclination angle of 30° from the horizontal would yield acceptable results for the purpose of this research.

Simulation of the ETC in ANSYS Fluent

ANSYS Fluent is a powerful CFD software which uses the finite element method in order to numerically solve fluid dynamics problems. It uses the conservation of mass equation as well as a turbulence model for the conservation of momentum equation in conjunction with an energy equation in order to solve fluid dynamics and thermodynamics problems. In order to setup a simulation, the following steps must be followed.

Geometry

The geometry of the evacuated tube was created using the CAD software Solidworks. The assembly of the ETC consists of a vacuum tube, a copper fin, a heat pipe and the water pipe. The detailed dimensions of the components can be found in Appendix K.

Mesh

For the mesh, due to the cylindrical shape of the heat pipe, copper fin and the vacuum tube, and also due to the direction of the heat flow going towards the axis, a well-aligned mesh in the axis is desired. The water, due to being a fluid, was set to tetrahedral so it would fit well with the heat pipe's condenser.

The relevance center was set to fine, the smoothing to high and the span angle center to fine as well. Pictures of the actual mesh can be found in Appendix L.

Named selections for inlet and outlet of the water in the pipe and at the outer wall of the vacuum tube for solar flux were defined.

The mesh has a total of 204,485 nodes and 159,643 elements.

Setup

The solver was set to pressure-based and as a steady state simulation. Gravity was turned on positive in the Z axis at 9.81 m2/s.

For the model of the ETC, several considerations and simplifications were taken into account. In order to avoid major computing loads for doing a two phase flow simulation using the volume of fluid (VOF) method for the heat pipe, it was agreed to use an effective thermal conductivity at the designed angle.

The energy equation was set to on and a standard k epsilon model with standard wall function was selected as the turbulence model. Also, a solar loading model was set to on with a direct solar irradiation of 1000 w/m2 and 0 diffuse solar irradiation.

The standard k epsilon model is a Reynolds Averaged Navier-Stokes based equation. It makes use of 2 transport equations, one for k, which is the turbulent kinetic energy, and ϵ, which is the dissipation of the kinetic energy.

The equations used by ANSYS Fluent are the following:

- For k:

$$\frac{\partial}{\partial t}\rho k + \frac{\partial}{\partial x_i}(\rho k u_i) = \frac{\partial}{\partial x_j}\left[\left(\mu + \frac{\mu_t}{\sigma_k}\right)\frac{\partial k}{\partial x_j}\right] + P_k + P_b - \rho\epsilon - Y_M + S_k$$

- For ϵ:

$$\frac{\partial}{\partial t}\rho\epsilon + \frac{\partial}{\partial x_i}(\rho\epsilon u_i) = \frac{\partial}{\partial x_j}\left[\left(\mu + \frac{\mu_t}{\sigma_\epsilon}\right)\frac{\partial \epsilon}{\partial x_j}\right] + C_{1\epsilon}\frac{\epsilon}{k}(P_k + C_{3\epsilon}P_b) - C_{2\epsilon}\rho\frac{\epsilon^2}{k} + S_\epsilon$$

Where:

k	Turbulence kinetic energy
u_i	Velocity component in tenor notation
μ_t	Turbulent viscosity
σ_k	Prandtl number for k
σ_ϵ	Prandtl number for ϵ
G_k	Production of turbulence kinetic energy due to mean velocity gradients
G_b	Production of turbulent kinetic energy due to buoyancy
Y_M	Contribution of fluctuating dilatation in compressible flow
S_k, S_ϵ	User defined source terms
C1ϵ, C2ϵ, C3ϵ	Constants.

The standard k epsilon model was selected as the turbulence model because it is a robust model that leads to stable calculations that doesn't have many issues converging. It also provides reasonable predictions for many types of flows.

In our case we are simply simulating the water pass by the condenser of the heat pipe in a reasonable velocity, as well as a buoyancy effect due to the heat transfer from the condenser to the fluid, therefore this simple model will be good enough for our purposes.

The energy equation used by ANSYS Fluent is the following:

$$\frac{\partial}{\partial t}\rho\epsilon + \nabla\cdot\left(\vec{v}(\rho E + p)\right) = \nabla\cdot\left(k_{eff}\nabla T - \sum_j h_j\vec{J}_j + \left(\overline{\overline{\tau_{eff}}}\cdot\vec{v}\right)\right) + S_h$$

$$E = h - \frac{p}{\rho} + \frac{v^2}{2}$$

Where:

k_{eff}	Is the effective thermal conductivity $k+k_t$, where k_t is the turbulence thermal conductivity of the model being used
$\vec{J}_j$	Is the diffusion flux of species j
$\overline{\overline{\tau_{eff}}}$	Is the effective shear force
h	Enthalpy of the flow according if its compressible or incompressible

The first three terms on the right represent the thermal conductivity, the species diffusion and the viscous dissipation.

Fluent's solar ray tracing uses an algorithm that models a beam from a "sun position" defined by the user and traces it as a vector. This vector can be applied to any wall, inlet or outlet boundary condition specified by the user as long as it is adjacent to a fluid zone. It can also perform a shade analysis depending if there is any shadow generating object in the vector path. The vector magnitude is defined by the user as a direct beam irradiation in W/m2.

This model also allows the use of a diffuse irradiation, which depends on a parameter named scattering fraction. What this option does is that whenever a beam strikes a fluid, it will distribute the heat flux to all adjacent walls according to the scattering fraction. In our case, using this option would cause some calculation issues; therefore we will set the scattering fraction to 0. It also offers an option for ground reflectivity, which is automatically set to 0.2, but we will turn it to 0 for this specific simulation.

When the solar vector is allowed in a wall, this wall can be defined to either semi-transparent or opaque. When the wall is semi-transparent, direct and infrared component of the absorptivity and transmissivity of the wall can be defined. The remaining vector will follow the original path and go through or strike another wall. When the wall is set to opaque, it won't let any ray go through and it will either absorb or reflect depending on its absorptivity.

Fluent offers a solar calculator option, which can calculate the ray vector position from a specific global position according to a user input latitude, longitude, time zone and time. Because our simulation is a steady state fix perpendicular ray, we won't use this option.

The material properties were set as follow in Table 5:

Type	Material	Section	Property	Value	Unit
Fluid	Water	Water in pipe	Density (Boussinesq)	1000	kg/m3
			Specific heat capacity	4182	J/Kg-K
			Thermal Conductivity	0.6	W/m-K
			Thermal expansion coefficient	8.80E-05	1/k
	Air	Vacuum tube	Density (Boussinesq)	1.25	kg/m3
			Specific heat capacity	1006.43	J/Kg-K
			Thermal Conductivity	0.02	W/m-K
Solid	Heatpipe	Heat pipe	Density	8978	kg/m3
			Specific heat capacity	381	J/Kg-K
			Thermal Conductivity	16000	W/m-K
	Copper	Pipe walls	Density	8978	kg/m3
			Specific heat capacity	381	J/Kg-K
			Thermal Conductivity	387.6	W/m-K

Table 5. Material properties used in simulation of ETC.

The vacuum tube material was set to air in order to use the solar loading model, which is only compatible with a fluid's surface.

A material called "heatpipe" was created with a thermal conductivity of 16,000 W/mK, which is an approximate effective thermal conductivity of a heat pipe at the selected inclination angle according to Dahn et al. (2011).

The densities of the fluids were set to Boussinesq in order to account for the buoyancy effects.

The boundary conditions were set as follows in Table 6:

Section	Type	Condition	Value	Unit	Participate in solar load model
Pipe inlet	Velocity inlet	Velocity	4.8	kg/s	No
		Temperature	358	K	
Pipe Outlet	Pressure outlet	Pressure	0	Pa	No
Solar_flux	Semi-transparent Wall	Transmissivity	0.9		Yes
Vacuum-to-fin-wall	Opaque Wall	Absorptivity	0.94		Yes

Table 6. Boundary conditions of simulation of ETC.

The flow recommended in order to obtain the performance is 0.02 kg/s*m2, where m2 is the area of absorber, but for the purpose of this research, a flow of 4.8 kg/s will be used, which is 40% of the rated flow of the heat medium of the absorption chiller.

We are interested in its performance when the mean inlet temperature is 85 °C, so this temperature will be used.

The vacuum tube will act as a semi-transparent body with a transmissivity of 0.9, and the copper fin will act as the absorber with an absorptivity of 0.9, which are common values for this type of collector.

A coupled wall mesh interface was set between the walls of the components.

A standard initialization was performed and the simulation was ran with 350 iterations.

Results

The calculation converged at iteration 336. The results can be seen in Figure 33.

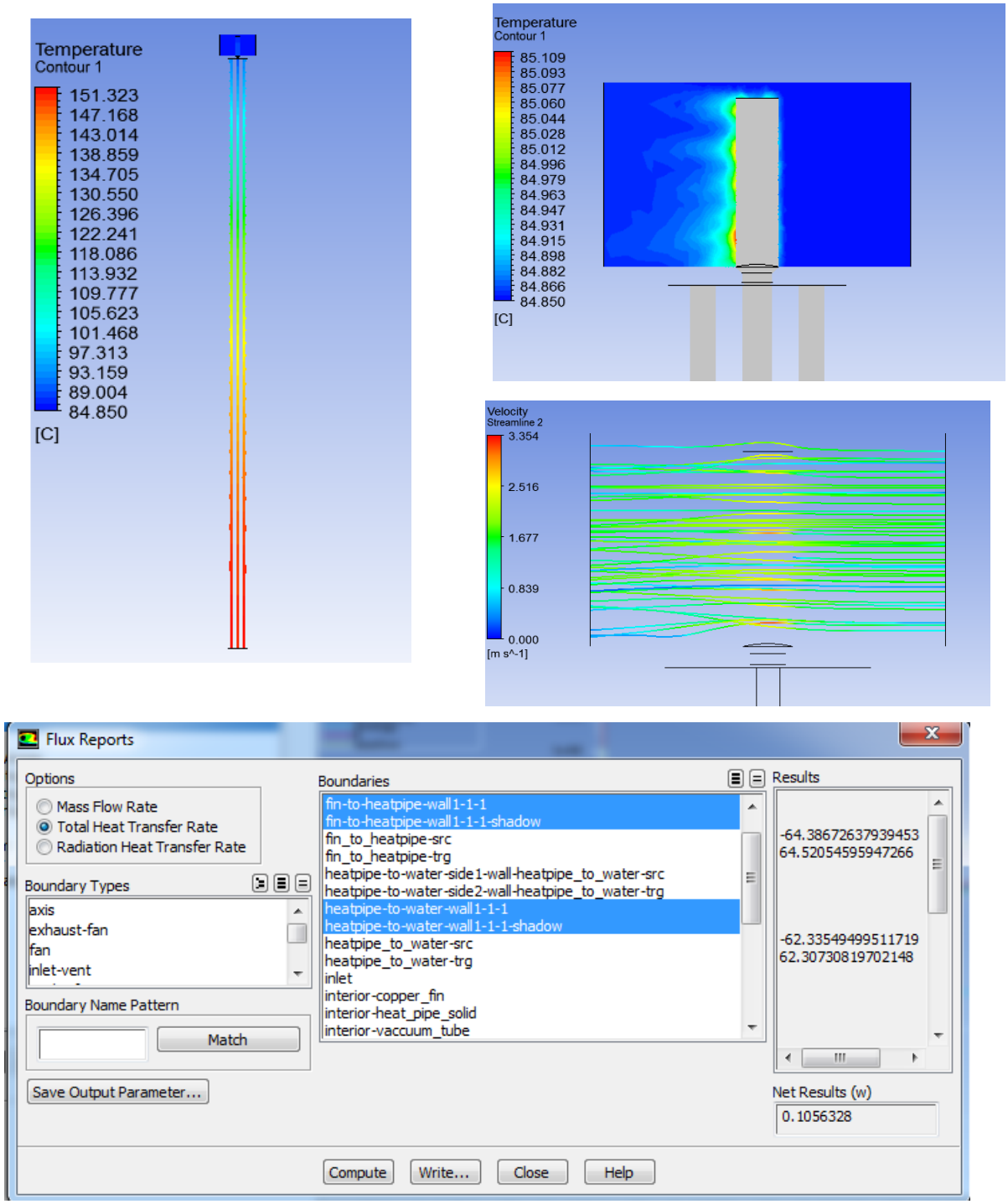

Figure 33. Results of simulation of ETC: Temperature contour throughout the vertical. Temperature contour of the water flowing. Streamlines of the water flow. Flux report of the total heat transfer at the ETC.

The flux report of the simulation indicates a total heat transfer rate of 62.3 W from the heat pipe to the water, and a heat transfer rate of approximately 64.5 W from the absorber (copper fin) to the heat pipe (see Figure 34). This yields a heat transfer efficiency of 0.96 (Usual values are around 0.96-0.99).

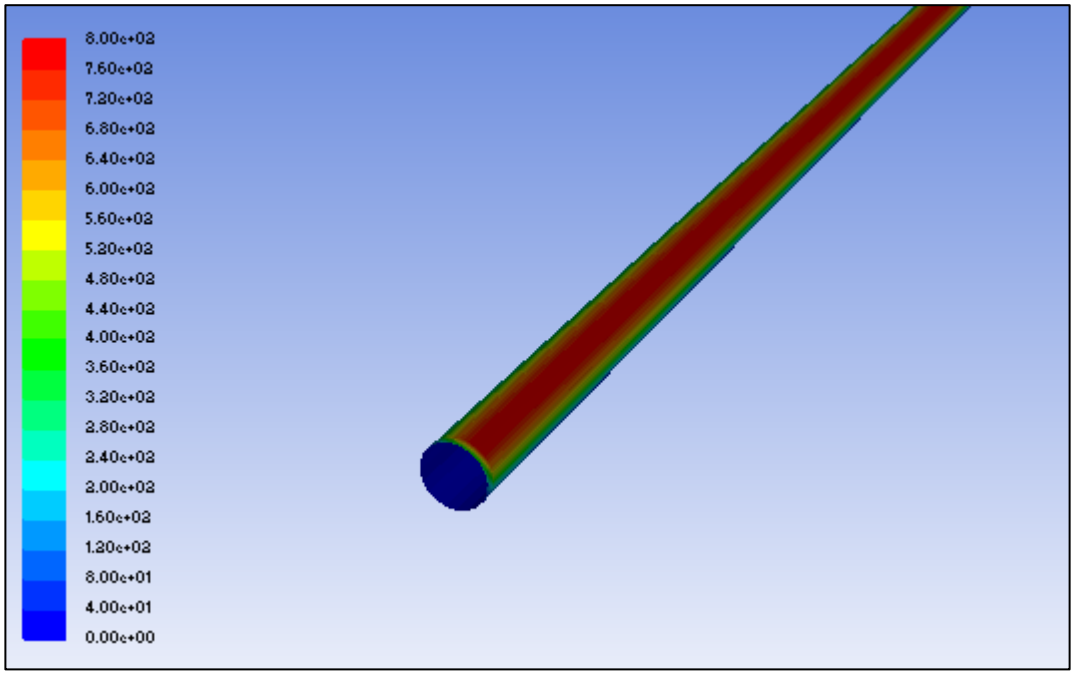

Figure 34. Solar heat flux at the surface of cylindrical absorber

As observed in Figure 34, the solar heat flux applied to the absorber is 800 W/m2, which already accounts for the optical losses due to absorptivity and transmissivity.

Therefore, the zeroth loss coefficient for this particular ETC is equal to:

$$F'(ta)en\ 0.96*(800/1000) = 0.768$$

This result is very similar to the results obtained by Jack et al. (2011) in his work where he performed several evaluation methods for heat pipes in solar thermal collectors that were similar to the one used in this simulation.

One year simulation and ScenoCalc

In order to standardize the one-year performance of a solar thermal collector, Perers et al. (2012) developed at tool for the calculation. This tool was created based on tests according to EN12975. This tool yields an annual energy output for a specified collector in order to facilitate comparisons among them. It also outputs an annual performance result of the collector in interest.

In order to maintain the standardization of our design in accordance to EN12975, we decided to use this tool in order to perform the annual calculation of the thermal performance of the ETC collector.

This tool is capable of calculation the output of the solar thermal collector by using local weather data of interest. It calculates the collector output at 3 temperatures defined by the user, and presents a graph with monthly and annual output. It is important to mention that hourly output data can be obtained as well from this tool, which is what we need for the purpose of this research.

The 3 user defined temperatures that we chose were 80, 87 and 95 °C, which is the range of temperature in which our ETC will operate, and the gross area was set to 2.5 m2.

To use a quasi-dynamic testing method, it is necessary to provide the following collector characteristics: $\eta 0,b$, $K\theta,d$, c1, c2 and c3.

$\eta 0,b$ is the zero loss coefficient in steady state method. They design the tool this way to make it compatible in both steady-state and quasi-dynamic.

Petterson et al. (2011) performed a research on improving the compatibility between steady state and QDT for collector designs such as the ETC.

In his work, he suggest using the following relationship between $F'(\tau\alpha)_{en}$ and $\eta 0,b$:

$$\eta 0,b = F'(\tau\alpha)_{en} K_{\theta b}(\theta)\, a + F'(\tau\alpha)_{en} K_{\theta d}(1-a)$$

Where a is the fraction of direct irradiance and 1-a the fraction of diffuse irradiance.

Further in his work, he performs some adjustments and the above equation yields to the following form:

$$\eta 0,b = 0.85\ F'(\tau\alpha)_{en} K_{\theta b}(\theta = 15)\ + 0.15\ F'(\tau\alpha)_{en} K_{\theta d}$$

It is assumed that the direct irradiance is 85% and the diffuse irradiance is 15% of the global irradiance in all calculations. Therefore:

$$\eta 0,b = 0.85*0.768*1 + 0.15*0.768*1.4 = 0.81$$

We will assume a $K_{\theta d}$ = 1.4, c1 = 1.5 W/m2K, c2 = 0.01 W/m2K2, c3 = 0.2 J/m3K, which are some characteristic values for an ETC (Petterson, et al., 2011).

The IAM of a typical ETC that will be used for the purpose of this research can be observed in Figure 35 (Petterson et al., 2011)

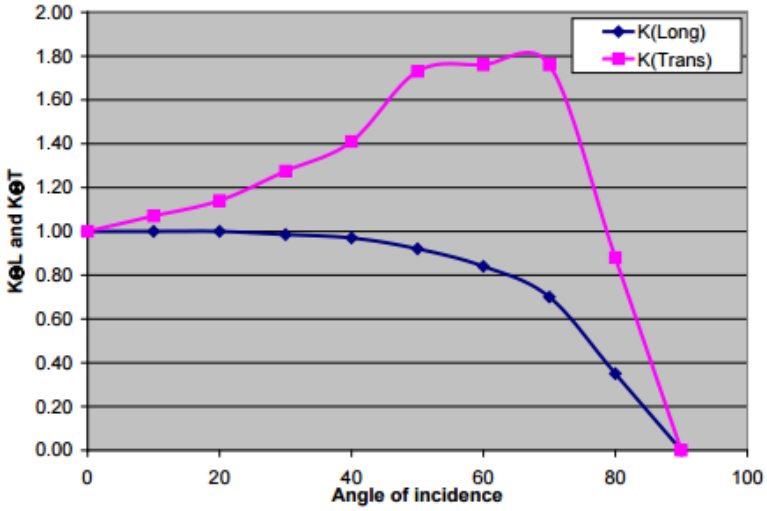

Angle of incidence [°]	0	10	20	30	40	50	60	70	80	90
$K_{\vartheta bL}$	1.000	1.000	1.000	0.985	0.970	0.920	0.840	0.700	0.350	0.000
$K_{\vartheta bT}$	1.000	1.070	1.140	1.275	1.410	1.730	1.760	1.760	0.880	0.000

Figure 35. Incident angle modifiers of a typical ETC. Petterson et al., 2011

In order to use this tool for our research, the following data must be provided.

- An hourly based ambient temperature data.
- An hourly based global horizontal irradiance data.
- An hourly based direct normal irradiance data.
- An hourly based wind speed data.
- An hourly based long wave irradiation data.

All of the above-mentioned data was obtain by the NSRDB, except for the long wave irradiance, which wasn't available; therefore, it must be calculated.

For this calculation we will use the calibrated Brunt model by Li et al. (2017).

$$LW_c = (0.618 + 0.056\sqrt{P_w})\sigma T_a^4$$

$$P = 610.94\left(\frac{\phi}{100}\right)\exp\left(\frac{17.625(T_a - 273.15)}{T_a - 30.11}\right)$$

Where Pw is the partial pressure of vapor (hPa), Ta is the ambient temperature (K), σ is the Stefan Boltzmann (W/m2k4) constant and ϕ is the relative humidity (%).

The latitude, longitude and STD longitude are also required. STD longitude is the time zone times 15. Mexico's time zone is 6, therefore it is 90 for the region.

After inputting all the data, the inclination angle is set to 30° and the Azimuth angle is set to 0° for maximum performance and we can calculate the annual thermal energy performance (see Figure 36).

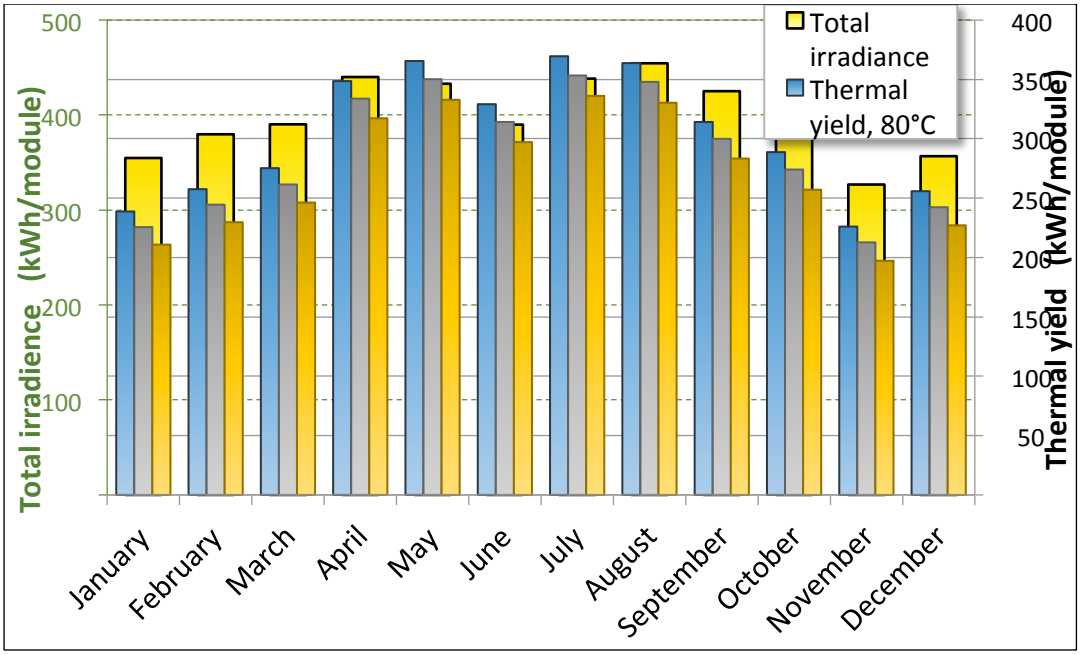

Figure 36. Annual thermal performance of the ETC.

By looking at the results, we can observe 2 things. First thing is that the heat output is just multiplied by the area and changes linearly as the area is increased.

Second thing we can observe is that the higher the fluid temperature, more convection losses occur and there is a lower thermal yield.

At this point, we still cannot estimate the minimum necessary collector area because we still have to calculate the heat losses of the hot buffer tank, the performance of the indirect seawater heat exchanger and the underground thermal storage tank.

Hot water buffer tank

The hot water buffer tank has the purpose of regulating the flow that comes from the collector's array in order to send it to the absorption chiller.

For the purpose of this research, we simplified the hot water buffer tank into a three-layer tank model (see Figure 37).

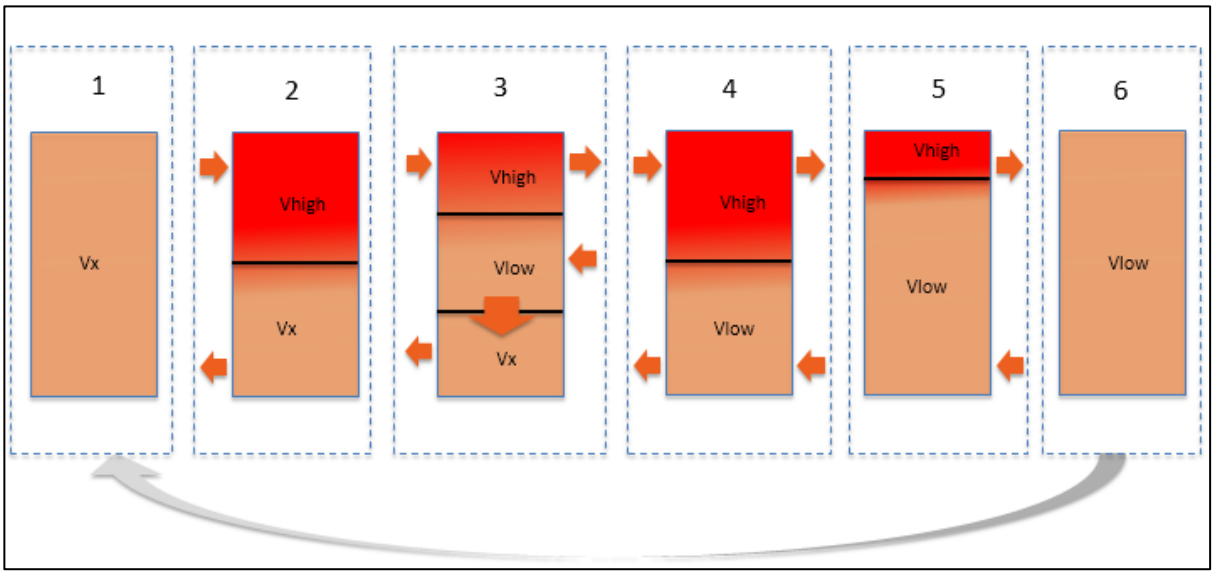

Figure 37. Flow diagram of the hot water tank logic

On step one, we have the remaining hot water (Vx) from the previous day, which is continuously losing heat through convection.

On step two, there is enough solar irradiation for the ETC collectors to provide hot water (Vhigh) to the buffer tank, so it starts charging.

On step three, the collectors continue to provide hot water (Vhigh). There is enough hot water in the buffer tank and the building requires cooling load, therefore, the absorption chiller turns on and starts extracting hot water (Vhigh) and discharging "cold water" (Vlow).

On step four, the remaining hot water (Vx) has depleted. The collectors continue to provide hot water and the absorption chiller keeps running.

On step five, there is no longer enough solar irradiation for the collectors to provide hot water. The absorption chiller keeps running and the hot water (Vhigh) is depleting.

On step six there is no more hot water (Vhigh) and the absorption chiller has to stop. The remaining water (Vlow) keeps losing heat through convection and becomes Vx to repeat the cycle.

The convection losses of the hot thermal storage tank works as follows.

When there is heat input from the collectors, it will take away the heat from the collectors on the next step equal to the convection losses corresponding to Vhigh and Vlow.

If there is no heat input from the collectors, the temperature Vx will start decreasing corresponding to the Vlossx every step.

If the volume of Vlow equals the total volume of the tank, the temperature of Vlow will start decreasing corresponding to the Vlosslow every step.

The convection losses were calculated according to Aerstin et al. (1989).

It is important to notice that we are assuming a perfect thermocline during the entire process and therefore ignoring the exergy losses that could occur due to it, as well as simplifying the model into only three layers.

The complete condition diagram of the model can be found in Appendix M.

Chapter 4. Indirect seawater heat exchanger

In order to perform an annual simulation of the performance of the indirect seawater heat exchanger in an analytical approach, it is necessary to understand the overall heat transfer of the heat exchanger, which in this case is composed by an array of helical coils. For us to propose a design of the heat exchanger array, it is necessary to know the heat transfer coefficient of a single helical coil as a first step.

The heat transfer coefficient is a value that depend on several characteristics of the heat exchanger such as the flow rates, the geometry of the heat exchanger and the fluid properties, therefore, it changes greatly depending on the specific application and scenario.

$$Q = hAdT_{lm}$$

h	Heat transfer coefficient
A	External area of helical coil
dT_{lm}	Logarithmic Mean Temperature Difference

It was decided to do simulation in ANSYS Fluent in order to obtain the heat transfer coefficient of our particular helical coil heat exchanger.

Designing the helical coil heat exchanger

According to the absorption chiller's datasheet, the rated heat rejection to the cooling tower is 427 kW with a flow rate of 0.0255 m3/s and the cooling water temperature enters the heat exchanger at 35°C and is expected to return to the chiller at 31 °C in rated conditions.

The tube diameter at the Chiller cooling water outlet is 10.16 cm (assuming a copper tubing), this gives a 9.55 cm inner diameter from a standard 0.12 inch wall thickness. In order to reduce the head loss of the system, it was decided to increase the outer diameter of the

main branch to 24 cm. For safety reasons, for a pipe to resist the operating pressures of the flow, it is important to consider a dimension ratio (DR). This dimension ratio is the outer diameter of the pipe divided by the thickness.

Lower DR means a higher resistance to pressure, but it also indicates a thick pipe wall, which in turn increases the thermal resistance, therefore we would look for the highest DR that would be able to resist the maximum operation pressure.

The maximum allowable operating pressure of the absorption chiller is 588 kPa, but it changes with the temperature of operation. The maximum temperature registered in the seawater temperature data is 32.7 °C, therefore it is assumed that the max temperature that will go through the pipe will be around 38 °C.

From Figure 38, we can observe that the DR 13.5 pipe at a temperature of 110 °F (43.3 °C) can resist a pressure of 90 PSI (620 kPa), therefore, this DR will be selected for this particular design.

Temp (°F)	Pipe DR					
	7	9	11	13.5	15.5	17
20	400	300	240	192	166	150
40	367	275	220	176	152	138
73.4	**267**	**200**	**160**	**128**	**110**	**100**
80	253	192	150	122	105	95
90	232	173	140	111	96	87
100	210	160	125	101	87	79
110	188	143	113	90	78	71
120	167	130	100	80	69	63
130	150	115	90	72	62	56
140	133	100	80	64	55	50

Figure 38. Pipe DR depending on temperature. Ground source heat pump residential and light commercial design and installation guide.

From Figure 39 we can observe that the DR 13.5 has a thermal resistivity of 0.117 hr-ft-F/BTU (67.65 mK/kW).

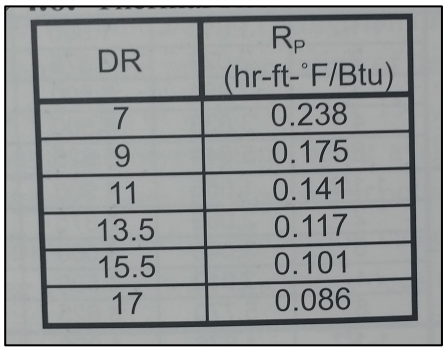

DR	R_P (hr-ft-°F/Btu)
7	0.238
9	0.175
11	0.141
13.5	0.117
15.5	0.101
17	0.086

Figure 39. Thermal resistivity according to DR. Ground source heat pump residential and light commercial design and installation guide.

This DR will be used for the entire design of the helical coils.

The rated flow rate of the cooling water, which will be constant at all times for this research, is 404.5 GPM (0.0255 m3/s).

It is well known that there is higher heat transfer when the flow is turbulent due to the agitation of the water particles. In order to know if a fluid has a laminar or turbulent flow, we can use the Reynolds number.

$$Re = 124\left(\frac{\rho V D_i}{\mu}\right) \quad , \quad V = 0.4085\,\frac{Q}{D_i^2}$$

Where:

Re	Reynolds number
V	Fluid velocity (ft/s)
D_i	Internal diameter (in)
μ	Fluid viscosity (cp)
ρ	Fluid density (lbm/ft^3)
Q	Flow rate (gpm)

In a pipe flow, a Reynolds number lower than 2300 is considered laminar and a Reynolds number greater than 10,000 is considered fully turbulent. The equation above is the formula for the Reynolds number on a straight pipe. For the case of a helical coil, the Reynolds number in which the flow becomes turbulent is a bit higher and it is a function of the pitch circle diameter.

A helical coil geometry is defined by the following characteristics in Figure 40.

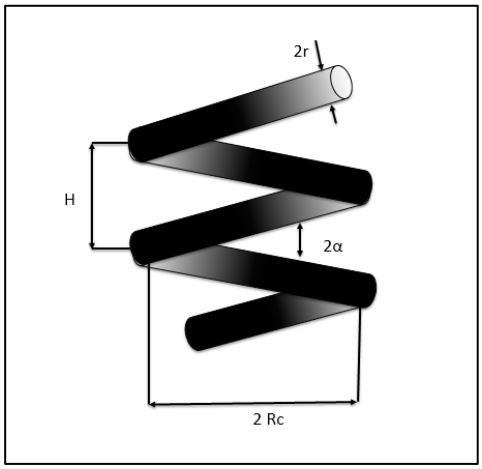

Figure 40. Helical coil geometry

Where:

2r	Pipe inner diameter
2Rc	Coil diameter = Pitch circle diameter (PCD)
H	Pitch
α	Helix angle

Other relations:

δ	Ratio of Pipe diameter to Coil diameter is called curvature ratio = r/Rc

λ Ratio of pitch to developed length of one turn (H/2pi*R) = non-dimensional pitch

Jayakumar (2012) did research on the helical coil heat exchanger. In his work he compares several critical Reynolds number on helical coil pipes obtained experimentally by various authors as a function of curvature ratio as observed in Figure 41.

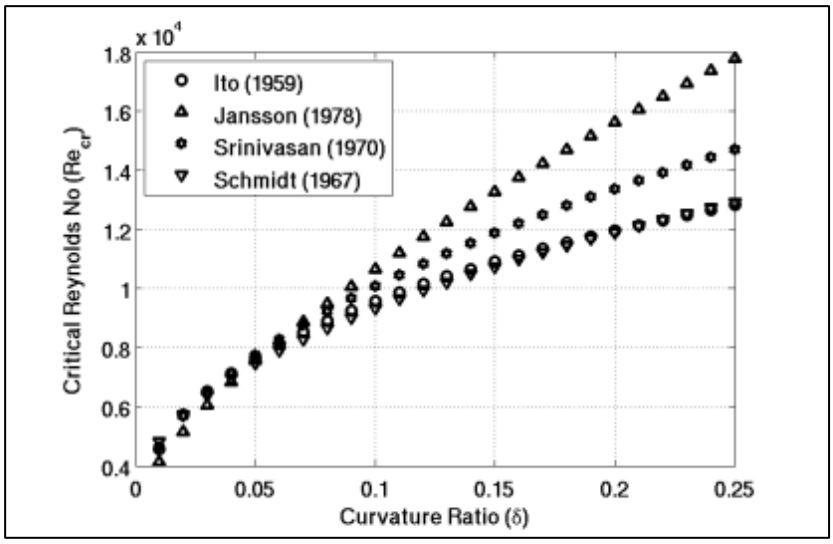

Figure 41. Critical reynolds number vs curvature ratio of a helical coil heat exchanger. Jayakumar (2012)

The effect of PCD in the flow of a helical coil influences the centrifugal force on the moving fluid. This will in turn affect the secondary flows along the pipe cross-section. As the PCD is increased, the effect of coil curvature on flow decreases and hence centrifugal forces play a lesser role in flow characteristics.

In his work, he did several comparisons using CFD to observe the change of Nusselt number as a function of PCD. His results indicated that higher PCDs lead to higher Nusselt numbers, and he proposed the following empirical equation:

$$Nu = 265.65(\delta^{0.11})$$

From this, we can point out that because a smaller coil diameter leads to higher curvature ratio, it would also lead to higher Nusselt Numbers, but as mentioned earlier, a higher curvature ratio also leads to a higher critical Reynolds number for a fully turbulent flow, therefore we need a healthy balance between these two parameters.

The pitch of the helical coil affects the heat transfer by increasing the torsion of the flow. This effect on the heat transfer can be observed when the pitch is smaller than the diameter, but for pitches greater than the diameter it is insignificant, therefore a pitch slightly greater than the OD was selected.

After some calculations, we chose a standard size pipe with outer diameter of 2.375 in (0.0603 m), which with the DR leads to an inner diameter of 0.0514 m. We set the coil diameter to 1 m, giving a curvature ratio of 0.0514. With this, we did 12 parallel branches, which yielded a velocity of 1.02 m/s per branch. This gives a Reynolds number of 65,782.9, which is a fully turbulent flow. This also gives a Nusselt Number of 191.18, which is acceptable compared to Jayakumar's results.

Methodology of the simulation

In order to do a mathematical calculation of the annual performance of the helical coil heat exchangers, we decided to use the Logarithmic mean temperature difference (LMTD) method.

In heat exchanger theory, the LMTD method is used to obtain the overall heat transfer coefficient of a heat exchanger when the inlet and outlet temperature and the flow rates are known values through experimental data. It represents a logarithmic average of the temperature difference of the cold and hot fluid inlet and outlet in a heat exchanger. Large ΔT_{lm} values indicate more heat transfer through the heat exchanger.

For this method, the following equations are used:

$$q = UA\Delta T_{lm}$$

$$\Delta T_{lm} = \frac{\Delta T_1 - \Delta T_2}{\ln\left(\frac{\Delta T_1}{\Delta T_2}\right)}$$

$$\Delta T_1 = T_{hin} - T_{cout} \quad , \quad \Delta T_2 = T_{hout} - T_{cin}$$

Where:

q	Total heat transferred (W)
U	Overall heat transfer coefficient (W/m2K)
ΔT_{lm}	Logarithmic mean temperature difference (K)
A	Total surface area of contact (m2)
T_{hin}, T_{hout}	Inlet and outlet temperature of the hot fluid (K)
T_{cin}, T_{cout}	Inlet and outlet temperature of the cold fluid (K)

In order to use this method, several assumptions have to be made, the first one being that the U is independent of the temperature of the fluids. Another important assumption that we will make is that T_{cin} and T_{cout} are equal. This assumption can be done because the flow rate of the sea is very big.

The following equation is also an important heat exchanger equation, which derives from the conservation of energy and mass:

$$q = \dot{m} C_p \Delta T$$

Where:

$\dot{m}$	Is the mass flow rate (kg/s)
C_p	Is the specific heat capacity of the fluid (kJ/kgK)

ΔT Is the difference of temperature between the inlet and the outlet (K)

When using this equation, a third assumption must be done, and that is that the C_p remains constant during the entire process for both working fluids.

With these equations, it is clear that we must obtain T_{hout} and q in order to obtain the U of our heat exchanger.

It is worth mentioning that fluent does calculate a heat transfer coefficient, but it uses a reference temperature for the calculation, and this is not acceptable for using the LMTD method, therefore, a simulation will be done in order to obtain the total heat transferred, q.

In order to use the LMTD method, first, we need to obtain the current velocity and temperature of the cold fluid, which in this case is the sea.

Several data taken from buoys in Mexico were searched, but due to a lack of available data, very few options could be found.

A buoy at Campeche Bay, which is property of the NOAA was the closest one to the target region, therefore, it was decided to use this buoy, but this buoy doesn't measure current data, therefore other options were looked for.

Another available buoy is called the Holbox buoy, which is composed by the buoy itself and an RDCP (Recording Doppler Current Profiler), which is located below it. The RDCP had data of the current speed at different depths; therefore due to the lack of current velocity data from the Campeche Bay buoy, this database was used for current velocities at a depth of 2.5m.

Another inconvenience was that the RDCP data was lacking current velocity information from May 24th to July 9th and from November 2nd to December 31th due to

maintenance, therefore, additional data had to be obtained from the buoy on top, which also measured the average current speed, but at a surface level (see Figure 42).

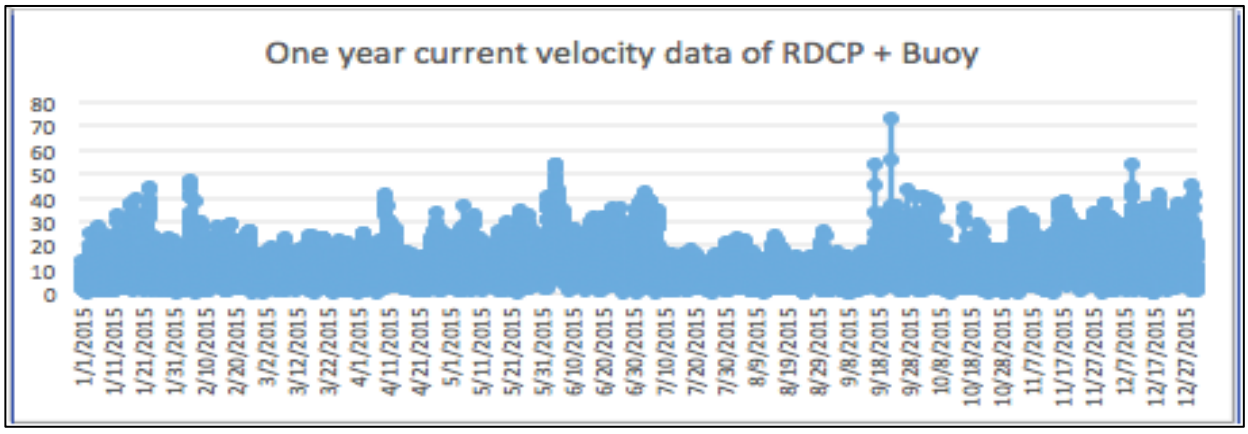

Figure 42. Annual data of sea current velocity at cm/s

As observed, there is a noticeable difference in the magnitude of the current flow data between the buoy measured current velocity and the RDCP measured current velocity, therefore, a scatter plot was analyzed in order to see if they were compatible.

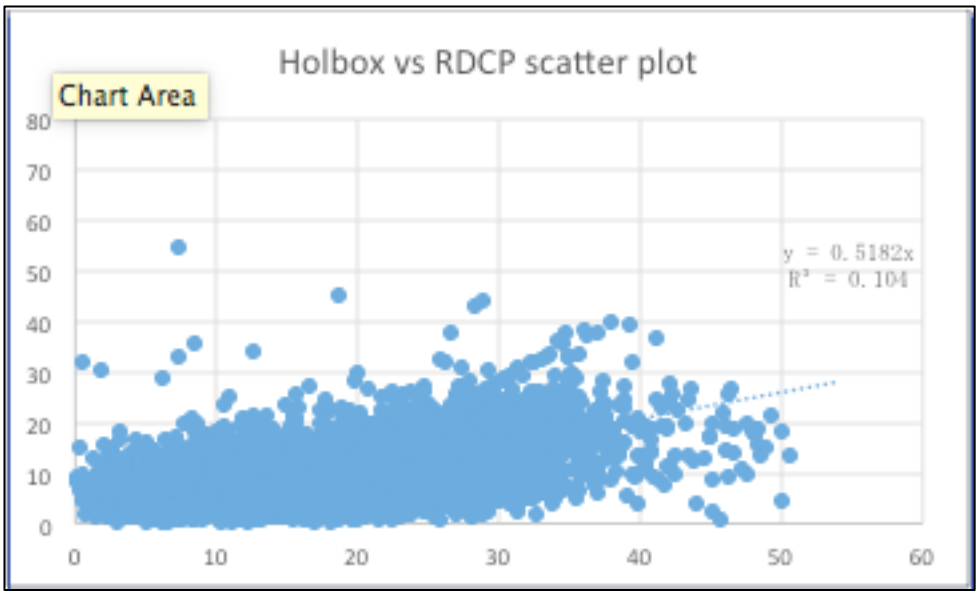

Figure 43. Scatter plot of Holbox current data vs RDCP current data

The scatter plot showed a trend, therefore, a linear interpolation was performed in order to adjust the data from the buoy.

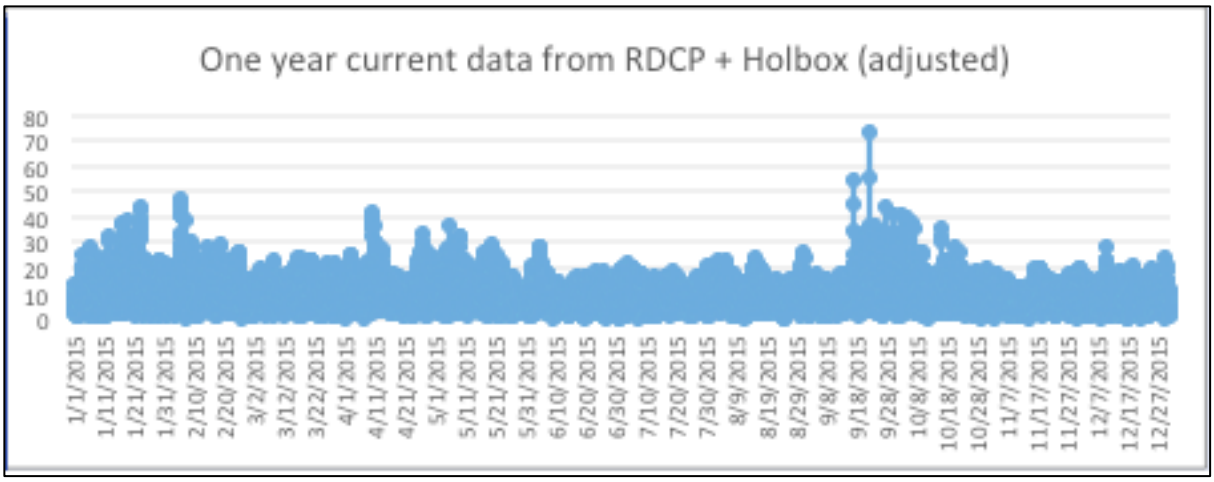

Figure 44. Adjusted data of the sea current combining RDCP and Holbox

The data was adjusted with the linear interpolation and now looks more acceptable.

In order for us to do the mathematical calculation, we decided to do several simulations of a helical coil heat exchanger under different sea current velocities and see how much heat is transferred in steady state in each case. With the transferred heat value, it is possible to obtain the overall heat transfer coefficient U during each of those cases. Then, it was agreed to do an interpolation with the heat transfer coefficients in order to obtain a curve in function of any sea current velocity.

Simulation of the helical coil heat exchanger

Geometry

The geometry of the helical coil heat exchanger was created using CAD software Solidworks. The parts consisted of a helical coil pipe, water and the sea. The detailed information about the geometry of the helical coil pipe can be found in Appendix N.

Mesh

For the mesh several adjustments had to be made for a correct convergence rate.

Edge sizing's had to be created at the edges of the water, pipe and sea in order for them to fit tightly. Face meshing was done at the face of the pipe and water to create a uniform figure along the helix. The geometry of the sea had to be extended in the outlet in order to reduce reverse flows, also the face of the outlet mesh of the sea was face meshed and an inflation was set in order to create finer meshes in the outlet. Pictures of the mesh can be found in Appendix O.

The relevance center was set to coarse, smoothing to high and span angle to coarse in order to not surpass the 512,000 elements restriction of the student version of Fluent.

Named selections were created at the inlet and outlet of the water inside the pipe, as well as at the sea inlet and outlet.

The mesh produced a total of 490,800 elements and 264,043 nodes.

Setup

A pressure-based solver was selected in steady state mode. Gravity was set to a value of -9.81 m2/s at the Y-axis.

Energy equation was turned to On and the Standard k-epsilon turbulence model with standard wall function was selected. The materials were assigned as indicated by Table 7.

Type	Material	Section	Property	Value	Unit
Fluid	Water	Pipe internal fluid & Sea	Density	1000	kg/m3
			Specific Heat	4182	J/Kg-K
			Thermal Conductivity	0.6	W/m-K
Solid	HDPE	Helical Coil pipe	Density	950	kg/m3
			Specific Heat	2250	J/Kg-K
			Thermal Conductivity	0.47	W/m-K

Table 7. Material properties for the simulation of the helical coil heat exchanger

The boundary conditions were set as follows in Table 8.

Section	Type	Condition	Value	Unit
Water inlet	Velocity inlet	Velocity	1	m/s
		Temperature	308	K
Water outlet	Pressure outlet	Pressure	0	Pa
Sea inlet	Velocity inlet	Velocity	x	m/s
		Temperature	298	K
Sea outlet	Pressure outlet	Pressure	0	Pa

Table 8. Boundary conditions of the simulation of the helical coil

The velocity of the sea inlet was modified in each of the trials as follows in Table 9.

V1	V2	V3	V4	V5	V6
0.0013	0.011	0.0924	0.2	0.31	0.73

Table 9. Velocities used for the simulation of the helical coil heat exchanger (m/s).

V1 was the minimum current velocity from the data and V6 was the maximum. V3 was the annual average velocity. The others are high and low representative data.

The mesh interfaces between the helical coil pipe, the water and the sea were set as coupled walls.

A standard initialization was done and the calculation was run with 300 iterations.

Results

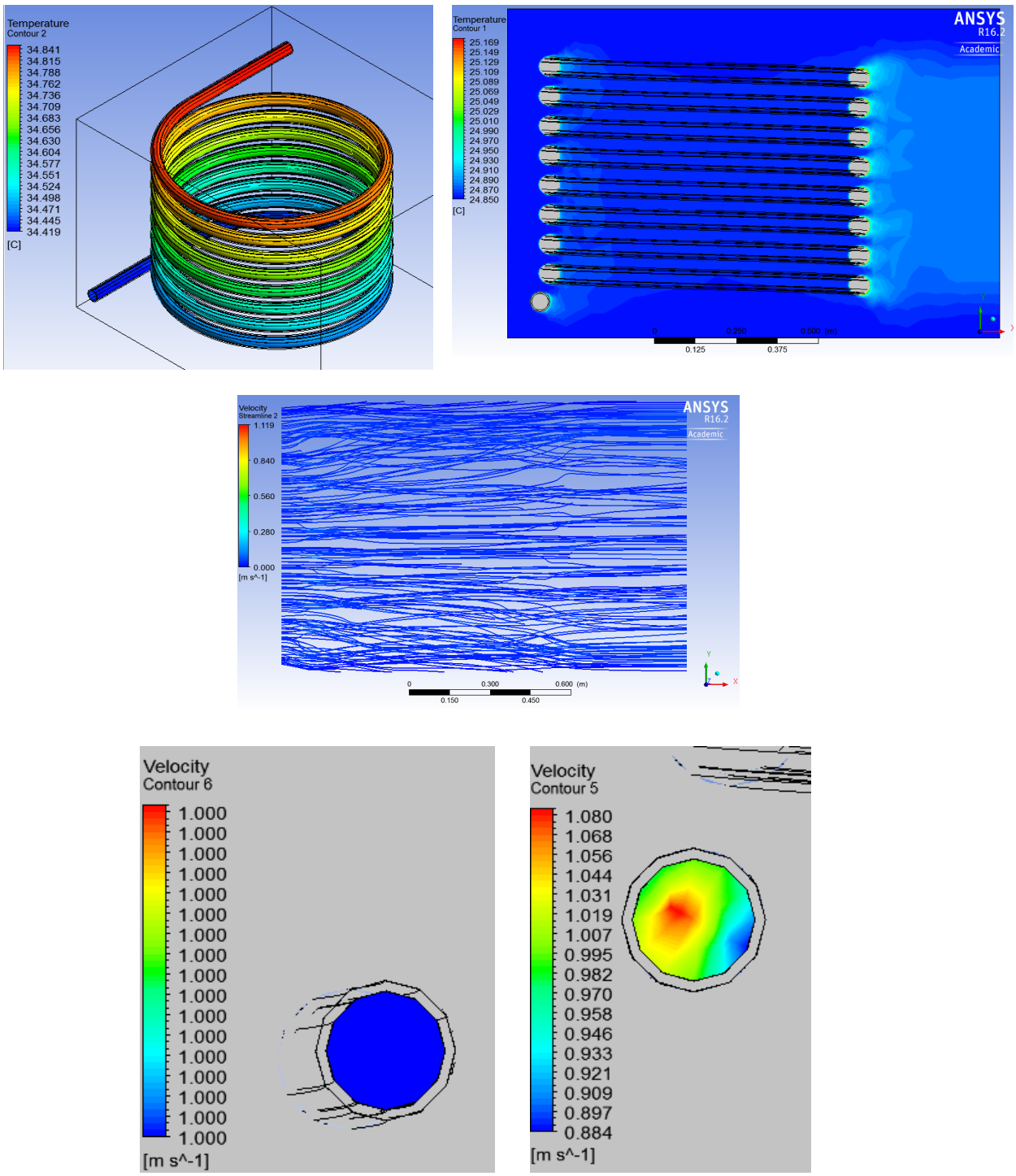

Figure 45. Results of the simulation. Temperature contour of the fluid inside the helical coil. Temperature contour of a section view of the sea. Steamlines of the sea. Contour of inlet velocity at helical coil. Contour of outlet velocity at helical coil.

We can observe the heat transfer going through the walls of the helical coil. We can also observe that turbulence is formed at the streamline after they strike the helical coils, which is why there seems to be a higher heat transfer when they strike the pipes after the helical coil axis.

We can also see the effect of the centrifugal force, which is creating a higher velocity at the outer part of the cross section view of the out and a lower velocity at the inner part.

The simulations yielded the following values for the total heat transferred (see Table 10).

Total heat transferred at each trial (W)

q1	q2	q3	q4	q5	q6
3472	3715.6	3952.1	3996.5	4037.3	4110.8

Table 10. Total heat transferred at each trial (W).

With this information, it is possible to calculate the U for each trial.

First, we used equation to calculate ΔT, with which we can use to calculate T_{out}. We use T_{out} for equation and we obtained the following U values in Table 11.

Overall heat transfer coefficient at each trial (W/m2K)

U1	U2	U3	U4	U5	U6
66.077	70.808	75.414	76.280	77.076	78.511

Table 11. Overall heat transfer coefficient at each trial (W/m2K)

If we graph U vs v, we obtain the following graph:

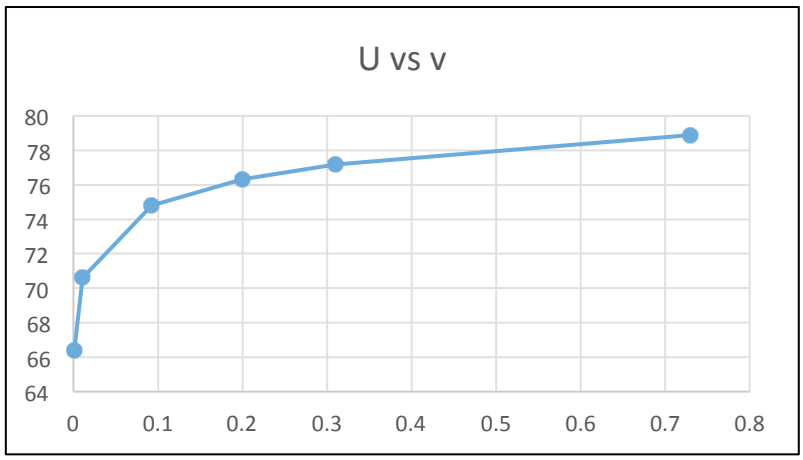

Figure 46. Graph of overall heat transfer coefficient vs velocity

We fit the graph by using a power function and we obtain the following fitting:

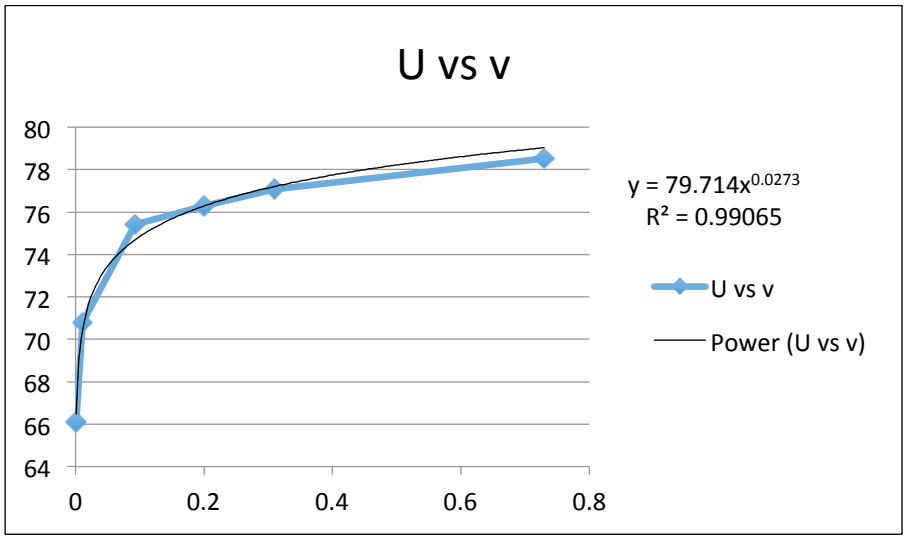

Figure 47. Graph of overall heat tranfer coefficieny vs velocity and power function interpolation.

It yields a very good fit, therefore, we will use this power function in order to characterize our U over any sea current velocity during the year, and with it, we can obtain the heat transferred at any time step.

We estimated the time that it would take for a water particle to do a complete loop through the entire heat exchanger and it was approximately 15 minutes, therefore, for the case of the cooling water, we would divide the step into 15 minutes in order to get a more precise result.

Chapter 5. Underground thermal storage tank

In order to size the underground thermal storage tank, we first need to know how much cooling loads we want to cover with it.

In Mexico, the electric bill works as shown in Figure 48.

First Sunday of April until the Saturaday before the last Sunday of October

Day of the week	Base	Intermedium	Peak
Monday to Friday	0:00-6:00	6:00-20:00 22:00-24:00	20:00-22:00
Saturday	0:00-7:00	7:00-24:00	
Sunday and festive days	0:00-19:00	19:00-24:00	

Last Sunday of October until the Saturday before the first Sunday of April

Day of the week	Base	Intermedium	Peak
Monday to Friday	0:00-6:00	6:00-18:00 22:00-24:00	18:00-22:00
Saturday	0:00-8:00	8:00-19:00 21:00-24:00	19:00-21:00
Sunday and festive days	0:00-18:00	18:00-24:00	

Region	kWh at Peak	kWh at Intermedium	kWh at Base
South	$2.5536	$1.4055	$1.1695

'

Figure 48. Hour table and electric bills in Mexico's southern region, CFE

As observed, depending on the season the electricity bill changes.

Peak hour electric bill is very high, therefore it is important that the UTS can at least cover the peak hour loads. Therefore, we size the UTS so that it can cover at least 4 hours of cooling loads.

Now that we know the heat medium's temperature and the cooling water's temperature, it is possible to simulate the solar absorption chiller system. We simulate the peak day, which happens in April 27th and use the results to size the UTS.

The approximate minimum UTS size for covering the peak hour even at the peak day considering zero thermal losses is approximately 55 m3, but we do several manual adjustments through the Excel tool and we decide that with a volume of 127 m3 it is possible to cover a greater amount of hours.

Because this is a single UTS tank, it is important to take account for the thermocline losses that occur.

In order to do this, we used the method proposed by Bayon et al (2014). In their work, the authors propose an analytical function describing the behavior of a thermocline storage tank with the objective of facilitating annual simulations of this type of thermal storage system.

Their method was created for the purpose of doing annual simulations of solar thermal molten salt storage technology, although they do validation of their function with other types of thermal storage tank and mention that this analytical function is applicable for a wide range of other thermal storage systems.

One important detail of this analytical function is that it does not take account for thermal losses to the exterior because molten salt thermal storage tanks are very well insulated and they present minimal heat; therefore, in order to use this function for our research, it is important to first demonstrate that the underground thermal storage tank has negligible heat loss.

In order to do this, a transient simulation was proposed to observe the heat transfer through the walls of the UTS. We decided to do a transient simulation because the heat

transfer rate should start declining as the temperature of the ground around the UTS starts to decline.

Simulation of underground thermal storage tank

Geometry

The geometry of the underground thermal storage tank was created using Solidworks. The details of the parts and the assembly can be found at Appendix P.

The tank has a 5.6 m diameter and 5.16 m height and it is buried at a 1 m depth.

Mesh

Several details had to be taken care for the meshing of this assembly.

Meshes plane on top and symmetrical along the axis were desired for this simulation in order to simulate correctly the heat transfer from the top soil towards the underground tank, therefore, a MultiZone meshing method was used. For a successful MultiZone meshing, face meshing in top and bottom surfaces were performed. Face sizing was created in order to achieve a symmetrical shape above the UTS tank.

The mesh created 107,145 elements and 116,528 nodes.

The details of the mesh can be found in Appendix Q.

Named selections where created at the upper surface of the top soil to put radiation and convection boundary conditions, at the bottom of the ground to act as a reservoir, and at the upper and lower surface at the tanks interior to simulate the upper hot part and lower cold part.

Setup

A pressure-based solver was selected in transient mode. Gravity was set to -9.81 m/s2 at the Y axis.

We have no fluids on this simulation, so only the energy equation was set to On. The materials were set as shown in Table 12.

Type	Material	Section	Property	Value	Unit
Solid	Concrete	Tank	Density	2300	kg/m3
			Specific Heat	750	J/Kg-K
			Thermal Conductivity	0.8	W/m-K
	Sand	Ground and top soil	Density	1520	kg/m3
			Specific Heat	800	J/Kg-K
			Thermal Conductivity	0.77	W/m-K

Table 12. Materials of the simulation of the UTS

Coupled walls were created between all surfaces in contact as mesh interfaces.

Boundary conditions were set as shown in Table 13.

Section	Type	Condition	Value	Unit
Hot	Wall	Temperature	286	K
Cold	Wall	Temperature	280	K
Reservoir	Wall	Temperature	298	K
Surface	Wall	Convection	h	W/m2K
			Tamb	K
		Radiation	Trad	K

Table 13. Boundary conditions of the simulation of the UTS

In order to do a transient simulation with variable boundary conditions, we used a transient table profile for the film transfer coefficient h, the ambient temperature Tamb and the radiation temperature Trad. We used the data from the annual weather data of Veracruz.

Afterwards, we did a standard initialization from all zones and we did a temperature patch at the ground to set it to 25 °C, which is the annual average temperature of the region.

A time step of 3600 s and a number of time steps of 1000 was set. It was possible to set a very high time step because there were no fluids present in this simulation, only conduction heat transfer through solids. The max iteration was set to 100.

Results

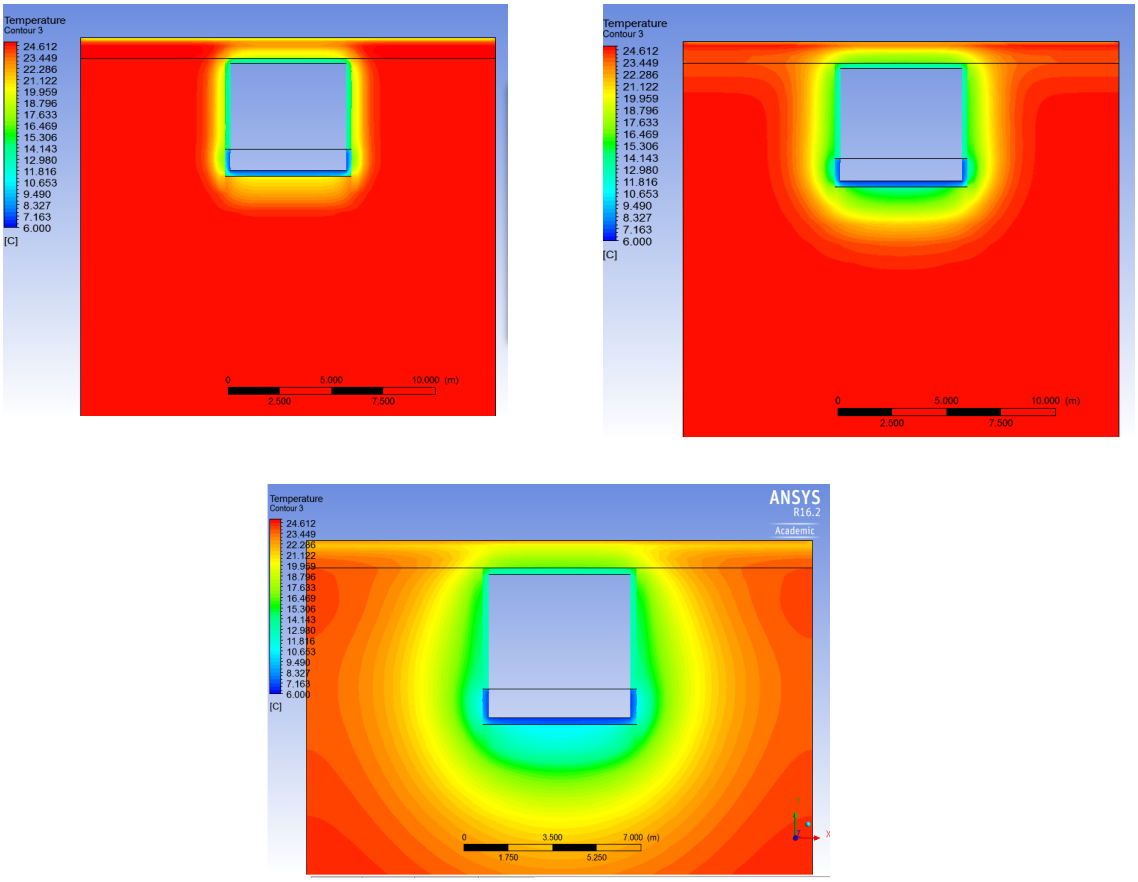

Figure 49. Temperature contour of the cross section of the ground. Temperature contour at 10 hours. Temperature contour at 100 hours. Temperature contour after 7 months.

As observed, the ground starts to cool with time. This affects the total heat transfer rate as observed in Figure 50.

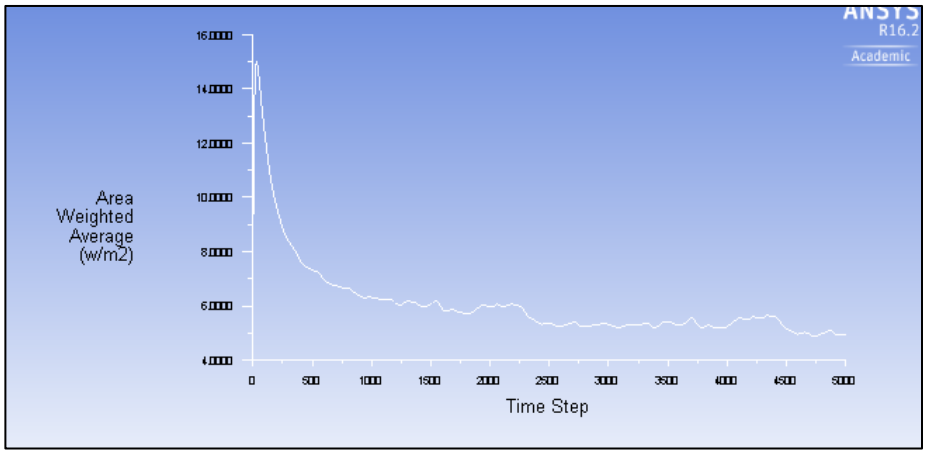

Figure 50. Area weighted average (W/m2) vs time step. Time step is 1 hour.

The heat required to raise 1 K the temperature of all the water inside the UTS is 532,132.3 kJ. Therefore, for it to increase its temperature 1 K in 1 hour it would require a constant heat flux of 147.8 kWh.

The total outer surface area of the tank is 166.8 m2. The highest area weighted average heat flux registered is 15 W/m2, which would yield a total heat transfer of 2503.7 W.

If we consider the total volume of the tank, this would result on an overall decrease in temperature of 0.017 °C in one hour, which is a very small dT/dt.

If we take into account that the charge and discharge cycle would end every 24 hours, at most we would get a total dT of 0.4 K, therefore, we agreed that it was acceptable to consider the UTS adiabatic and possible to use the thermocline function proposed by Bayon.

Thermocline function

A thermocline is the layer that forms when there is a temperature difference between the fluid at the upper and lower part. This layers thickness tends to increase with time and

also with the charging and discharging velocity of the tank. Depending on the characteristics of the tank, the losses generated by the thermocline can be severe.

The thermocline function proposed by Bayon is described by a logistic cumulative distribution function (CDF) and it is in dimensionless form. It uses a parameter S, which is related to the tank characteristics such as height and velocity, and this parameter is used to describe the thickness of the thermocline.

The value of the S parameter changes depending if the tank is in a dynamic state (charging or discharging) or in a static state.

In their work, the authors function is created in order to support a completely liquid tank or a liquid + solids tank, therefore she uses effective properties. For the purpose of this research, a completely liquid water tank is being considered, therefore, the equations of the author can be written in their dimensionless form as:

$$TC^*(z_c^*) = 2nS\ ln(2+\sqrt{3})$$

$$S(v^*, t^*) = \frac{\pi\sqrt{v^* t^*}}{60(2 - \frac{5}{\pi} e^{\frac{-v^*}{555}})}$$

$$S(t^*) = \frac{5\sqrt{t^*}}{2}$$

$$t^* = \frac{t \propto}{L^2}$$

$$z^* = \frac{z}{L}$$

$$z_c^* = v^* t^* \qquad \text{In discharge}$$

$$z_c^* = 1 - v^* t^* \qquad \text{In charge}$$

Where:

$TC^*(z^*_c)$	Dimensionless thermocline thickness
$S(v^*,t^*)$	S parameter function in dynamic state (discharging)
$S(t^*)$	S parameter function in static state
v^*	Dimensionless velocity of the thermocline
t^*	Dimensionless time
z^*	Dimensionless tank height
z^*_c	Dimensionless thermocline position at a certain time
α	Thermal diffusivity

n is a statistical parameter which indicates what percent of the thermocline is considered in the thickness. It can be obtained from the relationships obtained by the author in Figure 51.

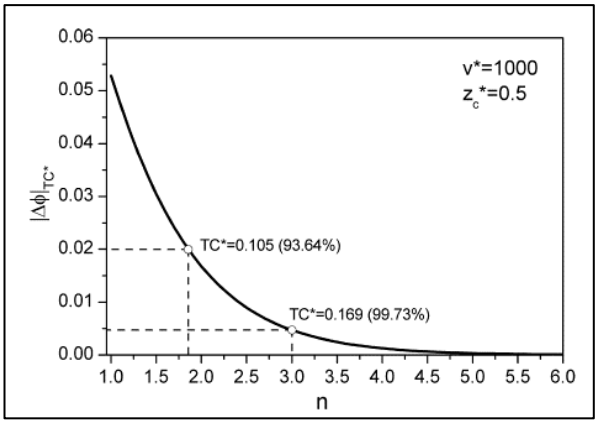

Figure 51. Graph of the temperature difference in function of the dimensionless thermocline thickness vs n. (Rojas et al.)

Whenever the chiller is running and it already covered the step's cooling load, the excess load goes to charge the UTS. The UTS only discharges when the chiller is not running. The charge flow rate always adjusts in order to charge the UTS at a temperature of 7 °C and the discharge flow rate adjusts so the water reentering the UTS always enters at 12.5 °C.

With these control considerations and the equations above, it is possible to calculate the thermocline thickness as a function of each time step.

With the thermocline thickness at each step, it is possible to calculate the sigmoidal temperature profile at each step by using the following equations:

$$\phi_{OUT-DISCHARGE}(v^*t^*)|_{z^*=0} = \phi_{min} + \frac{\phi_{max} - \phi_{min}}{1 + e^{\frac{-(1-z_c^*)}{S}}}$$

$$\phi_{OUT-CHARGE}(v^*t^*)|_{z^*=0} = \phi_{min} + \frac{\phi_{max} - \phi_{min}}{1 + e^{\frac{(z_c^*)}{S}}}$$

As an example, if we graph ϕ for charging over the dimensionless time t^* we obtain the following graph (see Figure 52).

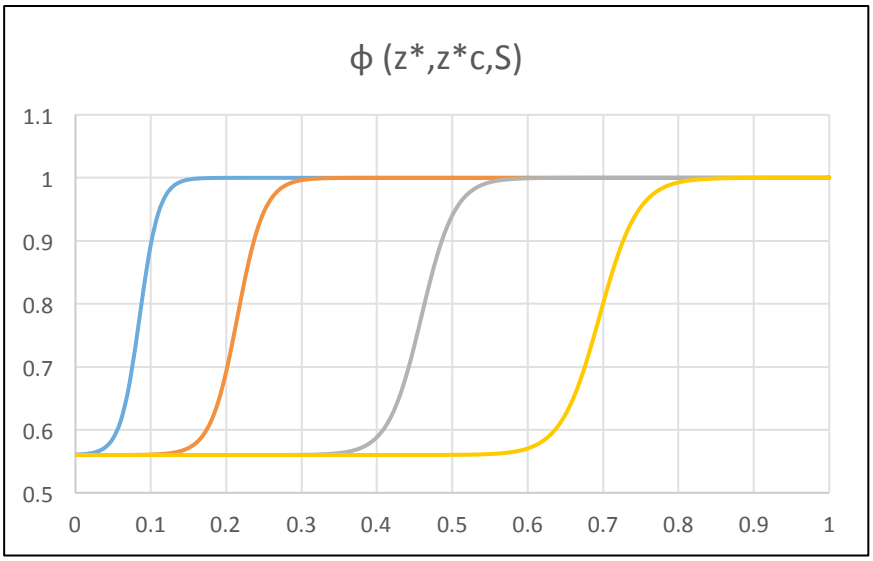

Figure 52. Graph of dimensionless temperature vs dimensionless height during a charging process.

Chapter 6. The system level simulation

Now that we have all the equations and data required, it is possible to do an annual simulation in Excel.

An Excel worksheet was created in which all the gathered information was input. The worksheet consists of a one-hour step rows in the Y axis and the calculation of each of the components in the X axis. In this worksheet, it is possible to observe what is happening at every hour. Several control parameters had to be implemented in order to gather the multiple components. Once the control parameters were set, the simulation was run.

Covered cooling load

When using a 570 m2 area of collector, 1500 m2 area of the indirect seawater heat exchanger, 200 m3 of the underground thermal storage and a 60 m3 of volume of the hot buffer tank, the entire system performed as follows in Figure 53.

ANALYSIS (Thermocline UTS)		
Solar ETC Area	570	m2
Seawater HC Area	1500	m2
UTS Volume	200.00	m3
Hot Storage Volume	60	m3
Total year building loa	593,815.08	kw
Chiller covered load	237,002.05	kw
T UTS covered load	162,312.57	kw
Total covered load	399,314.61	kw
Chiller covered %	40%	
T UTS covered %	27%	
Total covered %	67%	

Figure 53. Results of the Excel tool to calculate the performance of the designed system

We can observe that the designed entire system is capable of covering 67 % of the cooling loads throughout the year, therefore, it is necessary to have a backup chiller to cover 33 %. We can also observe that the thermocline UTS is covering only 27 %, so we simulated a two underground storage tank model, which doesn't has the thermocline losses and compared the results as observed in Figure 54.

ANALYSIS (Two UTS model)		
Solar ETC Area	570	m2
Seawater HC Area	1500	m2
UTS Volume	200	m3
Hot Storage Volume	60	m3
Total year building loa	593,815.08	kw
Chiller covered load	237,002.05	kw
UTS covered load	212,082.93	kw
Total covered load	449,084.98	kw
Total uncovered load	144,730.10	kw
Chiller covered %	40%	
UTS covered %	36%	
Total covered %	76%	

Figure 54. Results of the simulation of the proposed design with two cold storage underground tanks.

As observed, without the thermocline losses it is possible to cover 76% of the annual load of the target location.

It is also important to mention that with this design, there were 118,684 kWh available to use for domestic hot water generation, which is a significant amount of heat that could be used for shower, pool heating, laundry, cooking, etc. The amount of remaining heat is due to the size of the UTS.

Comparison of indirect seawater cooling and cooling tower

We also compared the performance of two water source chillers, one with the indirect seawater cooling system and the other one using a wet cooling tower. For the chiller, we used the specification sheets of a YORK chiller from Johnsons Control as shown in Figure 55:

FORM 150.26-EG1 (116)

Ratings - Standard Efficiency

MODEL: YCWL0056SE											IPLV= 21.3	
	ENTERING CONDENSER WATER TEMPERATURE (°F)											
LCWT	75.0				85.0				95.0			
(°F)	TONS	KW	MBH	EER	TONS	KW	MBH	EER	TONS	KW	MBH	EER
40.0	50.7	33.9	724.0	17.9	48.1	37.7	705.0	15.3	45.3	42.0	686.0	12.9
42.0	52.6	34.1	747.0	18.5	49.8	37.8	727.0	15.8	47.0	42.2	708.0	13.4
44.0	54.4	34.3	770.0	19.0	51.6	37.9	749.0	16.3	48.8	42.3	729.0	13.8
46.0	56.4	34.5	794.0	19.6	53.5	38.1	771.0	16.8	50.5	42.4	751.0	14.3
48.0	58.3	34.7	818.0	20.2	55.4	38.3	795.0	17.4	52.3	42.5	773.0	14.8
50.0	60.3	34.9	843.0	20.7	57.3	38.5	819.0	17.9	54.2	42.7	796.0	15.2

Figure 55. YORK chiller model YCWL0056SE specifications, Johnson Controls

The results are shown in Figure 55.

	Chiller with cooling tower (kWh)	Chiller with indirect seawater cooling (kWh)
Annual electric power consumption	132,858.15	148,789.34

Table 14. Annual electric power used by a water source chiller.

As observed, the chiller with the indirect sea cooling system uses slightly more electricity. This is due to the wet bulb temperature being slightly above the seawater temperature throughout the year, even though the seawater temperature is lower than the dry bulb temperature. This can be observed on Figure 56.

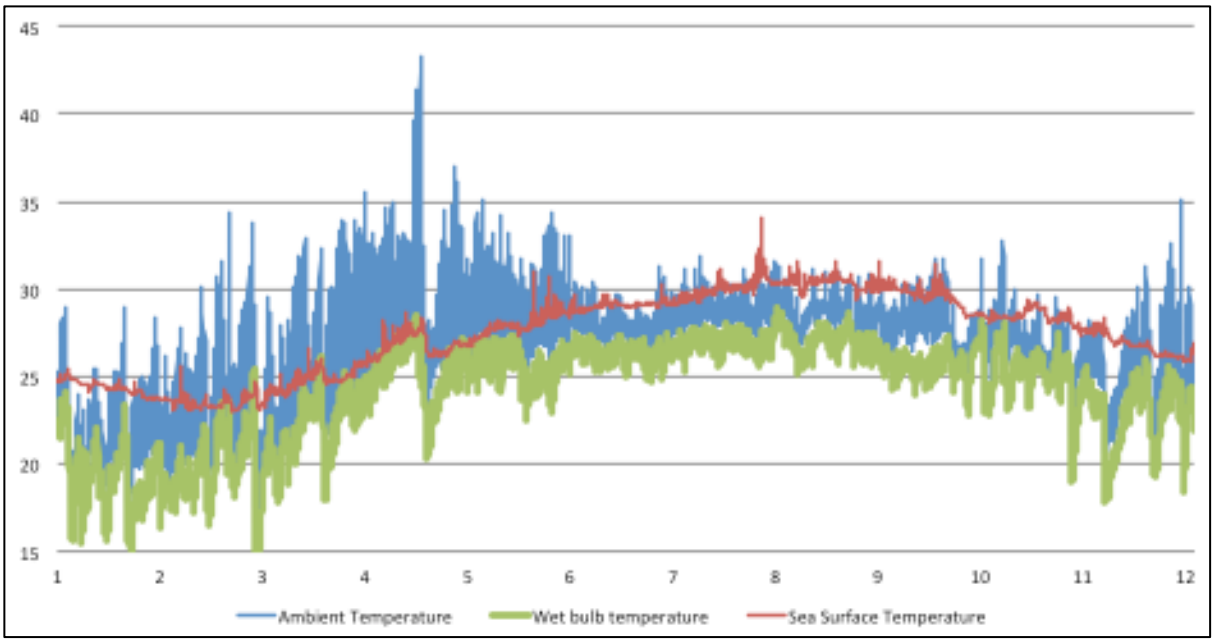

Figure 56. Graph of temperature vs time of the dry bulb temperature, wet bulb temperature and the sea surface temperature.

Even though electricity consumption of the chiller with cooling tower is slightly less, in order to do a more precise comparison, it is necessary to include the cooling tower pumping costs and the indirect seawater system pumping costs, as well as the water costs consumed by the cooling tower.

Electricity consumption of the absorption chiller components

We then calculated the electricity consumption of each of the pumps of the absorption chiller in order to understand which spent the most amount of power.

In order to do this calculation, we first need to know an approximate value of the head loss of each of the circuits; therefore, the Hazen-Williams equation was used:

$$S = \frac{h_f}{L} = \frac{10.67Q^{1.852}}{C^{1.852}d^{4.8704}}$$

Where:

S	Heat loss per length of pipe
h_f	Head loss of water over the length of pipe (m)
L	Length of pipe
Q	Volumetric flow rate (m3/s)
C	Pipe roughness coefficient
d	Inside pipe diameter (m)

The pipe roughness coefficient values were set as indicated in table 15.

	Pump ETC to buffer tank	Pump buffer tank to chiller	Pump cooling water to chiller	Pump chilled water to fan coil	Pump UTS
C	135	150	140	140	140

Table 15. Pipe roughness coefficient and hydraulic radius of each of the circuits.

We then followed to calculate the power consumed by the pump by using the following equations:

$$P_h = \frac{q \rho g h_f}{3.6\ 10^6}$$

$$P_s = \frac{P_h}{\eta}$$

Where:

P_h	Hydraulic pump power (kW)
q	Flow capacity (m3/h)
P_s	Shaft power (kW)
η	Pump efficiency

We set all pumps efficiency as a constant of 0.8.

Figure 57 shows the result of the power consumption of each of the pumps of the system:

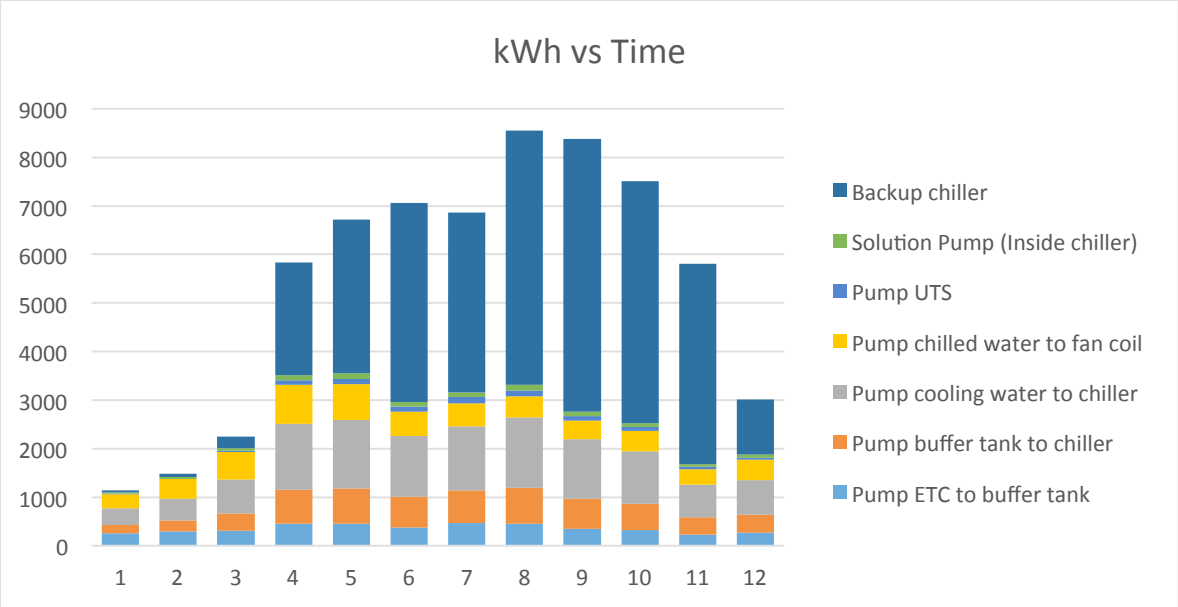

Figure 57. Graph of electricity consumption of the several components of the solar absorption chiller system (kWh)

As observed, the component that uses most of the electricity is the backup chiller followed by the cooling water, which is the indirect seawater system. This is due to the length of the entire array of helical coils, which generate a considerable head loss, increasing the pumping electricity consumption.

Cost evaluation

We then performed an annual costs calculation in order to compare the systems. In order to perform a more precise comparison with systems using cooling tower with the indirect seawater systems, we decided to remove the indirect seawater cooling system's pumping costs to just compare the chiller components.

The costs were calculated by using the electric bills shown in Figure 48 earlier.

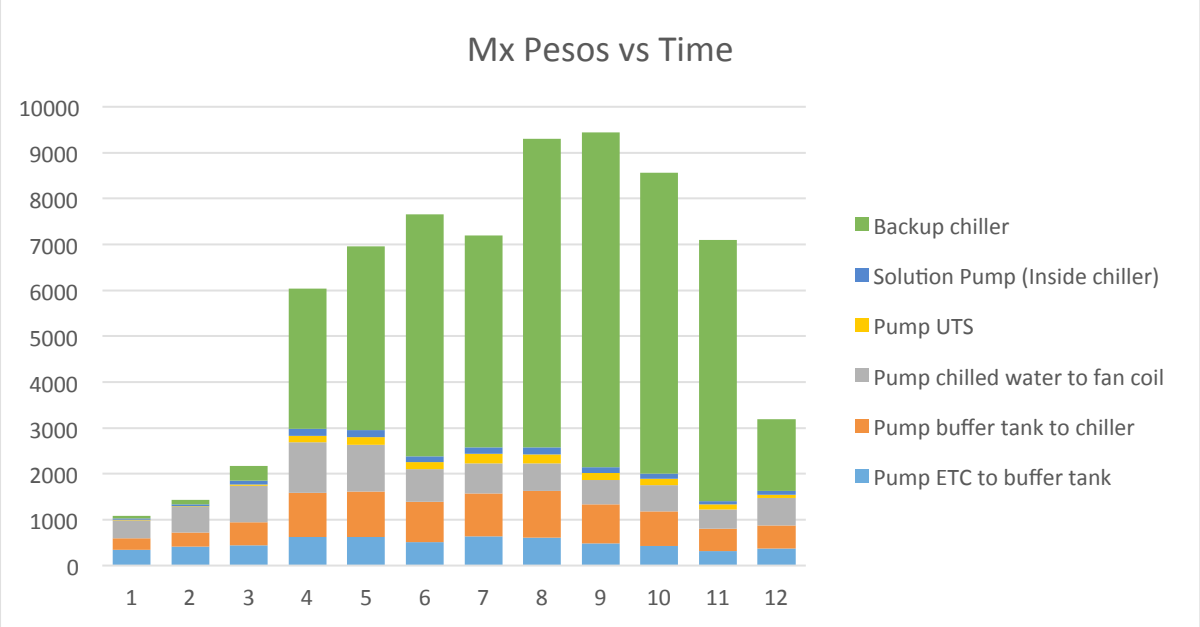

Figure 58. Annual electric bill costs per component of the absorption chiller system.

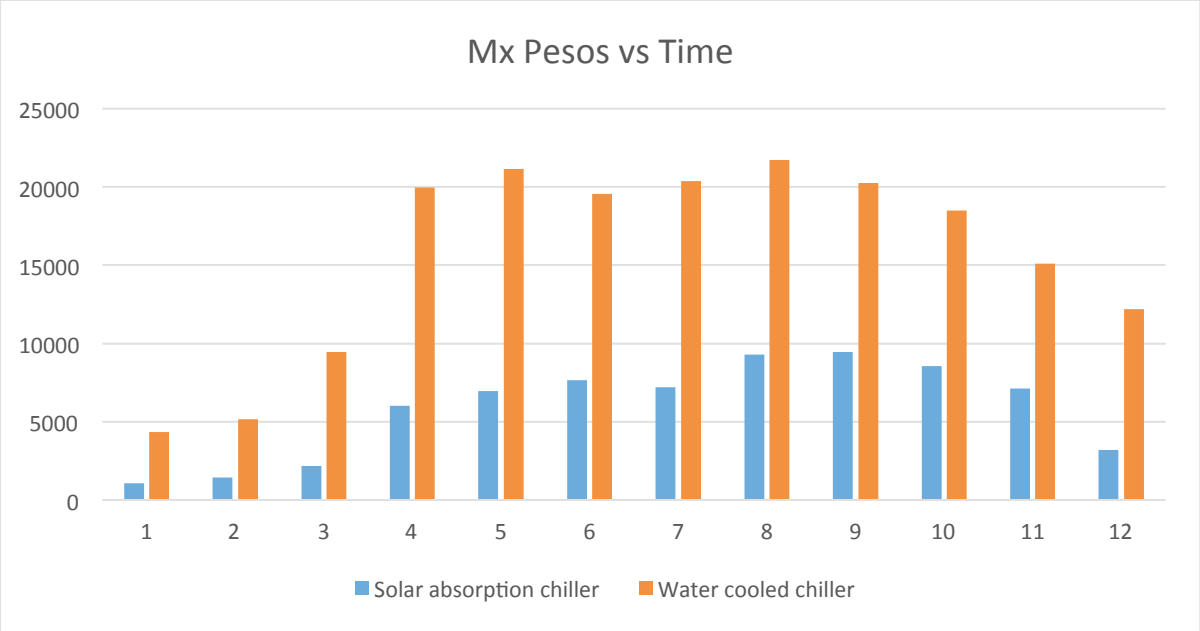

Figure 59. Annual operation costs of the proposed solar absorption chiller system and a water-cooled chiller with a cooling tower.

	Solar absorption chiller	Water cooled chiller
Total annual costs	70,133.98	187,722.21

Table 16. Cost comparison between the solar absorption chiller and a water cooled chiller with cooling tower

As observed, the solar absorption chiller system consumes almost 63% less electricity than the traditional water-cooled chiller. It is important to mention that both water powered chiller's additional equipment costs such as cooling tower pumping costs, water costs, indirect sea cooling system pumping costs are not included in this analysis, which would further increase the gap between them and the solar absorption chiller. Nonetheless, the installation costs of the solar absorption chiller are well known to be high, therefore, further cost analysis is required for a more detailed economic comparison.

Chapter 7: Summary and recommendations

Summary

An analytical approach based on CFD was performed in order to simulate a one-year performance of a solar absorption chiller with an underground cold thermal storage tank and an indirect seawater cooling system.

The results indicated that the proposed solar absorption design would be able to save approximately 63% in electric costs compared to a traditional water powered chiller with a cooling tower. It is also important to notice that the costs of the water powered chiller don't include the cooling tower additional operation costs such as pumping and water consumption, which would further increase the gap in operation costs.

Recommendations

Solar thermal collector costs are decreasing rapidly with the expansion of China's manufacturers through Asia and Europe, therefore, it is of our interest to know at what point the costs reduce enough to make the solar absorption chiller economically feasible.

In the case the technology is not economically feasible due to high initial costs, it is recommended to understand the required subsidy amounts in future researches.

Further, it is recommended to improve the heat buffer tank model and create an analytical function that could describe the hot buffer tank thermocline losses while considering the convection losses to the ambient air. Also, improving the Excel worksheet tool to include a design optimization function in order to provide the most profitable results while including the installation costs is recommended. Finally, an experimental validation of the annual simulation is recommended for future research.

References

Abhat A, et al., Development of a modular heat exchanger with an integrated latent heat storage. Report no. BMFT FBT 81-050. Germany Ministry of Science and Technology Bonn; 1981.

ACCA, "Manual J - Residential Load Calculation" (ANSI/ACCA 2 Manual J – 2006).

Aerstin, F., & Street, G. (1989). *Applied Chemical Process Design*. New York: Plenum Press.

The use of phase change material (PCM) to improve the coefficient of performance of a chiller for meeting domestic cooling in Wales, F., Agyenim, M. Rhodes, I. Knight, 2nd PALENC Conference and 28th AIVC Conference on Building Low Energy Cooling and 1 Advanced Ventilation Technologies in the 21st Century, September 2007, Crete island, Greece

Agyenim, F. (2016). The use of enhanced heat transfer phase change materials (PCM) to improve the coefficient of performance (COP) of solar powered LiBr/H2O absorption cooling systems. *ELSEVIER, 87*(1), 229-239.

Akashi, Akashi, Y., and T. Watanabe. 2003. Energy and cost performance of a cooling plant system with indirect seawater utilization for airconditioning in a commercial building. Journal of Asian Architecture and Building Engineering 2(1):67–73.

Ali, M., PE Senior Design Engineer at ADC Energy Systems, UAE Solar Absorption Air-Conditioning Systems

ASHRAE (2009), Handbook of fundamentals, SI Edition

Bayon, R., & Rojas, E. (2014). Analytical function describing the behaviour of a thermocline storage tank: A requirement for annual simulations of solar thermal power plants. *International Journal of Heat and Mass Transfer, 68*, 641 - 648.

Buddhi D, Sawhney RL.In: Proceedings on thermal energy storage and energy conversion; 1994.

Cabeza, Experimental analysis of the effectiveness of a high temperature thermal storage tank for solar cooling applications, Appl. Therm. Eng. 54 (May (2)) -2013 521–527. [58]

Chien, P.Y.B., V.K.C. Tse, and D.P.L. Yeung. 1986. Using seawater for cooling. ASHRAE Journal 28(9):18–24.

CONUEE Analisis, CFE 2006

Danh, D., & Torii, S. (2011). Heat transfer performance of a self-oscillating heat pipe using pure water and effect of inclination to this performance. *ASEAN Engineering Journal Part A, 2*(1), 93 - 101.

Elsafty, A. (2009). Sea Water Air Conditioning [SWAC]: A Cost Effective Alternative. *International Journal of Engineering (IJE),3*(3), 346 - 358.

Felinski, P., & Sekret, R. (2016). Experimental study of evacuated tube collector/storage system containing paraffin as a PCM. *ELSEVIER, 114*, 1063-1072.

Fischer S., Heidemann W., Müller-Steinhagen H., Perers B., Bergquist P., Hellström B. (2004) “Collector test method under quasi dynamic conditions according to the European Standard EN 12975-2” Solar Energy. Vol 76 pp 117-123

S. Fischer, (2012) Topic report for WP2 Solar thermal collectors *Performance testing of evacuated tubular collectors*, QAiST

George A. Hand book of thermal design. In: Guyer C, editor. Phase change thermal storage materials. McGraw Hill Book Co.; 1989 [chapter 1].

A.A. Gil, C. Barreneche, P. Moreno, C. Solé, A. Inés Fernández, L.F. Cabeza, Thermal behaviour of d-mannitol when used as PCM: comparison of results obtained by DSC and in a thermal energy storage unit at pilot plant scale, Appl. Energy 111 (November) -2013 1107–1113. [57] A. Gil, E. Oró, A. Castell, L.F.

A. Gil, E. Oró, L. Miró, G. Peiró, Á. Ruiz, J.M. Salmerón, L.F. Cabeza, Experimental analysis of hydroquinone used as phase change material (PCM) to be applied in solar cooling refrigeration, Int. J. Refrig. 39 -2014 95–103)

Helm, M., Keil, C., Hiebler, S., Mehling, H., & Schweigler, C. (2009). Solar heating and cooling system with absorption chiller and low temperature latent heat storage: Energetic performance and operational experience. *ELSEVIER, 32*(4), 596-606.

S. Jack, N. Katenbrink, F. Schubert, (2011). Evaluation Methods for Heat Pipes in Solar Thermal Collectors - Test Equipment and First Results. *ISES Solar World Congress 28 August - 2 September 2011.*

J. S. Jayakumar (2012). Helically Coiled Heat Exchangers, Heat Exchangers - Basics Design Applications, Dr. Jovan Mitrovic (Ed.), ISBN: 978-953-51-0278-6, InTech, Available from: http://www.intechopen.com/books/heat-exchangers-basics-design-applications/helically-coiled-heatexchangers

Kumar B. Design, development and performance evaluation of a latent heat storage unit for evening and morning hot water using a box type solar collector. Project report, M Tech (energy management). Indore, India: School of Energy and Environmental Studies, Devi Ahilya University; 2001.

Li, M., Jiang, Y., & Coimbra, C. (2017). On the determination of atmospheric longwave irradiance under all-sky conditions. *Solar Energy, 144*, 40-48.

Matt S. Mitchell & Jeffrey D. Spitler (2013): Open-loop direct surface water cooling and surface water heat pump systems —A review, HVAC&R Research, 19:2, 125-140

Mettawee E-BS, Assassa GM. Experimental study of a compact PCM solar collector. Energy 2006;31:2958–68.)

National Solar Radiation Data Base (NSRDB) [Internet]. National Renewable Energy Laboratory (US), National Solar Radiation Data Base; [2015] - [cited 2017 Feb 10]. Available from: https://maps.nrel.gov/nsrdb-viewer/

D.N. Nkwetta, J. Sandercock / Renewable and Sustainable Energy Reviews 60 (2016) 1351–1366 1359

Noro, M., Lazzarin, R., & Busato, F. (2014). Solar cooling and heating plants: An energy and economic analysis of liquid sensible vs phase change material (PCM) heat storage. *ELSEVIER, 39*, 104-116.

Patil, R., Shende, B., & Ghosh, P. (1982). Designing a helical-coil heat exchanger. *Research Gate,* , 85 - 88.

Perers, B., Kovacs, P., Olsson, M., & Pettersson, U. (2012). A Tool for Standardized Collector Performance Calculations Including PVT. *Energy Procedia, 30*, 1354-1364.

U. Pettersson, P. Kovacs, B. Perers, (2011). Improving the compatibility of collector parameters between Steady state and Quasi-dynamic testing for new collector designs. ISES Kassel.

Pintaldi, S., Sethuvenkatraman, S., White, S., & Rosengarten, G. (2017). Energetic evaluation of thermal energy storage options for high efficiency solar cooling systems. *ELSEVIER,188*, 160-177.

Rabin Y, Bar-Niv I, Korin E, Mikic B. Integrated solar collector storage system based on a salt-hydrate phase-change material. Sol Energy 1995;55:435–44.

Serag, M. (2013). Design of Heat Storage for a Solar Concentrator Driving an Absorption Chiller. *Scientific Research,5*(1A), 107-116.

Song, Y., Akashi, Y., & Yee, J. (2007). Effects of utilizing seawater as a cooling source system in a commercial complex. *ELSEVIER, 39*(10), 1080-1087.

Stalin, J., Barath, ., & Manikandan, G. (2014). Air Conditioning Using Waste Heat and Solar Energy with Phase Change Materials. *ELSEVIER, 52*, 579-587.

Yap C, Khor TH. Outdoor testing of evacuated-tube heat pipe solar collectors. Proc. Inst. Mech. Eng. E., J Process Mech Eng 1999;214(1):23–30.

Zhen, L., Lin, D., Shu, H., Jiang, S., & Zhu, Y. (2007). District cooling and heating with seawater as heat source and sink in Dalian, China. *ELSEVIER, 32*(15), 2603 - 2616.

Appendix A

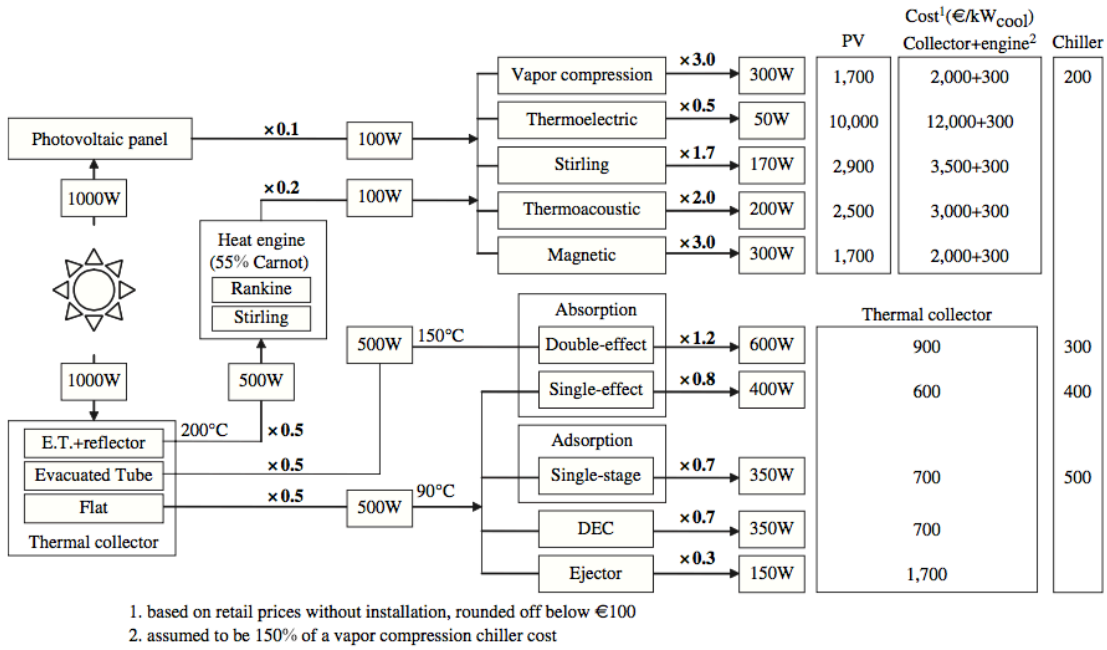

1. based on retail prices without installation, rounded off below €100
2. assumed to be 150% of a vapor compression chiller cost

Fig. 8 – Performance and cost of various solar refrigeration systems.

Kim et al.

Appendix B

Table 3
Cost of different types of complete solar cooling units.

Sr. no.	Type	Cost of complete solar cooling kit (€/kW$_c$)	Remarks
1	H_2O–LiBr absorption cooling system with FPC	1500–2000	FPC: 150–200 €/m^2 Chiller cost: 300–350 €/kW$_c$ Backup boiler: 150–200 €/kW Storage tank: 500–600 €/m^3 Cooling tower: 80–100 €/kW Mountings and accessories: 200–300 €/kW (fan coils, pipe work, pumps, sensors and controllers etc.) Installation cost: 150–200 €/kW$_c$ (10% of capital investment)
2	NH_3–H_2O absorption cooling system with ETC	2500–3000	ETC: 250–300 €/m^2 Chiller cost: 500–600 €/kW$_c$ (rest of components same as above)
3	Adsorption chiller using FPC	2000–2500	Chiller cost: 400–450 €/kW$_c$ (rest of components same as above)
4	Desiccant evaporative cooling system with FPC	3000–4000	Complete DEC system cost: 2000–2500 coupled with FPC

Worldwide overview of solar thermal cooling systems, Gadoof. 2015

Appendix C

Table 1
Small capacity absorption chillers available in the market [28,29,31].

Manufacturer	Country	Capacity (kW)	Type	Working pair	Driving temp. (°C)	Cooling temp. (°C)	Chilled temp. (°C)	COP
Rotartica	Spain	4.5	Ab[a]	H_2O–LiBr	90/85	30/35	13/10	0.67
Climatewell	Sweden	10	Ab	H_2O–LiCl	83/–	30/–	–/15	0.68
Pink	Austria	10	Ab	NH3–H_2O	85/78	24/29	12/6	0.63
Sonnenklima	Germany	10	Ab	H_2O–LiBr	75/65	27/35	18/15	0.77
EAW	Germany	15	Ab	H_2O–LiBr	90/80	30/35	17/11	0.71
Yazaki	Japan	17.6	Ab	H_2O–LiBr	88/83	31/35	12.5/7	0.70

[a] Ab = Absorption.

Worldwide overview of solar thermal cooling systems. Gadoof. 2015

Appendix D

Specifications - Imperial Units

YAZAKI

Specifications			WFC-	SC5	SC/SH10	SC/SH20	SC/SH30	SC50
Cooling Capacity			Mbtuh	60.0	120.0	240.0	360.0	600.0
Heating Capacity {WFC-SH Only}			Mbtuh	---	166.3	332.6	498.9	---
Chilled/Hot Water	Cooling Temperature		°F	54.5 Inlet / 44.6 Outlet				
	Heating Temperature		°F	117.3 Inlet / 131.0 Outlet {WFC-SH Models Only}				
	Evaporator Pressure Loss		PSI	7.6	8.1	9.6	10.1	6.4
	Max Operating Pressure		PSI	85.3 / {High Pressure Option Available on Select Sizes}				
	Rated Water Flow		GPM	12.1	24.2	48.4	72.6	121.1
	Allowable Water Flow		% of Rated	80% - 120%				
	Water Retention Volume		Gal	2.1	4.5	12.4	19.3	33.6
Cooling Water	Heat Rejection		Mbtuh	145.7	291.4	582.8	874.2	1457.0
	Temperature		°F	87.8 Inlet / 95.0 Outlet				
	Absorber Pressure Loss		PSI	5.6	12.3	6.6	6.7	6.6
	Condenser Pressure Loss		PSI	5.6	Included in Absorber	6.6	6.7	3.2
	Max Operating Pressure		PSI	85.3 / {High Pressure Option Available on Select Sizes}				
	Rated Water Flow[1]		GPM	40.4	80.8	161.7	242.5	404.5
	Allowable Water Flow		% of Rated	100% - 120%				
	Water Retention Volume		Gal	9.8	17.4	33.0	51.3	87.2
Heat Medium	Heat Input		Mbtuh	85.7	171.4	342.8	514.2	857.0
	Temperature		°F	190.4 Inlet / 181.4 Outlet				
	Allowable Temperature		°F	158.0 - 203.0				
	Generator Pressure Loss		PSI	11.2	13.1	6.7	8.8	13.6
	Max Operating Pressure		PSI	85.3 / {No High Pressure Option on Any Size}				
	Rated Water Flow		GPM	19.0	38.0	76.1	114.1	190.4
	Allowable Water Flow		% of Rated	30% - 120%				
	Water Retention Volume		Gal	2.6	5.5	14.3	22.2	39.7
Electrical	Power Supply			115 / 60 / 1	208 volts AC / 60 Hz / 3-Phase			
	Consumption[2]		Watts	48	210	260	310	670
	Minimum Circuit Amps		Amps	0.89	0.6	0.9	2.6	4.7
	MOCP		Amps	15				
Capacity Control				On - Off				
Construction	Dimensions[3]	Width	Inches	23.4	29.9	41.9	54.3	70.3
		Depth	Inches	29.3	38.2	51.2	60.8	77.2
		Height	Inches	69.1	74.8	79.1	80.5	82.1
	Weight	Dry	lbs	805	1100	2050	3200	4740
		Operating	lbs	926	1329	2548	3975	5955
	Noise Level		dB(A)	38	49		46	51
Piping	Chilled/Hot Water		Inches	1-1/4 NPT	1-1/2 NPT	2 NPT		3 NPT
	Cooling Water		Inches	1-1/2 NPT	2 NPT		2-1/2 NPT	3 NPT
	Heat Medium		Inches	1-1/2 NPT		2 NPT	2-1/2 NPT	3 NPT

1 - Minimum cooling water flow is 100%.

2 - Power consumption does not include external pumps or motors.

3 - Height does not include removable lifting lugs but does include level bolts. Width/Depth does not include the junction box or mounting plates.

4 - All specifications are based on water in all circuits and a fouling factor of 0.0005 ft²hr°F/BTU.

5 - If heat medium temperature exceeds 204.8°F (96°C), the chiller or chiller/heater will shut down and require manual reset.

6 - Do not exceed 85.3 PSI (588 kPa) in any operating circuit unless the high pressure option is chosen. High pressure option allows 113.9 PSI (785 kPa) in the Chilled/Hot Water and Cooling Water circuits only. There is no high pressure option for the Heat Medium circuit.

7 - Noise level is measured in a free field at a points 1m away from the cabinet and 1.5m above ground level.

Appendix D (Continuation)

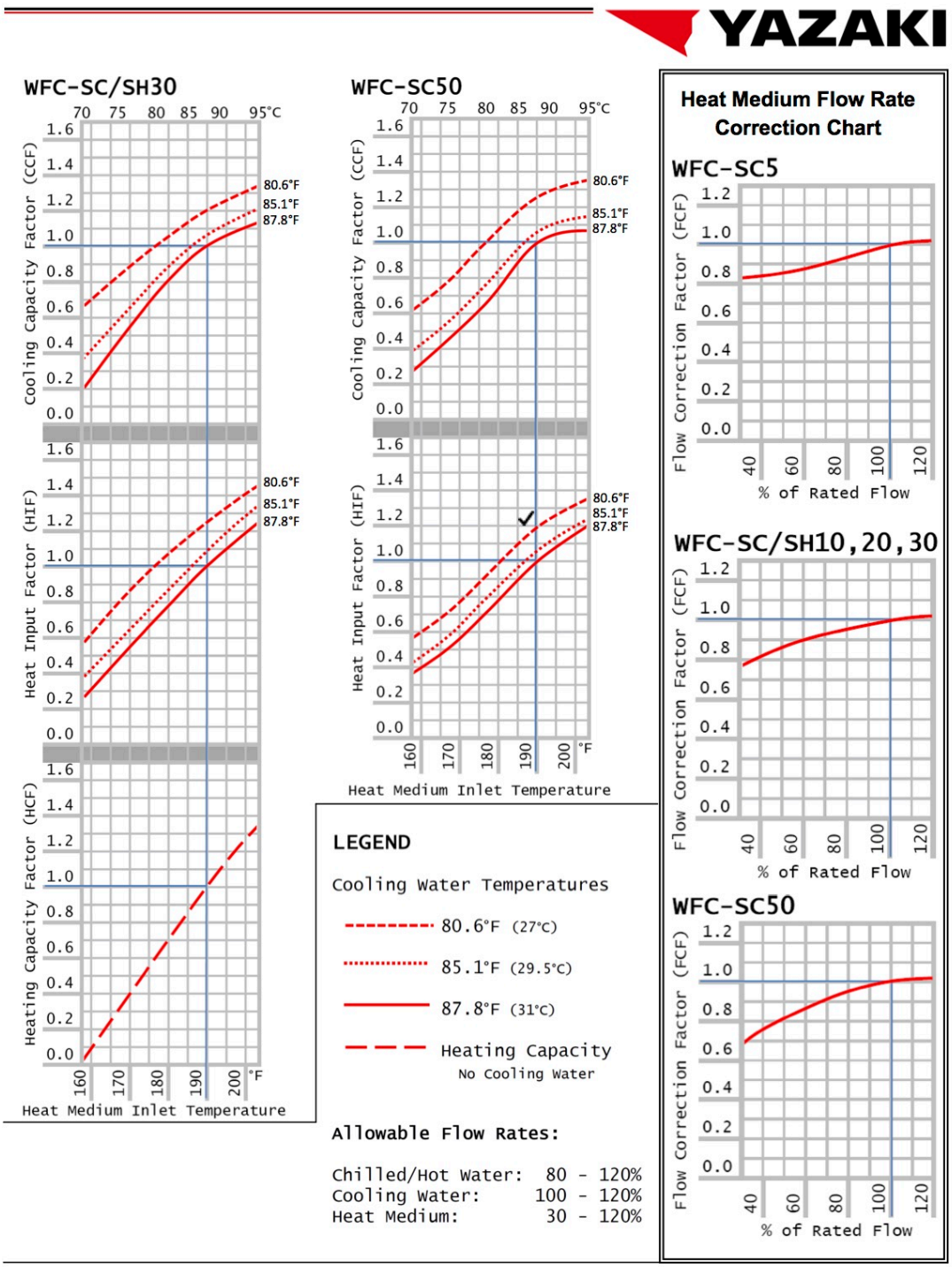

Appendix E

Table 2
Characteristics of a typical water FPC system

Parameter	Simple flat plate collector	Advanced flat plate collector
Fixing of risers on the absorber plate	Embedded	Ultrasonically welded
Absorber coating	Black mat paint	Chromium selective coating
Glazing	Low-iron glass	Low-iron glass
Efficiency mode	$nv_s(T_i - T_a)/G$	$nv_s(T_i - T_a)/G$
G_{test}-flow rate per unit area at test conditions (kg/s m^2)	0.015	0.015
c_o-intercept efficiency	0.79	0.80
c_1-negative of the first-order coefficient of the efficiency (W/m^2 °C)	6.67	4.78
b_0-incidence angle modifier constant	0.1	0.1
Collector slope angle	Latitude +5 to 10°	Latitude +5 to 10°

Appendix F

Table 4
Characteristics of a typical ETC system

Parameter	Value
Glass tube diameter	65 mm
Glass thickness	1.6 mm
Collector length	1965 mm
Absorber plate	Copper
Coating	Selective
Absorber area for each collector	0.1 m^2
Efficiency mode	$nv_s(T_i - T_a)/G$
G_{test} : flow rate per unit area at test conditions (kg/s m^2)	0.014
c_0 : intercept efficiency	0.82
c_1 : negative of the first-order coefficient of the efficiency (W/m^2 °C)	2.19
b_0 : incidence angle modifier constant	0.2
Collector slope angle	Latitude +5 to 10°

Appendix G

Table 3
Characteristics of a typical CPC system

Parameter	Value
F' : collector fin efficiency factor	0.9
U_L : overall loss coefficient of collector per unit aperture area (W/m^2 °C)	1.5
ρ_R : reflectivity of walls of CPC	0.85
θ_c : half-acceptance angle of CPC (degrees)	45
Ratio of truncated to full height of CPC	0.67
Axis orientation	Receiver axis is horizontal and in a plane with a slope of 35° (transverse)
a: absorbtance of absorber plate	0.95
N_G : number of cover plates	1
η_R : index of refraction of cover material	1.526
K_L : product of extinction coefficient and the thickness of each cover plate	0.0375
Collector slope angle	(local latitude)

Appendix H

Table 2. Absorption Chillers Heat Source Requirement

Type	COP	Heat Source Temp (°C)	Type of solar collectors matched
Single Effect	0.75	98 °C hot water	Evacuated tube collectors
Double Effect	1.4	180 °C hot water	Compound parabolic collectors/Parabolic trough collectors/Linear fresnel reflector
Triple Effect	1.8	250 °C steam at 40 bars	Parabolic trough collectors/Linear fresnel reflector

Appendix I

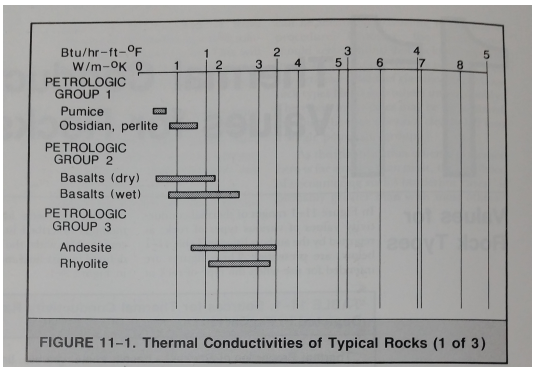

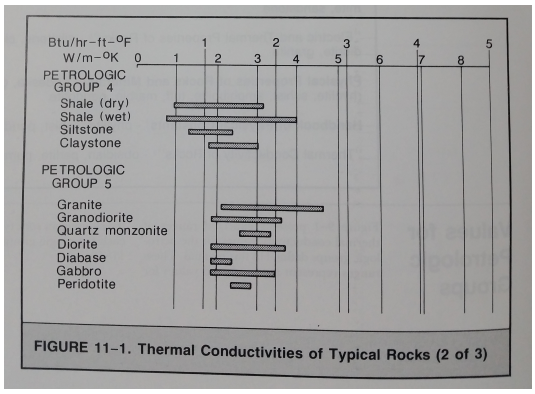

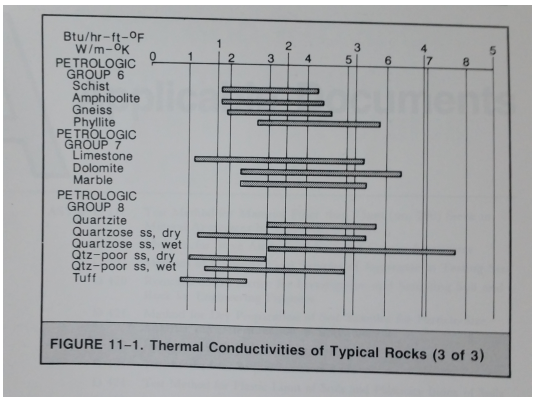

Thermal conductivity of typical rocks (Soil and rock classification for the design of ground-coupled heat pump systems - Field manual)

Appendix K (units in m)

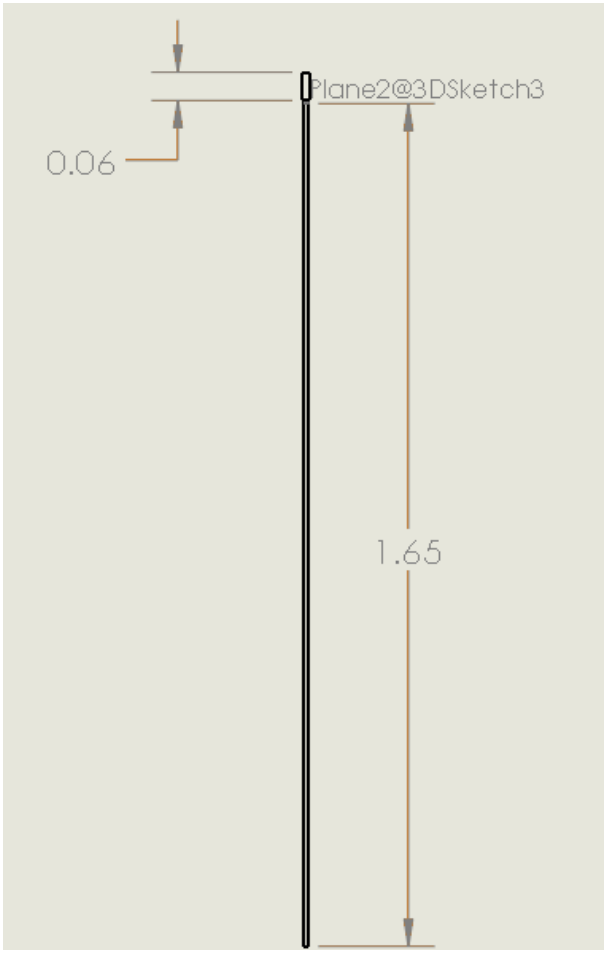

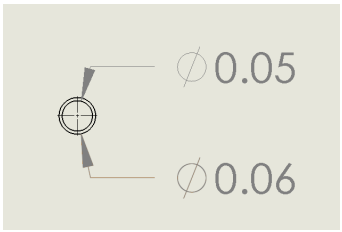

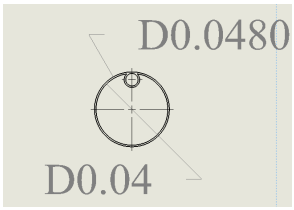

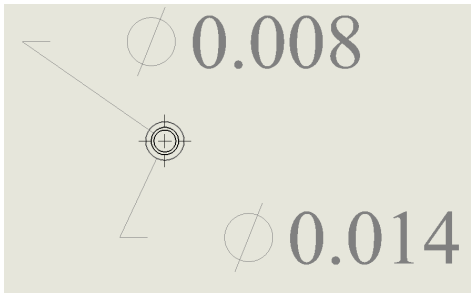

Appendix L

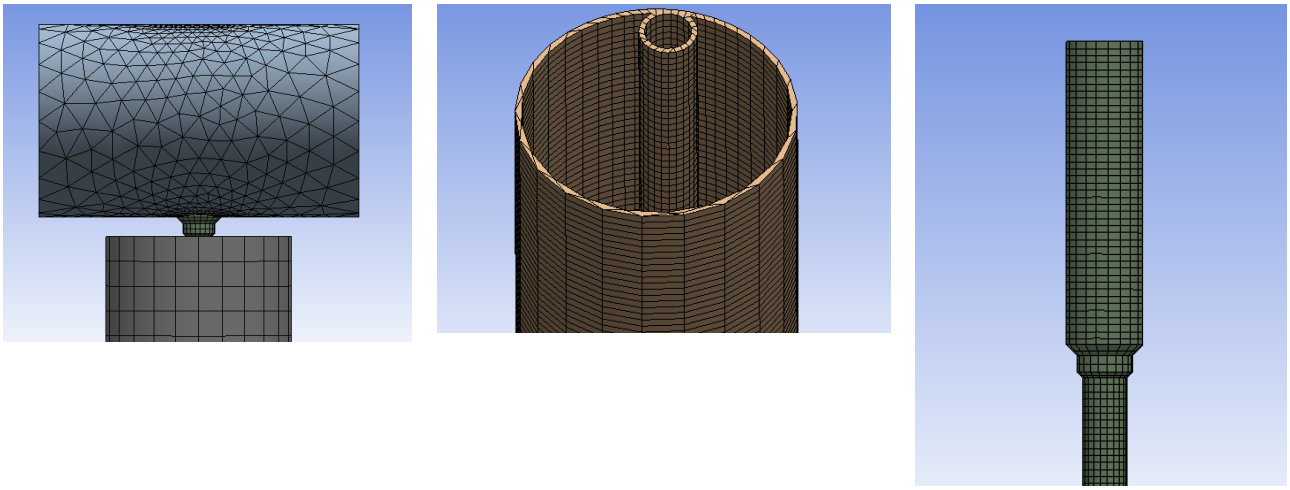

Appendix M

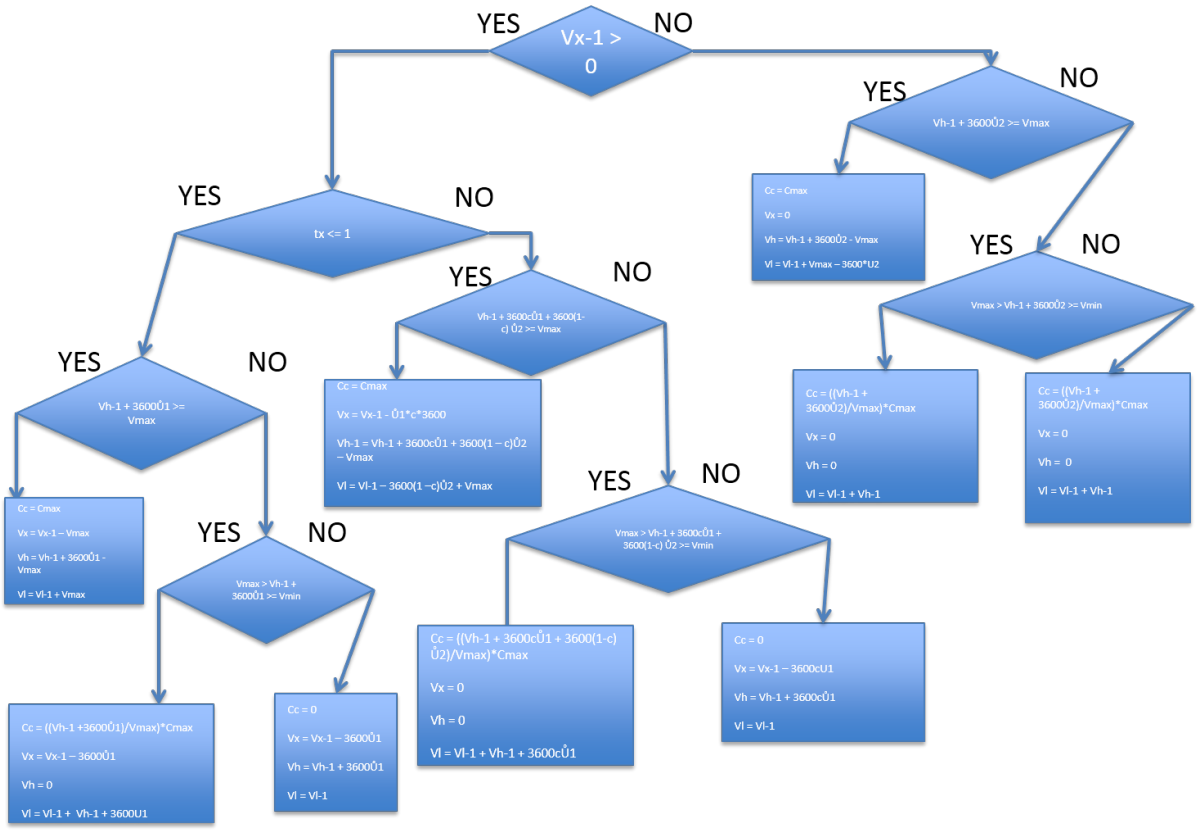

Appendix N

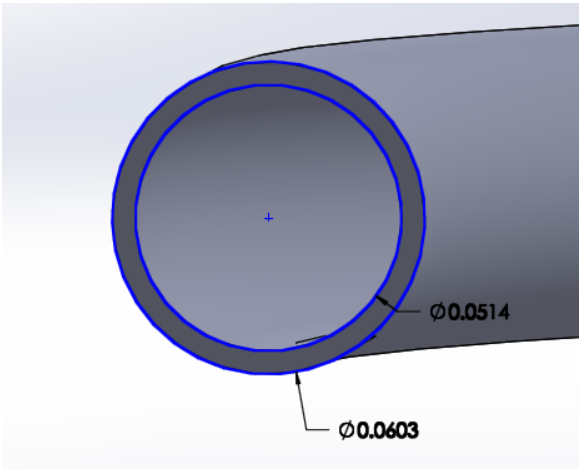

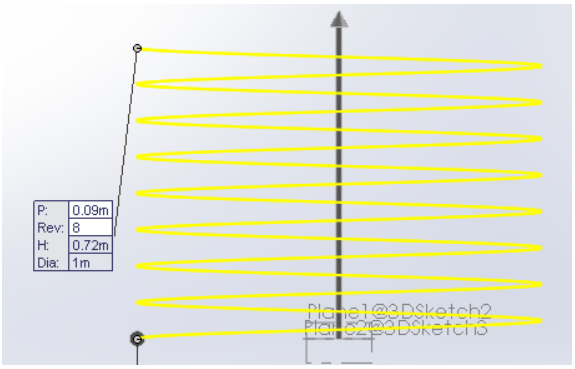

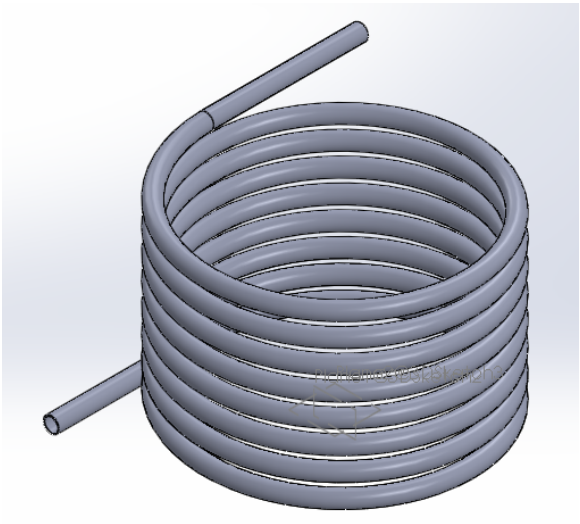

Appendix O

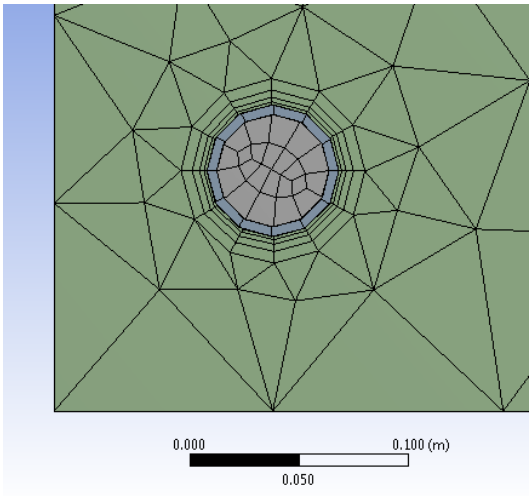
0.000
0.100 (m)
0.050

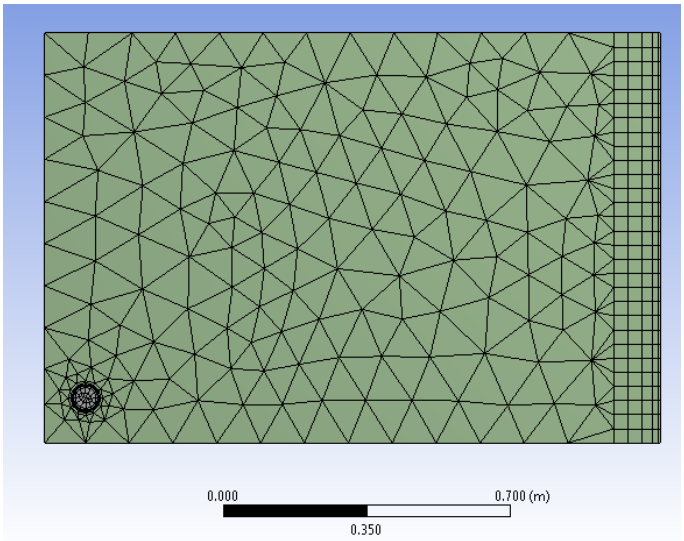
0.000
0.700 (m)
0.350

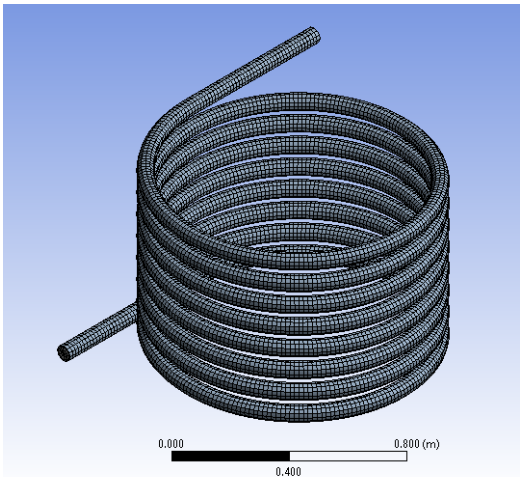
0.000
0.800 (m)
0.400

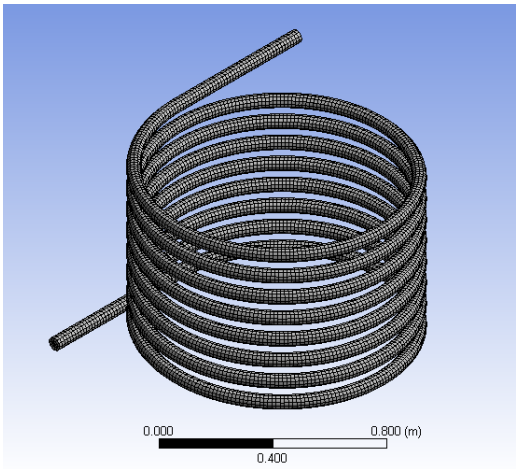
0.000
0.800 (m)
0.400

Appendix P

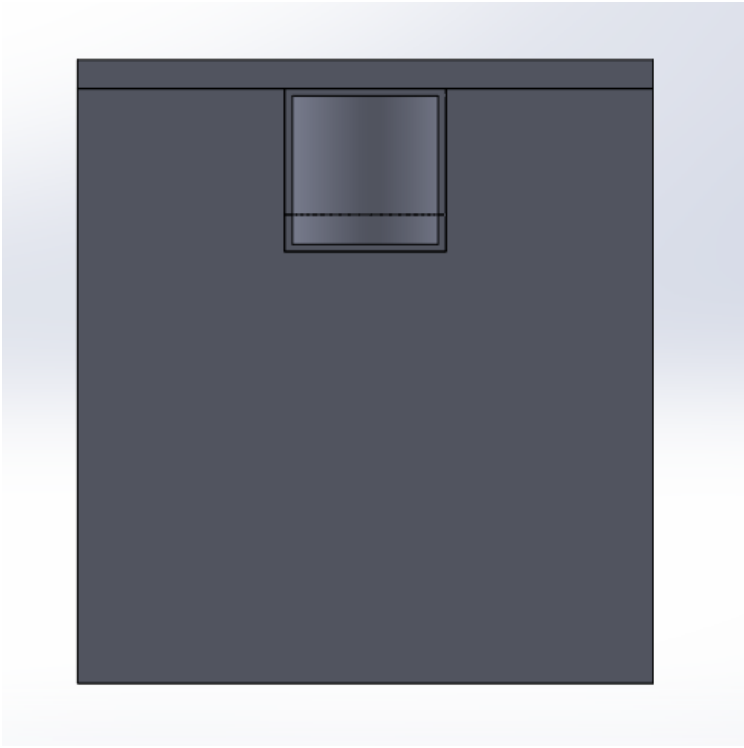

Appendix Q